Performance Assessment of Advanced Digital Measurement and Protection Systems

Final Project Report
Part I

Power Systems Engineering Research Center

A National Science Foundation
Industry/University Cooperative Research Center
since 1996

Power Systems Engineering Research Center

Performance Assessment of Advanced Digital Measurement and Protection Systems

Final Report for PSERC Project T-22
Part I

George G Karady, Project Leader
Sadik Kucuksari, Graduate Student
Yan Ma, Graduate Student
Arizona State University

PSERC Publication 06-23

August 2006

Information about this project

For information about this project contact:

George G. Karady
Professor
Arizona State University
Department of Electrical Engineering
Tempe, AZ 85287
Tel: 480-965-6569
Fax: 480-965-0745
Email: karady@asu.edu

Power Systems Engineering Research Center

This is a project report from the Power Systems Engineering Research Center (PSERC). PSERC is a multi-university Center conducting research on challenges facing a restructuring electric power industry and educating the next generation of power engineers. More information about PSERC can be found at the Center's website: http://www.pserc.org.

For additional information, contact:

Power Systems Engineering Research Center
Arizona State University
577 Engineering Research Center
Box 878606
Tempe, AZ 85287-8606
Phone: 480-965-1643
FAX: 480-965-0745

Notice Concerning Copyright Material

Acknowledgements

This is Part I of the final report on the Power Systems Engineering Research Center (PSERC) project "Performance Assessment of Advanced Digital Measurement and Protection Systems (T-22)."

- Part I: compares the accuracy and other performance characteristics of optical instrument transformers to magnetic instrument transformers in a high voltage laboratory and using data from field testing.
- Part II: compares the performance of the optical and magnetic transformer systems by evaluating their relative performance when supporting the functions of protection, revenue metering, and power quality metering using field testing results and model simulation techniques.

We express our appreciation for the support provided by the PSERC industrial members and by the National Science Foundation under grant NSF EEC-0001880 received from the Industry / University Cooperative Research Center program. We also express our appreciation for the support provided by Farnoosh Rahmatian (NxtPhase), Dylan Steward (NxtPhase) and Dale Krummen (AEP). We also acknowledge the assistance of Dr. Mladen Kezunovic of Texas A&M University.

Executive Summary

Traditional measurement and protection systems consist of current and voltage transformers (CTs and PTs) that produce analog signals that are transported through electrical cables to the substation control room. The primary sides of the instrument transformers are supplied by the network voltage and current. The secondary side supplies the protection relays or energy measurement systems. Recently developed optical voltage and current transducers produce digital and analog signals representing secondary current and voltage. These signals are transported to the control room through fiber-optic cables. In the control room the optical instrument transformer may supply digital relays, a digital energy metering system, power quality meters, among other devices or systems. The conventional instrument transformers have one output, 1 A or 5 A for CTs, and 69V or 115V for PTs. The optical instrument transformers have three outputs: (1) Digital; (2) Low Energy Analog (LEA): Optical CT = 4 V, Optical PT= 4 V; and (3) High Energy Analog (HEA): Optical CT = 1 or 5 A, Optical PT =69/120V.

The suggested advantages of optical systems over traditional magnetic systems include improved safety, smaller size, immunity from electromagnetic interferences, better transient response (wider frequency band), a broader dynamic range, and higher accuracy. It is expected that the optical and digital system will provide advantages in relaying and metering applications. The wider frequency band and improved dynamic performance should make the relaying applications less prone to misoperation as a result of transformer saturation or input signal distortions. The higher accuracy should result in more reliable revenue metering. The wider frequency bandwidth should also improve accuracy of harmonic monitoring, which would enable improved assessment of power quality. The immunity from electromagnetic disturbances should increase reliability. These suggested benefits of optical instrument transformers motivated a systematic quantitative comparison of an integrated measurement and protection system based on optical CTs and PTs with a system using magnetic CTs and PTs in this research project.

At Arizona State University, a high-current generator was developed to produce up to 1,200 A. It was used in the High-Voltage Laboratory for laboratory comparison of instrument transformer performance. Field testing using installed conventional and optical CTs and PTs for protection and metering was done at AEP's Corridor substation. The instrument transformer outputs were observed and recorded by a Tesla event recorder.

In general, the results show that the performance of the optical instrument transformers is quite comparable to the magnetic instrument transformers. Differences found in the field and laboratory measurements were within acceptable levels of the test and data acquisition equipment used. The following specific results were obtained.

1. The test of metering accuracy of the OCT verified the manufacturer's specified accuracy of 0.2%. The field measurements showed a 2% difference between the OCT and magnetic transformer-measured RMS values, but these differences are within the allowed limits of the test and recording equipment used.

2. The steady state performance was compared using the ASU's current generator. The RMS current difference between the two transformers was less than 2% in the 200 A to 750 A range. A small phase shift (less than one degree) was observed between the two transformers. This was due to the OCT optical system having a 40 μs inherent delay that was not compensated for in these tests.
3. The steady state performances of the OPT and a standard magnetic PT were compared using ASU's high voltage laboratory. The difference between the two PTs was less than one percent under the rated voltage, but increased rapidly above the rated voltage due to saturation of magnetic PT. The OPT output was highly linear. The comparison of wave shapes produced less than a 3% difference and a 42 μs phase delay. The field test showed less than 0.5% differences between the magnetic and optical PTs, which is well within the accuracy of test and recording equipment.
4. The transient performance of the OCT was assessed by comparing the reproduction of short circuit current and the direct measurement of frequency characteristics. Laboratory testing showed around a 2.3% differences in peak short circuit current reproduction. The field test showed a maximum 2.8% difference in LEA output of OCT in the reproduction of RMS values of the first to third cycles after short circuit. Both the field and laboratory tests showed around 2.5% differences between the instantaneous short circuit current values. The OCT response was tested using a DC pulse. The OCT signal showed a 68 μs delay and the rise time of the pulse appeared increased. The frequency characteristics of the OCT were measured. The results showed that the amplitude decreases with frequency. The slope was around 3 dB/octave. The amplitude is zero above around 20 kHz. The phase angle changes more or less linearly by the frequency. At 7.6 kHz the phase angle is 180 degrees.
5. The transient performance of the OPT was evaluated, comparing the PT responses to short-circuit produced voltage drop in the field, a lightning impulse test, and direct measurement of frequency characteristics. The short circuit generated a voltage drop with less than 0.25% differences in RMS voltages. The instantaneous voltage values showed less than a 1.8% difference. The lightning impulse test showed that the magnetic PT and the OPTs HEA output did not reproduce the lightning impulse well, but that the LEA output did. A higher bandwidth LEA would be necessary for reproducing lightning impulses accurately. The OPT's frequency characteristic showed that the amplitude decreased with frequency, with a slope of around 3 dB/octave. The amplitude was zero above around 40 kHz. The phase angle changed more or less linearly by the frequency.
6. The field test permitted the calculation of impedance trajectories in the cases of different faults. The trajectories were calculated by using data from the optical and magnetic instrument transformers. The point-by-point comparison of the data showed around a 10% deviation.

The frequency test results suggested that both transformers could be modeled by a low-pass filter. A circuit model was developed to represent the OCT in protection system performance analysis (reported in Part II). The model consisted of an ideal current transformer, a sixth-order low-pass filter, and an ideal amplifier which converts the voltage signal to current.

Table of Contents

1 Introduction 1
2 Task #1 Literature Review and State-of-Art Report 2
2.1 Characteristics of Optical Transformers 2
2.2 Literature Review of Optical Current Transformer 3
2.2.1 General Literature Review 3
2.2.2 NxtPhase Company's Publications 18
2.3 Literature Review of Optical Voltage Transformers 21
2.3.1 General Literature Review 23
2.3.2 NxtPhase Company's Publications 26
2.4 Market Survey of Optical Instrument Transformers 29
2.4.1 Digital Optical Instrument Transducers (ABB) 29
2.4.2 Magneto-Optic Current Transducer (MOCT) 30
2.4.3 Electro-Optic Voltage Transducer (EOVT) 30
2.4.4 Fiber Optic Current Transducer (FOCT) 31
2.4.5 SEECO Current Sensor 31
2.4.6 AREVA Instrument Transformers 32
2.4.7 AIRAK Optical Current Transducer 34
2.4.8 NxtPhase T&D Optical Voltage and Current Transformers 35
2.4.9 Optically Powered Current Transformer 35
2.5 Conclusion of Literature and Market Survey 37
3 Task #2 Analysis of the Measurement and Protection System Operation 38
3.1 Study of Optical CT Operation 38
3.1.1 NxtPhase Optical Current Transformer 38
3.1.2 Current Generator and Test Setup 40
3.1.3 Comparison of Steady State Performance of the Magnetic and Optical CT in Protection Mode 45
3.1.4 Comparison of the Magnetic and Optical CT Wave Shape 51
3.1.5 Comparison of the Current Transformers Accuracy in Metering Mode 53
3.2 Study of Optical PT Operation 55
3.2.1 NxtPhase Optical Potential Transformer 55
3.2.2 High Voltage Test Setup 58
3.2.3 Comparison of Steady State Performance of an Optical and Magnetic PT 60
3.2.4 Comparison of the Magnetic and Optical PT Wave Shape 65
4 Task #3: Investigation of the Steady State and Transient Response of the Two System 67
4.1 Transient Response of Current Transformers 67
4.1.1 Reproduction of Short Circuit Current 68
4.1.2 Low Voltage DC Impulse Test 72
4.1.3 Temperature Effect 74
4.1.4 Measurement of OCT Frequency Characteristics 75
4.1.5 Electrical Circuit Model for OCT 79
4.1.6 Verification of the Model by PSPICE Simulation 81
4.2 Transient Response of Voltage Transformers 85
4.2.1 Transient Analysis of PTs 85

4.2.2 Frequency Characteristics of the PTs 89
4.3 Comparison of Magnetic and Optical Instrument Transformers Operation Based On Field Data 95
4.3.1 Case 1: Disturbance in C phase. 96
4.3.2 Case 2: Disturbance in Phase B 105
4.3.3 Case 3: Disturbance in Phase B 108
4.3.4 Case 4: Disturbance in Phase A 111
4.3.5 Case 5: Disturbance in Phase A 112
4.3.6 Case 6: Disturbance in Phase A 115
4.3.7 Case 7: Disturbance in Phase C 117
4.3.8 Case 8: Disturbance in Phase A 120
4.3.9 Case 9: Disturbance in Phase A 122
4.3.10 Case 10: Disturbance in Phase A 124
4.3.11 Case 11: Disturbance in Phase A 126
5 Conclusion 129
APPENDIX 132
REFERENCES 139

Table of Figures

Figure 2.1 Physical layout of an optical fiber current sensor [7] 4
Figure 2.2 Comparisons of measurement outputs for a 50 Hz primary current [7] 4
Figure 2.3 Linearity of the optical fiber current sensor [7] 5
Figure 2.4 Comparison of measurement outputs for direct current transients [7] 5
Figure 2.5 Test for ratio error and phase displacement characteristic [8] 6
Figure 2.6 Test for transient characteristics [8] 6
Figure 2.7 Magnetic core and sensor configuration [9] 7
Figure 2.8 Result of testing an optical sensor electronic interface of a microprocessor based protection relay [11] 9
Figure 2.9 Schematic diagram of the optical current sensing system [12] 10
Figure 2.10 The output characteristics of optical AC current sensing system [12] 11
Figure 2.11 Schematic illustration of ABBs' Optical current sensor [13] 11
Figure 2.12 Temperature dependence of power converter efficiency [13] 12
Figure 2.13 Frequency response of the phase angle [13] 12
Figure 2.14 Structural diagram of optical current transformer [14] 13
Figure 2.15 Principle set up of optical current sensor [15] 14
Figure 2.16 Short circuit-reference sensor (shunt) [15] 14
Figure 2.17 Short-circuit-optical sensor [15] 15
Figure 2.18 Typical 50 Hz test waveform [16] 15
Figure 2.19 Percentage difference between reference signal and OCT reading up to 3 kHz [16] 16
Figure 2.20 Sensing head drawing [17] 16
Figure 2.21 FOCS sensor head [17] 17
Figure 2.22 Relative FOCS output as a function of temperature [17] 17
Figure 2.23 Optical current sensor with low energy analog (LEA) output to analog meter or relay. [18] 18
Figure 2.24 Low energy analog (LEA) metrology setup, applicable for < 100 amp turns [5] 19
Figure 2.25 Saturated and non-saturated CT secondary output – conventional instrument transformer [3] 20
Figure 2.26 NXCT and Maxsys 2510 power meter accuracy error versus rated current (100% = 1 A secondary) [21] 21
Figure 2.27 Illustration of the Pockels effect (half-wave plate) [41] 22
Figure 2.28 MOCT based Optical PT [22] 23
Figure 2.29 Current and voltage transducers [24] 24
Figure 2.30 Block diagram of optical voltage transformer [27] 25
Figure 2.31 Schematic diagram of an optical DC voltage measuring system [30] 26
Figure 2.32 Digital Optical Instrument Transducers 30
Figure 2.33 SEECO Current and Voltage Sensors 32
Figure 2.34 AREVA Instrument Transformer system components 33
Figure 2.35 Optical Current Transducer 34
Figure 2.36 Optically-powered Current Transformer System 36
Figure 3.1 NXCT Optical Circuit [4] 39
Figure 3.2 NXCT Optical Current Transducer [4] 40

Figure 3.3 Experimental test setup connections diagram 41
Figure 3.4 Experimental test setup..... 41
Figure 3.5 Electronic Switch Block Diagram 42
Figure 3.6 Sample Current waveform with noise 43
Figure 3.7 Sample Current waveform without noise 44
Figure 3.8 Linearity of results..... 46
Figure 3.9 OCT current vs. Magnetic CT current..... 49
Figure 3.10 CT based percentage error vs. OCT current 50
Figure 3.11 OCT and Magnetic CT currents and difference between them, when the primary current is 730 A 51
Figure 3.12 Sine wave differences at steady state between them when the primary current is 109 A. 52
Figure 3.13 OCT measurement test setup..... 53
Figure 3.14 CT measurement test setup..... 54
Figure 3.15 NxtPhase Voltage Transducer 56
Figure 3.16 Connection diagram for the AC test of optical and magnetic PT..... 57
Figure 3.17. Experimental test setup..... 58
Figure 3.18 Sample OPT output voltage waveform with noise (most of noise is expected to have been caused by the oscilloscope's connection) 59
Figure 3.19 Error bar analysis of magnetic PT and OPT..... 63
Figure 3.20 OPT output voltage vs. magnetic PT output voltage..... 63
Figure 3.21 Difference between the magnetic and optical PT output voltages 64
Figure 3.22 Saturation caused distortion of magnetic PT output voltage at 80 kV applied voltage..... 64
Figure 3.23 Electrical field coupling effect; Magnetic PT energized, OPT floating..... 65
Figure 3.24 OPT and Magnetic PT voltages and difference between them when the primary voltage is 70 kV..... 66
Figure 3.25 OPT and Magnetic PT voltages and difference between them when the primary voltage is 40 kV..... 66
Figure 3.26 Error between magnetic PT and OPT at rated voltage 67
Figure 4.1 Transient short circuit current when the switching occurred at 90 degree voltage..... 68
Figure 4.2 Transient short circuit current when the switching occurred at voltage zero. 69
Figure 4.3 Typical recorded fault current 70
Figure 4.4 Short circuit simulation test setup 70
Figure 4.5 Simulated fault current 71
Figure 4.6 Short circuit simulations for CT and OCT 72
Figure 4.7 DC impulse test setup..... 73
Figure 4.8 DC test results..... 73
Figure 4.9 Temperature effect on optical CT reading..... 74
Figure 4.10 Frequency response experimental test setup 75
Figure 4.11 Current and OCT signals at 2 kHz 76
Figure 4.12 Input current and OCT output signals at 4 kHz..... 77
Figure 4.13 Normalized amplitude-frequency characteristics of OCT..... 78
Figure 4.14 Phase angle-frequency characteristics of OCT..... 78
Figure 4.15 Electrical circuit model for OCT 79

Figure 4.16 Comparisons of circuit model amplitude frequency characteristics with the measured values. 80
Figure 4.17 Comparisons of circuit model phase-angle frequency characteristics with the measured values. 81
Figure 4.18 PSPICE circuit model 81
Figure 4.19 60 Hz Steady State 82
Figure 4.20 60 Hz Steady State phase difference 82
Figure 4.21 ATP simulation; input current 84
Figure 4.22 ATP simulation; output voltage 84
Figure 4.23 Phase delay 85
Figure 4.24 Optical PT response to lightning impulse HEA output 86
Figure 4.25 OPT impulse test HEA output 87
Figure 4.26 Optical PT lightning impulse test LEA output 87
Figure 4.27 Lightning impulse test of magnetic PT 88
Figure 4.28 NXVT Frequency response test setup 89
Figure 4.29 Applied voltage and NXVT output voltage at 3 kHz 90
Figure 4.30 Normalized amplitude-frequency response 91
Figure 4.31 Phase angle-frequency characteristics 92
Figure 4.32 Applied voltage NXVT output voltage changing by frequency 93
Figure 4.33 Normalized amplitude-frequency response 94
Figure 4.34 Phase angle-frequency characteristics 94
Figure 4.35 Corridor substation Instrument transformer connection 95
Figure 4.36 Current measurements Case 1 97
Figure 4.37 Voltage measurements 99
Figure 4.38 Voltage-current overlap sine waves 100
Figure 4.39 Comparison of voltage sine waves, Case 1 101
Figure 4.40 Comparison of current sine waves, Case 1 102
Figure 4.41 Percentage difference between the R and X values Case 1 102
Figure 4.42 Impedance trajectories, Case 1 104
Figure 4.43 Current measurements Case 2 106
Figure 4.44 Percentage difference between the R and X values Case 2 107
Figure 4.45 Impedance trajectories with magnetic transformers, Case 3 109
Figure 4.46 Impedance trajectories with optical transformers, Case 3 110
Figure 4.47 Percentage difference between the R and X values Case 3 110
Figure 4.48 Percentage difference between the R and X values, Case 4 112
Figure 4.49 Current sine waves, Case 5 113
Figure 4.50 Percentage difference between the R and X values, Case 5 115
Figure 4.51 Percentage difference between the R and X values, Case 6 116
Figure 4.52 Voltage and current sine waves, Case 7 118
Figure 4.53 Percentage difference between the R and X values, Case 7 119
Figure 4.54 Recorded current sine waves, Case 8 120
Figure 4.55 Percentage difference between the R and X values, Case 8 122
Figure 4.56 Percentage difference between the R and X values, Case 9 124
Figure 4.57 Percentage difference between the R and X values, Case 10 126
Figure 4.58 Voltage and current sine waves, Case 11 127
Figure 4.59 Percentage difference between the R and X values, Case 11 128

Figure A. 1 Experimental amplitude-frequency response 133
Figure A. 2 Experimental phase-frequency response 134
Figure A. 3 Ladder network..... 134
Figure A. 4 Experimental and calculated data, amplitude-frequency..... 137
Figure A. 5 Experimental and calculated data, phase-frequency..... 138

List of Tables

Table 2.1 The results of cross-talk tests [11] 9
Table 2.2 Measurement of harmonic content [32] 27
Table 2.3 Accuracy measurement under various drybanding (DB) [34] 28
Table 2.4 Technical Data 33
Table 2.5 Optical Current Transducer Specifications 35
Table 3.1 ASA Accuracy Classes for Metering Current Transformers [37] 42
Table 3.2 ASA Standard Burdens for Current Transformers at 60 Cycles [37] 43
Table 3.3 Test results 48
Table 3.4 Repetition of current measurement using precision CT and ampere meters 50
Table 3.5 Test results 54
Table 3.6 Primary current vs. magnetic CT output 55
Table 3.7 CT comparisons 55
Table 3.8 Test results 61
Table 4.1 Difference between peak currents 72
Table 4.2 Temperature effect on OCT 74
Table 4.3 Frequency characteristics of the OCT test results 77
Table 4.4 Frequency characteristics of the NXVT test results 91
Table 4.5 Frequency characteristics of the NXVT test results 93
Table 4.6 Metering current comparison Case 1 98
Table 4.7 Comparison of fault currents Case 1 98
Table 4.8 Comparison of voltages during the fault in Case 1 100
Table 4.9 Metering current comparison Case 2 105
Table 4.10 Comparison of fault currents Case 2 106
Table 4.11 Comparison of voltages during the fault in Case 2 107
Table 4.12 Metering current comparison Case 3 108
Table 4.13 Comparison of fault currents Case 3 108
Table 4.14 Comparison of voltages during the fault in Case 3 109
Table 4.15 Compares the metering CT outputs. The results are very similar to the previous cases. The maximum difference between magnetic and optical CTs is 0.47%. 111
Table 4.16 Metering current comparison, Case 4 111
Table 4.17 Comparison of fault currents, Case 4 111
Table 4.18 Comparison of voltages during the fault, Case 4 112
Table 4.19 Metering current comparison, Case 5 113
Table 4.20 Comparison of fault currents, Case 5 114
Table 4.21 Comparison of voltages during the fault, Case 5 114
Table 4.22 Metering current comparison, Case 6 115
Table 4.23 Comparison of fault currents, Case 6 116
Table 4.24 Comparison of voltages during the fault, Case 6 116
Table 4.25 Metering current comparison, Case 7 117
Table 4.26 Comparison of fault currents Case 7 118
Table 4.27 Comparison of voltages during the fault, Case 7 119
Table 4.28 Metering current comparison, Case 8 120
Table 4.29 Comparison of fault currents, Case 8 121
Table 4.30 Comparison of voltages during the fault, Case 8 121

Table 4.31 Metering current comparison, Case 9 122
Table 4.32 Comparison of fault currents, Case 9..... 123
Table 4.33 Comparison of voltages during the fault, Case 9..... 123
Table 4.34 Metering current comparison, Case 10 124
Table 4.35 Comparison of fault currents, Case 10..... 125
Table 4.36 Comparison of voltages during the fault, Case 10..... 125
Table 4.37 Metering current comparison, Case 11 126
Table 4.38 Comparison of fault currents, Case 11..... 127
Table 4.39 Comparison of voltages during the fault, Case 11..... 128

1 Introduction

Traditional measurement and protection systems consist of current and voltage transformers that produce analog signals that are transported through electrical cables to the substation control room. The primary sides of the instrument transformers are supplied by the network voltage and current. The secondary side supplies the protection relays or energy measurement systems.

This project deals with the new advanced digital instrumentation and protection system. Recently developed optical voltage and current transducers have become available, that produce digital and analog signals representing the secondary current and voltage. These signals are transported to the control room through fiber-optic cables. In the control room the optical instrument transformer may supply a digital relay, a digital energy metering system, a power quality meter, etc.

The major advantages of the optical system are improved safety, smaller size, and immunity from electromagnetic interferences, better transient response (wider frequency band), a larger dynamic range, and higher accuracy than the traditional magnetic system. It is expected that the optical and digital system will provide advantages for utilities both in the relaying and metering applications. The wider frequency band and improved dynamic performance make the relaying applications less prone to miss operations as a result of transformer saturation and input signal distortions. The higher level of accuracy results in more accurate revenue metering, which affects the billing and may improve revenue. The wider frequency bandwidth also improves accuracy of harmonic monitoring, which enables improved assessment of power quality. The immunity from electromagnetic disturbances increases reliability.

Qualitative technical system analysis verifies all previously mentioned advantages through measurements and associated comparisons. However, it fails to evaluate quantitatively the effect of digital systems on measurement and protection performance, as well as to provide estimates of the related financial consequences. A cursory review of literature did not produce any papers or studies that compare quantitatively the two systems in an authentic environment. The potential for major benefits of the innovative sensory system provides the motivation for systematic research that compares conventional systems with the proposed optical system.

The objective of this project is to provide quantitative comparisons between an integrated measurement and protection solution based on optical CTs and PTs and the traditional magnetic CTs and PTs connected to the measurement and protection systems.

2 Task #1 Literature Review and State-of-Art Report

The project started with a review of the literature published in the last 15 years. This review evaluated papers dealing with the accuracy, transient behavior, bandwidth, and flexibility of digital and analog systems. The results of this study identified the present state-of-the-art. The market offerings were reviewed using the web sites of manufacturers. The available products and their technical specifications have been identified. In the educational component of this work, the participating students learned the subject and became familiar with related theoretical and practical problems.

2.1 Characteristics of Optical Transformers

The function of current and voltage transformers is to transform the power system currents and voltages to a lower value and provide isolation between the power network, relays, and other instruments. Operating voltages and currents in a power system are usually at kilovolt and kiloampere levels. However, for measurement or digital processing the current and voltage levels must be reduced. Typical output values are 1 A or 5 A for current transformers and 120 V for voltage transformers.

Recently, a number of Optical Current Transformers (OCT) and Optical Voltage Transformers (OPT) have been developed. The manufacturers claim that these devices offer many advantages when compared to traditional magnetic instrument transformers. Most of the practical OCTs are based upon Faraday's observation that the magnetic field of a current-carrying conductor changes the polarization angle of polarized light beam in a fiber optic cable [1].

In industrial applications and market, traditional sensors have a multitude of applications that are accepted by many users. They have had a wide application area since the beginning of power transmission, and optical systems must compete with them as new application system development [2].

Traditional magnetic transformers have an iron core in order to convert the primary current to a secondary manageable current level (5 A or 1 A for CT and 120 V for PT). As a result of saturation of the magnetic core, these signals can be distorted. In optical current sensors no saturation occurs, but optical systems must be used appropriately in order to present distortion-free signal duplication [3]. The most advantageous optical systems are lightweight, which allows easy installation. Optical sensors have a large dynamic range and they do not reveal hysteresis [4].

The primary advantages of optical current sensors are their large dynamic range and higher degree of accuracy than magnetic current transformers. Because optical systems do not contain magnetic resources, there is no saturation or hysteresis effect. The Faraday Effect is used to sense the flowing current, making them inherently linear; this linearity allows them to measure a wide range of current from 1 A to high current levels, DC current, and harmonic measurements. All these applications can be installed in one OCT [5].

Optical current sensors merge the measuring ability of magnetic transformers with the isolation features of optical systems, making optical systems exciting. Current is sensed in the high voltage conductor and converted to a secondary side by using light through fiber-optic cable. Optical current transformers are connected to metering and relaying equipment. Their accuracy for metering is 0.2%, and protection accuracy is 2%. They have also wide bandwidth, from 1 Hz to 20 kHz [6].

2.2 Literature Review of Optical Current Transformer

The literature review is divided into two parts: general literature review and NxtPhase-related literature review The NxtPhase Company sponsors the project and provides the Optical Current Transformers for the work. NxtPhase has published several papers describing their OCT. This literature was reviewed separately because NxtPhase instrument transformers are used for the experimental work.

2.2.1 General Literature Review

The first studies on the Optical Current Transformers (OCT) were published at the end of 1970s and during the 1980s. Those studies mainly focused on the feasible power system application of optical sensors. Most of the studies concentrated on the development of a Faraday Effect-based low-voltage optical current sensor. In late 1980s and the early 1990s, researchers began to study the HV applications of optical current sensors. Some researchers investigated the transient behaviors of OCTs. From the beginning of the 1990s until today, large numbers of studies dealt with the performance improvement of OCTs that are used for power system protection. Different variations of the Faraday Effect and also the effect of various environmental conditions were studied. At present several different OCTs have been developed and offered for applications in power systems.

A.P. Steer, S.J. Turner, et al [7] presented a comparison between OCTs and conventional CTs in their paper, which describes the design and test of an OCT. They also mention two broad categories of optical fibers that are available: multimode and single mode. Single mode is most appropriate for current sensors. The principle of OCT is the Faraday Effect: the change of polarization angle (azimuth) is proportional to the part of the magnetic field parallel to the propagation direction of the light. If the fiber forms a closed path around a conductor, the change of the polarization angle depends on the number of ampere-turns. Vibration or a change in temperature of the sensing fiber could affect the accuracy of readings [7].

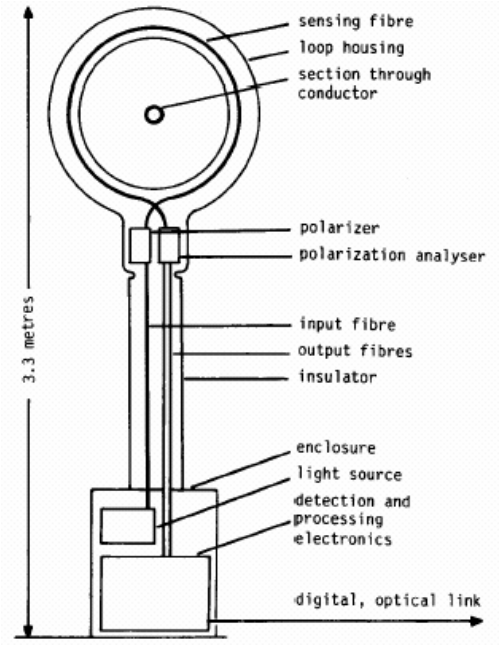

Figure 2.1 Physical layout of an optical fiber current sensor [7]

The designed [7] OCT was tested by using 25 turns of cable around the sensing head. Passing 400 A through the cable simulated a 10 kA current. A direct current test was also performed for this transformer. Figure 2.1 shows the arrangement of the tested system.

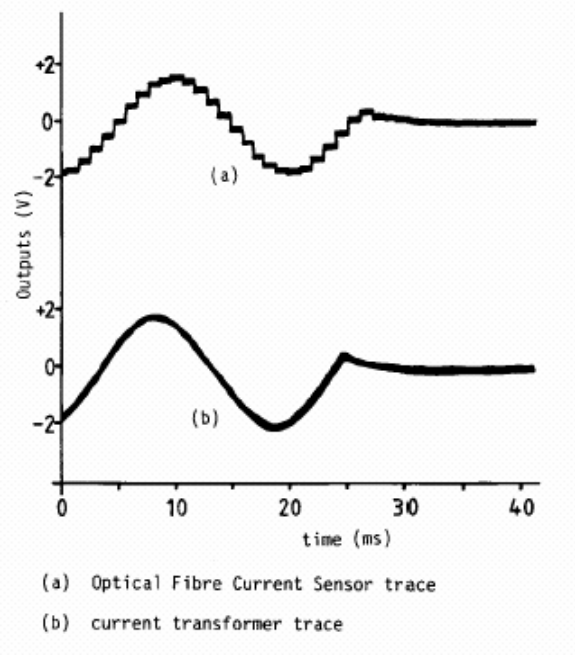

Figure 2.2 Comparisons of measurement outputs for a 50 Hz primary current [7]

In order to make a comparison, a shunt was connected to the cable that makes 500 turns at the current transformer. The voltage across the shunt was recorded to compare the output voltage of optical fiber current sensor.

Figure 2.2 shows the amplitude response of the two readings. The current transformer output has been scaled to obtain the same current level with 25 turns of cable around the fiber loop. The current transformer output was linear and well below the saturation limit. A traditional ampere meter was used to measure the applied current; it limits the accuracy of the readings for this experiment by 1%. The difference in linearity was not larger than this limit. However, some deviations were observed at high current levels due to the linear birefringence of the light beam.

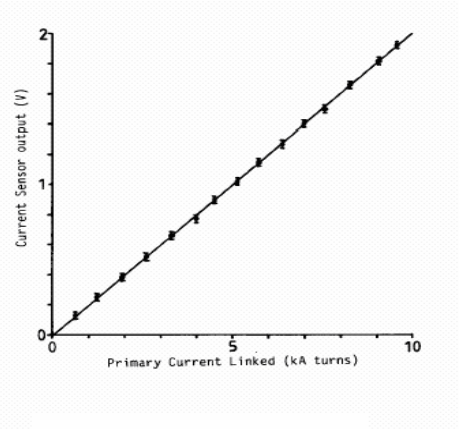

Figure 2.3 Linearity of the optical fiber current sensor [7]

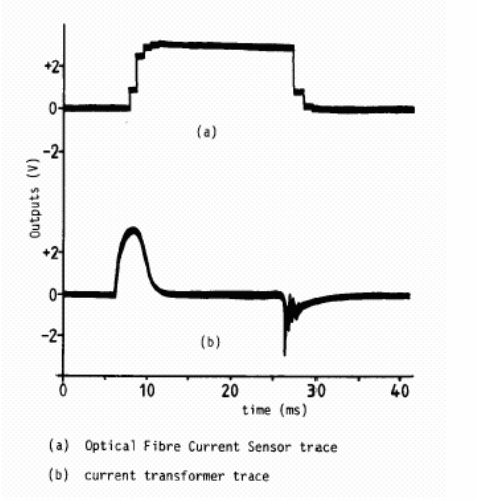

Figure 2.4 Comparison of measurement outputs for direct current transients [7]

Figure 2.4 shows the step function response of the two devices. A DC pulse was applied on the OCT and conventional magnetic CT. The figure demonstrates that the traditional

CT saturated and differentiated the pulse. There is a 1 ms delay in the current reading for the optical system as a result of the digital processing technique.

T. Sawa, K. Kurosawa and other Japanese researchers [8] presented a paper that is frequently cited as a reference. Toshiba Electric Power Co. and Toshiba Corp. performed the study. They developed a Gas Insulated Switchgear (GIS) type OCT. This device is different than the HV OCTs described in [7]. The paper shows that there are two practical methods for detecting the Faraday rotation angle:

- Light power amplitude detection
- Light power phase detection.

The results of ratio error and phase displacement tests are shown in Figure 2.5. It is evident that the accuracy of the OCT is better than required by JEC 1201 standard.

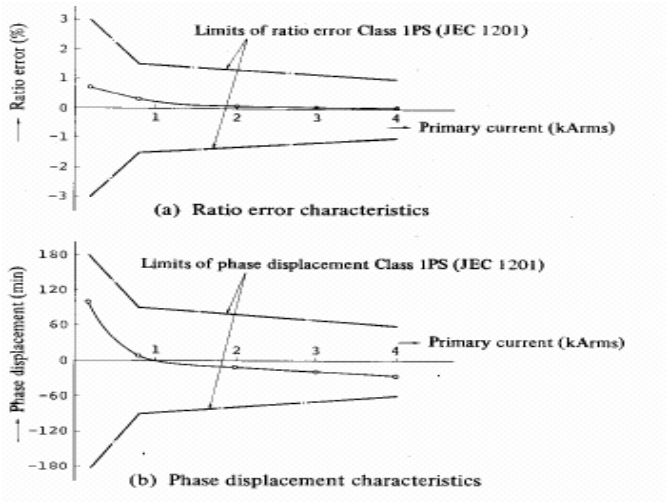

Figure 2.5 Test for ratio error and phase displacement characteristic [8]

The paper also presents temperature characteristics and transient characteristics of the CTs. The transient response of this OCT is shown on Figure 2.6.

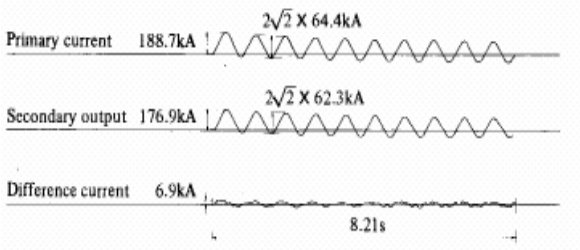

Figure 2.6 Test for transient characteristics [8]

The output waveforms and transient errors of the optical CT were measured using 10 cycles of a 63 kA RMS transient primary current (primary time constant: 0.1 s, 100% DC

component superimposed). The figure shows that the optical CT output is not saturated. The transient error is 3.6%, which meets the requirement of 10% or less requirement.

A circular sensor was developed and used as a Faraday sensor in order to avoid the effects from a neighboring magnetic field. SF6 was used for electrical insulation to transmit the light from GIS tank to the sensor element of the GIS-type optical CT. A light-powered detection was developed for signal detection, allowing easy error control.

Frankie Y.C. Leung and others [9] developed a fiber-optic current sensor for power system measurements. The paper describes two types of Fiber-optic sensors:

- Magneto-striction-based sensors and
- Faraday-rotation sensors.

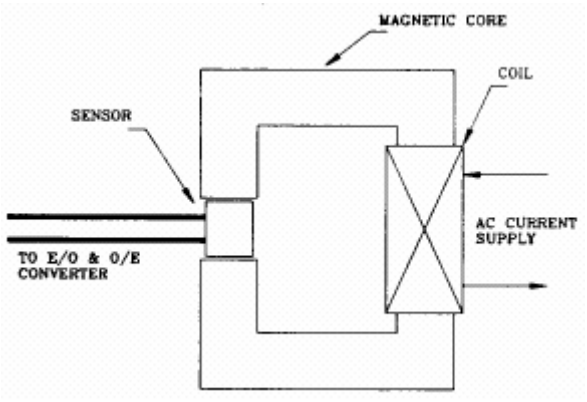

Figure 2.7 Magnetic core and sensor configuration [9]

The Faraday sensors are suitable for ac current applications ranging from power line frequencies (50-60 Hz) to well over 100 MHz. However, the Faraday sensor is not suitable for applications that require high sensitivity, because it is inherently less sensitive. The typical value for Faraday sensor is 8 x 10^{-4} A/m RMS/√Hz, compared to the 8 x10^{-11} A/m RMS/√Hz to that of the magneto-strictive sensors. This represents a significant difference.

Due to the difficulty of generating a high current in the laboratory environment, a coil of N turns carrying a small current is turned around a magnetic core. This simulates a high current passing through the center of the core, and shows an identical magnetic field effect to that of the high current. The test setup can be seen in Figure 2.7. The optical axis of the Faraday cell was arranged with the direction of the magnetic field in order to obtain maximum sensitivity. The input-output characteristics show strong linearity between the conductor current and output voltage of the transformer.

The Verdet constant (the strength of the magnetic field and a proportionality constant) of the Faraday cell is temperature dependent and affects the voltage output of the transformer. However, the applied current and magnetic field do not change as the temperature changes, and creating an error between the primary current and transformer

output. This temperature variation must be considered in the design of the signal processing unit.

The optical fiber current sensor applications in high voltage current readings have great potential in terms of accuracy, ease of use, safety, and economy. The described [9] optical magnetic field sensor prototype can be used as a current transducer, and the total cost of its components is $2,500 USD.

A. Cruden and others [10] described a Faraday Effect-based measuring device, which meets with the British Standard BS3938 specifications. The performance of the sensor is also discussed with respect to harmonic content, vibration, and temperature effects. TGG crystal is used. This crystal has a Verdet Constant of 82 μradians / Ampere-turns. Different uses of high frequency applications of optical current transformers show that the described optical devices will present important improvements in conventional CT bandwidth. The designed optical CT was tested in a current range of 0 to 5000 A, and the spectrum analysis of the sensor was compared to the output from Class 0.1%.

Cruden [11] used both the same principle and same crystal as in [10]. The optical sensor supplied a microprocessor based on over current relay. The operation of the system was tested by large short circuit current. A 75 kA short circuit current was switched to the optical sensor for approximately 10 cycles. Typical result is shown in
Figure **2.8**.

The over-current relay was set to trip at 6 times the rated current using the “high set” trip features.
Figure **2.8** shows that the current trips the relay at 34 ms.

Three main problems affecting the operation of the described device are the effects of neighboring conductors, temperature, and vibration of the optical system. To test the effect of neighboring conductors, a parallel horizontal 3-phase bus bar configuration with 5 conductors is simulated. The sensor is mounted on Phase B, and the results are given in Table 2.1.

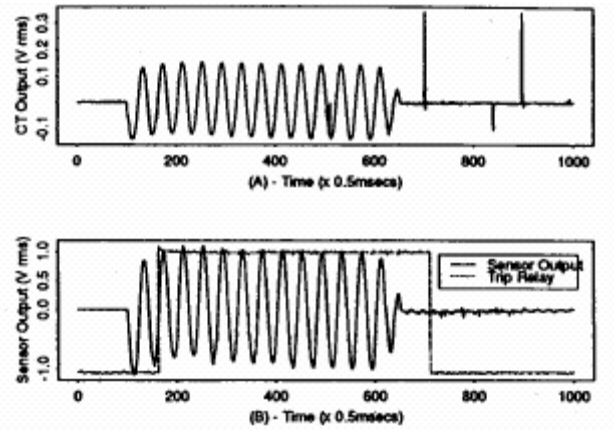

Figure 2.8 Result of testing an optical sensor electronic interface of a microprocessor based protection relay [11]

The magnetic shielding of neighboring phases by using a μ-metal enclosure is a good and practical solution to this affect.

Table 2.1 The results of cross-talk tests [11]

Phase A (amps)	Phase B (amps)	Phase C (amps)	Sensor Output (mV RMS)
0	989	0	52.9
1013	0	0	0.1
0	0	1008	0.1
1032	0	1003	0.1
999	989	1006	53.4

Vibration effects are a source of noise for the optical systems. The sources of vibration can be circuit breaker operation, environmental conditions, or human interference. A dual-wavelength referenced vibration compensation scheme was developed in this study, consisting of two separate wavelengths of light. One provides the measured signal, and the other provides the reference signal.

The magneto-optical crystal Terbium Gallium Garnet (TGG), which is an optimum material for Faraday devices, has a 1/T temperature dependence and requires compensation. The authors have developed a scheme using two different crystal materials to provide a temperature measurement and control the temperature sensitivity of the TGG.

Peng-Gang Zhang and Dave Irvine-Halliday [12] studied Faraday Effect-based optical current transformer. In this study the geometric compensation method was adopted and a closed loop current sensor with a frame structure was designed and fabricated.

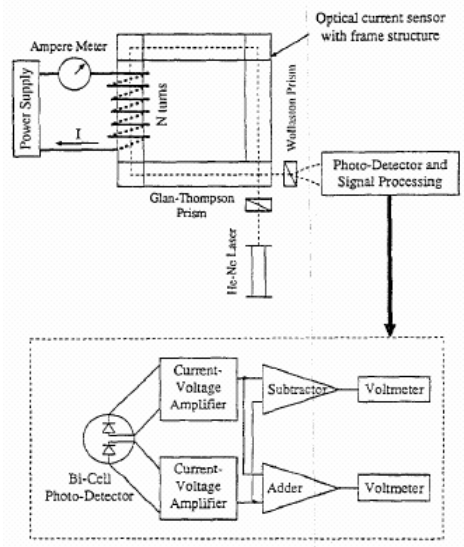

Figure 2.9 Schematic diagram of the optical current sensing system [12]

Faraday materials come in three basic classes: diamagnetic, paramagnetic and ferromagnetic. Diamagnetic material was used for the current sensor because of its low temperature dependence, which is an important factor for current-sensing in the power industry.
Figure **2.9** shows the system arrangement.

A Helium-Neon Laser was used to provide a fixed light source of constant intensity for this optical current-sensing system. The optical sensor has an enclosed structure that covers the current-carrying conductor. The effect of neighboring phase magnetic fields is eliminated in this study.

The paper reports an effective current measurement range from approximately 20 A to 1300 A. The input and output relationship is not linear, as shown in Figure 2.10. However, the relationship curve is smooth.

It is feasible for DC current-sensing to use the same system as is used for AC current-sensing is feasible. In this study, the average relative error is less than 0.13% within a range of 20 A to 1300 A for the AC current. For the DC current, the average relative error is less than 0.6%, within the range of 120 A to 300 A.

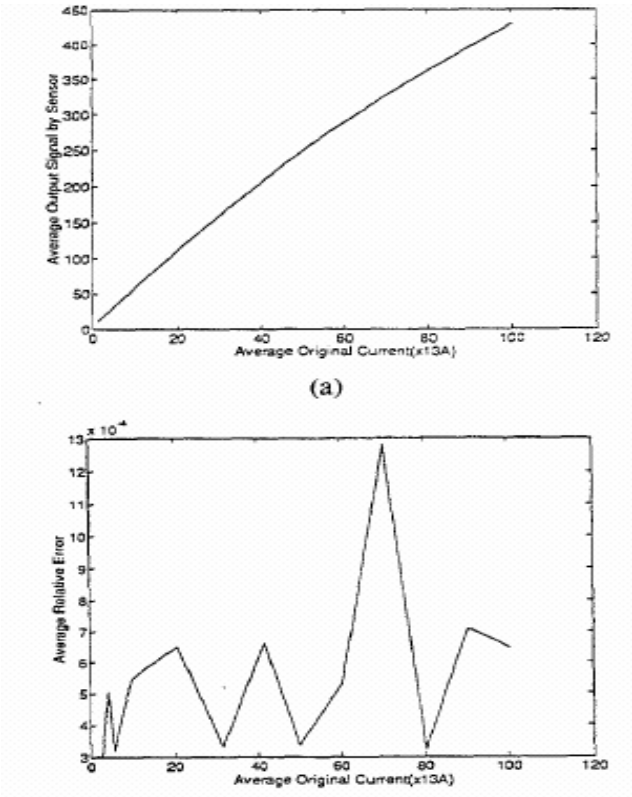

Figure 2.10 The output characteristics of optical AC current sensing system [12]

J.G. Werthen and others described the ABB Power System Company's optical current transformer [13]. The system, which is shown schematically in Figure 2.11, is divided into two modules, one located at high voltage and the other in a controlled environment at ground potential.

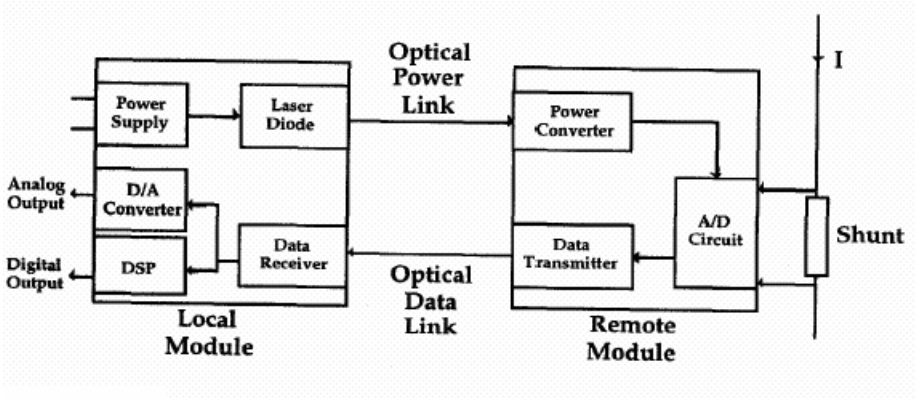

Figure 2.11 Schematic illustration of ABB's Optical current sensor [13]

The optical current transformer was effectively operated from DC to 10 kHz and 16 kHz. At 0.2 % accuracy, it met within system specifications. This offers a reliable system operation for protection of high voltage systems. Temperature range of the system is -40

°C to +85 °C and the temperature tests were conducted between -60 °C to +100 °C. The results are shown in Figure 2.12.

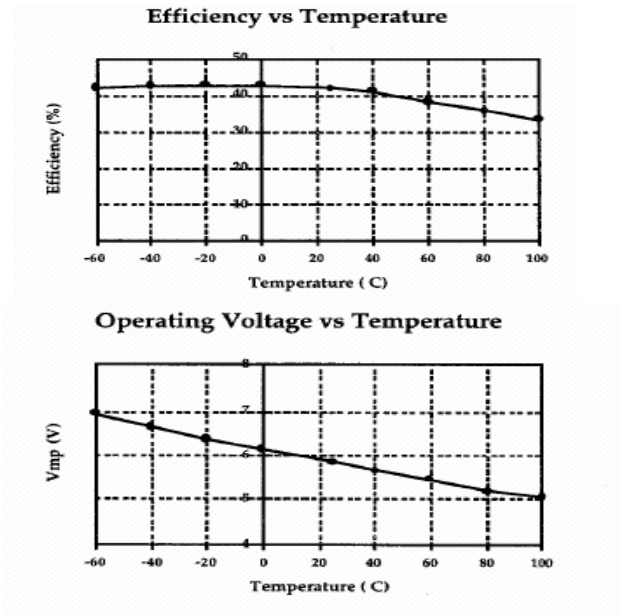

Figure 2.12 Temperature dependence of power converter efficiency [13]

A single-phase system has undergone a series of tests at Tokyo Electric Power in Japan [13] by using a resistive divider for voltage measurements. A 6.6 kV line was to be controlled with ±400 V. A simple filter was chosen in order to minimize the phase angle. As shown in Figure 2.13, a significant phase angle shift appears after 1 kHz.

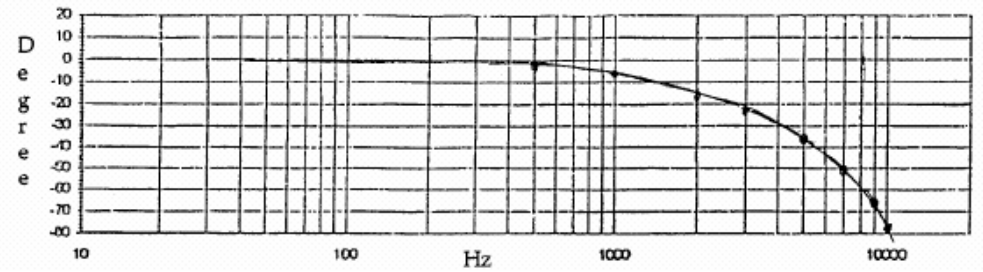

Figure 2.13 Frequency response of the phase angle [13]

Yixiong Nie and others described a practical optical current transformer [14]. The National Committee of Plan and Development of China supported to work. The current transformer described in this paper differs from the design of the high voltage CT. It exploits the magnetic potentiometer concept to sense the current and isolate the signal from high voltage by optic-fiber.

Figure 2.14 shows the structural diagram of this newly developed optical current transformer. Magnetic potentiometer produces a signal proportional with the line current. This signal is digitized with a high speed AC-DC Converter (ADC). The digital signal is

converted to a light signal by the signal processing circuit and is transferred to the ground via fiber-optic cable. At the ground an electric-optical converter converts the light signal to a digital signal, which can be used for measurement, protection, and fault recording.

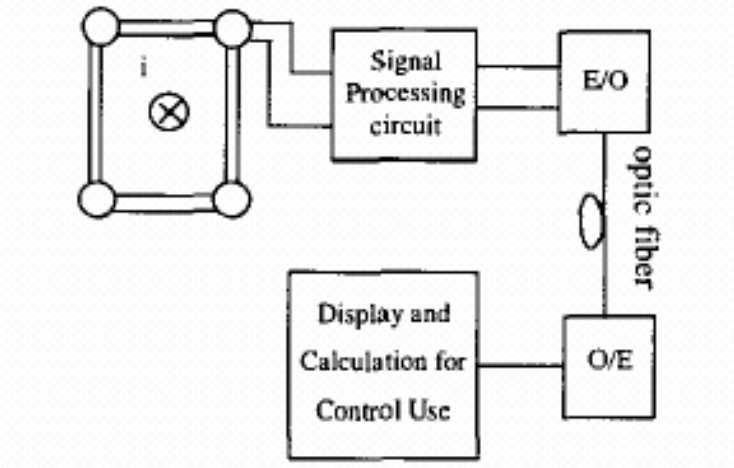

Figure 2.14 Structural diagram of optical current transformer [14]

Using ampere-turns, a heavy current generator tested the accuracy and the linearity of the optical transducer. The generated current range was from 0 to 15 kA. The error was less than 0.08%.

The temperature sensitivity was measured using a temperature-controlled box when the simulated current was a constant 3 kA. The results show that the error is negative at lower temperature and positive at the higher temperature. The expansion or shrinking of the winding at different temperature causes the error.

M. Willsch and T. Bosselmann, [15] presented studies for three magneto-optical current sensors (MOCT) that were placed inside a 120 MVA power generator. Tests were performed under the influence of high temperature, vibration, and current up to 120 kA [15]. The operating principle of the MOCTs can be seen in Figure 2.15.

Several types of tests were performed while a fast transient recorder monitored the three current sensors. The output signal versus the current characteristics of the MOCT is liner.

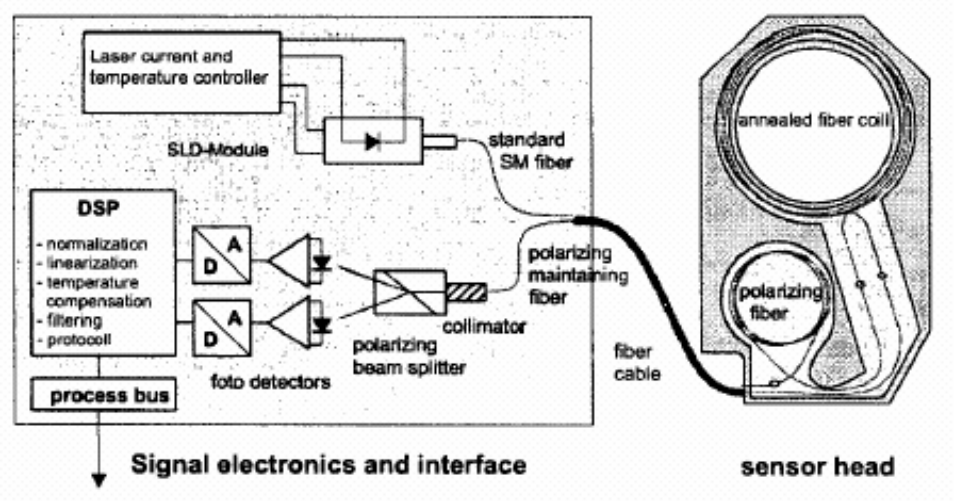

Figure 2.15 Principle set up of optical current sensor [15]

Figure 2.16 shows the transient short circuit current measured by a shunt. The conventional inductive CT was removed for this test.

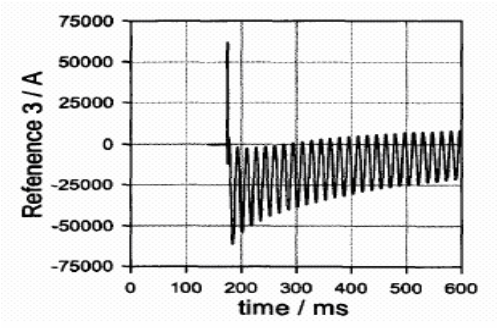

Figure 2.16 Short circuit-reference sensor (shunt) [15]

An electromagnetic spike can also be seen at the moment of switching. Figure 2.17 shows the corresponding signal of the optical sensor. The amplitude in the highest current region was reduced due to the non- linearity of the fiber coil sensor.

W.C Michie and others [16] presented a harmonic analysis of current waveforms using an optical current sensor. A computer interfaced with the Digital Signal Processing (DSP) unit in order to further process signals using LabView®. A variety of test signals were synthesized using a signal generator. The amplified signal supplied the coil surrounding the OCT. The 3-dB bandwidth of the electrical system was in the region of 1 kHz; therefore, signals above this frequency were significantly attenuated.

Comparing the OCT readings with the reference voltage signal could make an effective assessment of the OCT. A typical test waveform is shown in Figure 2.18.

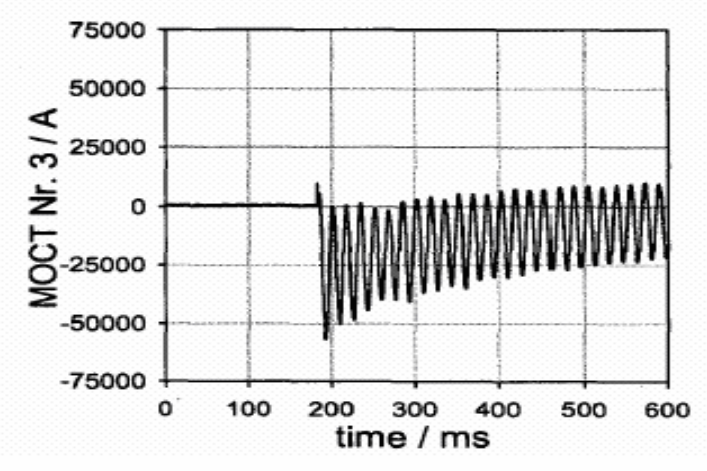

Figure 2.17 Short-circuit-optical sensor [15]

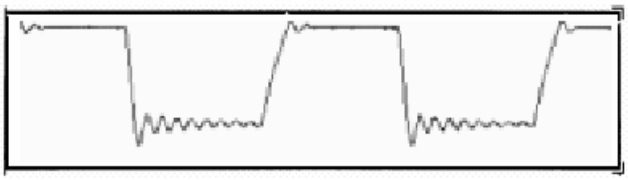

Figure 2.18 Typical 50 Hz test waveform [16]

The OCT output signal and reference voltage were analyzed by Fast Fourier Transform (FFT) to make the harmonic analysis. Although the RMS values of the signals were different, the harmonic content was identical. Figure 2.19 shows the percentage difference between the OCT reading and the voltage reference. The maximum difference between the signals was less than 0.25%.

The 50 Hz high-current measurement proved that the OCT response is linear and has a minimum resolvable bus bar current of less than 1 A.

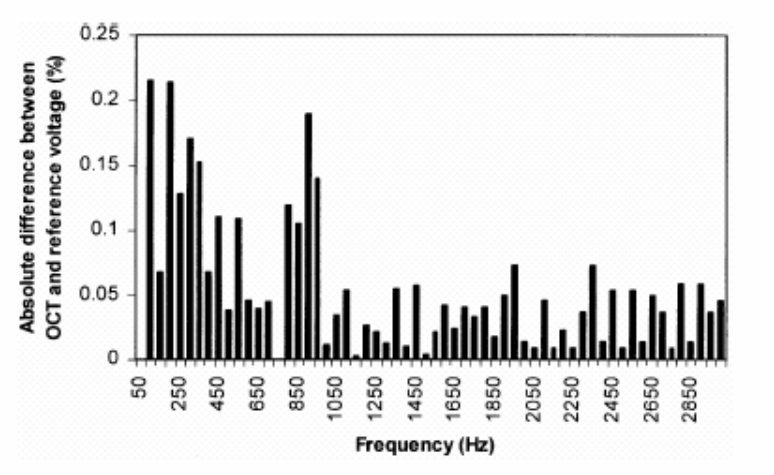

Figure 2.19 Percentage difference between reference signal and OCT reading up to 3 kHz [16]

Pedja Mihailov and others [17] studied a portable fiber-optic current sensor for power systems monitoring. The Fiber-Optic Current Sensor (FOCS) includes two major elements. The first element is an optical crystal (sensor) based on the Faraday Effect. The second element is a magnetic ring core that can open and encloses an electric conductor (Figure 2.20 and Figure 2.21). The magnetic field induced by the conductor in this magnetic circuit is concentrated in the gap containing the receptive crystal.

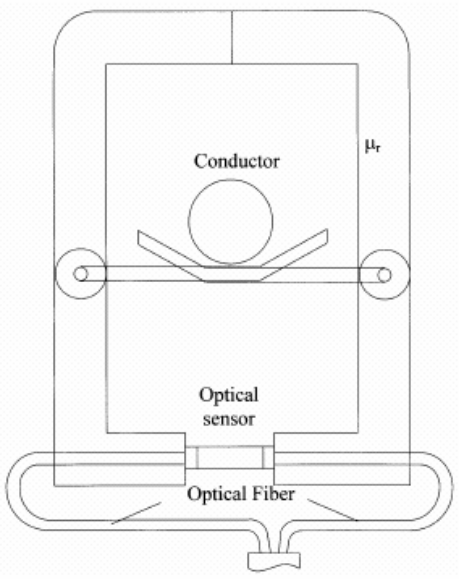

Figure 2.20 Sensing head drawing [17]

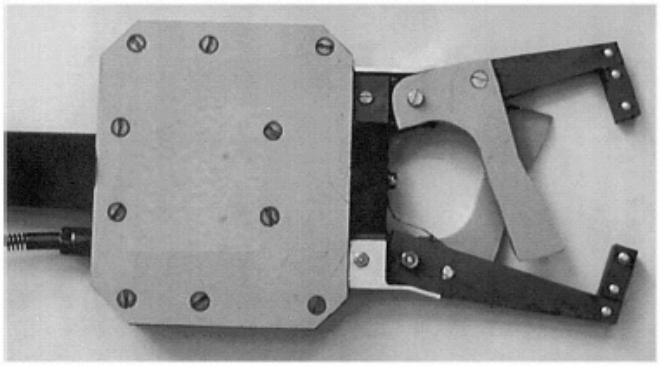

Figure 2.21 FOCS sensor head [17]

The current clamps enable measurements independently of the position of the conductor in the measurement area.

A polarized light beam is driven through the sensing crystal. The magnetic field changes the polarization angle. An electronic processing block monitors change with a signal processing unit and user interface.

In order to calibrate FOCS and to test its electrical performance, a series of experiments were conducted at the Institute of Electric Energy Systems and High Voltage Technology, University of Karlsruhe, Germany.

A 20-turn coil placed on the magnetic ring of the sensing head was used to generate excitation. A 50 Hz, 6 A sinusoidal current generated a total of 120 A of excitation. An ampere meter measured the magnitude of the current, and current was kept constant. The chamber was slowly heated from 0^{o} C to 45^{o} C, and the digital output of FOCS was monitored and recorded.

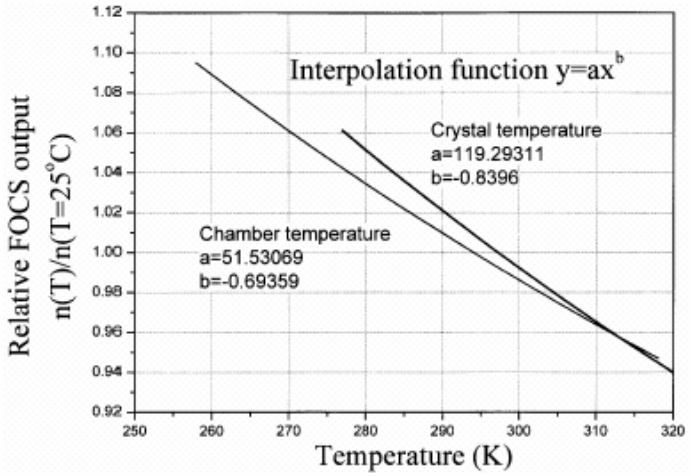

Figure 2.22 Relative FOCS output as a function of temperature [17]

Figure 2.22 shows FOCS output as a function of temperature, with a constant excitation current. Figure 2.22 shows two curves, one having chamber temperature and the other crystal temperature as independent variables. The figure shows that the temperature affects the accuracy of the FOCS.

2.2.2 NxtPhase Company's Publications

NxtPhase, one of the manufacturers of optical instrument transformers, published several papers describing the company-developed OCTs and OPTs. They tested the units extensively and installed several units in substations.

J.D.P Hrabliuk [18] studied interfacing of optical current sensors with the existing meters and relays in a substation. Interfacing optical current sensors with conventional meters and relays requires a new approach. The magnetic CTs, rated outputs are either 1 A or 5 A for both metering and protection. These relatively high current output signals are easy to obtain from "iron core" CTs, but difficult and expensive to produce using amplifiers. The optical CT output is an inherently digital signal. This digital signal is converted to an analog voltage signal and to analog current signal. The NxtPhase-produced OCTs are following the IEC standard (6044-8).
The device has three types of outputs:

- digital
- low-energy-analog (LEA) (e.g., 4 V represents rated current)
- high-energy-analog (HEA) (e.g., 1 A represents rated current).

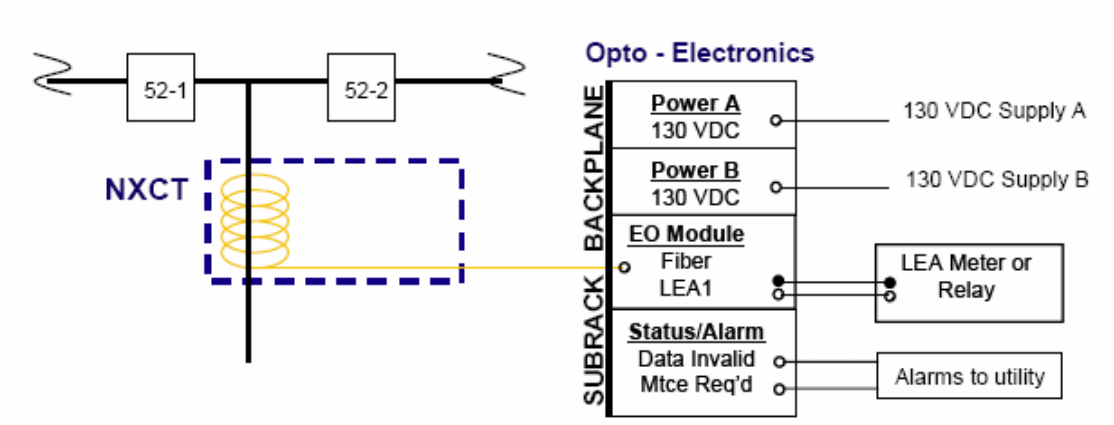

Figure 2.23 Optical current sensor with low energy analog (LEA) output to analog meter or relay. [18]

It is possible to obtain different output voltage ranges of low energy analog output from the electro-optics for the user's requirements. For metering applications, the output can be 2 V_{RMS} or 4 V_{RMS} nominal for the rated primary current. For protection applications, rated current is equal to a 200 mV_{RMS} signal, and the maximum short circuit current is 40 times the rated current, represented by 11.3 kV peak voltages.

Figure 2.23 shows a low-energy analog (LEA) signal generation concept for either metering or relaying.

High-energy analog (HEA) outputs will allow use of optical sensors in substations. A power amplifier allows the connection of an optical CT in parallel with a conventional CT. With this capability, an optical sensor can sum signals at a node.

NxtPhase optical current transducer output has an inherent noise that can affect the sensitivity of both meters and relays. These incorrect readings appear at low current levels, meaning 100 A. One effective method of reducing the signal-to-noise ratio is wrapping the conductor with multiple turns of fiber. This method increases the sensitivity of the sensor and reduces noise to an insignificant level.

G. Nicholson [19] provided a structure for the development of a reliability program for the OCTs. Military standards and handbooks are used to describe the planning methods and implementation techniques in this study. The Fiber Optic Gyroscope sensor, a gyroscope sensor designed for Aerospace and Space applications, forms the NxtPhase current sensor's basis. Due to the importance of dependability, reliability, maintainability and interchangeability must be implemented during the theoretical design.

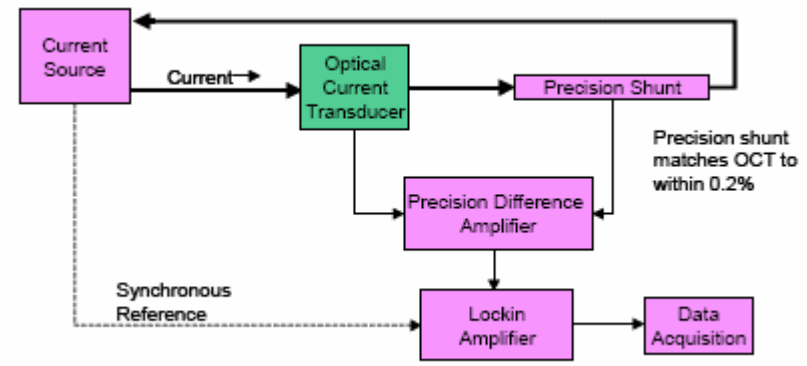

Figure 2.24 Low energy analog (LEA) metrology setup, applicable for < 100 amp turns [5]

Blake [5] studied the fiber optic current sensor calibration technique. The dynamic range for this study is ~1 amp to 3.6 kA. The optical sensor must have better than 0.2 % accuracy. The aim of the calibration is to prove this accuracy. Since the OCT has 3 different outputs, all three output must be calibrated. The OCT accuracy depends on the current level. Generally at low current the accuracy is decreasing. Consequently the calibration was performed in two levels: Low current levels (<100 A) and high current levels (100 to 3600 A). Each output (LEA and HEA) are calibrated with this two levels. Figure 2.24 shows the metrology setup for calibration of the OCT at low currents.

J.D.P Hrabliuk [3] studied CT saturation. Due to the magnetic core, conventional current transformers have saturation, which affects the secondary side output signal that is connected to meters and relays. On the other hand, in an optical current sensor there is no

saturation because it does not have an iron core. However, the distortion of signals can be a problem during the fault. The current changes rapidly and it affects the linearity of the signal. This is compensated for by the use of electronics. This paper discusses the characteristics of optical current sensors, and presents the compensation technique for non-linearity of the signal. Figure 2.25 below shows an example of a CT saturated output signal with a plot of the actual current.

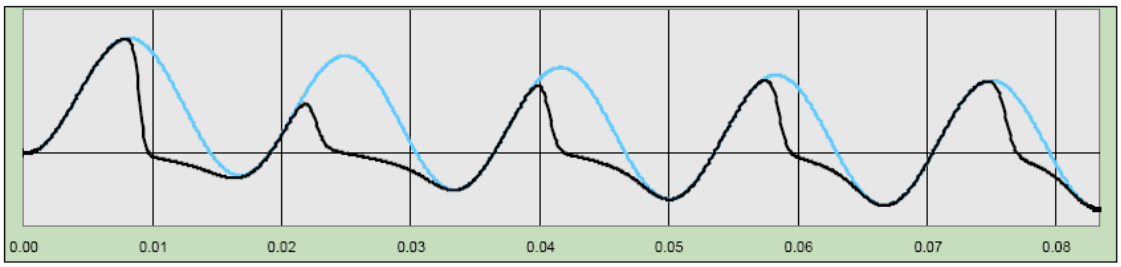

Figure 2.25 Saturated and non-saturated CT secondary output – conventional instrument transformer [3]

Farnoosh Rahmatian and Patrick P. Chavez [20] described the 550 kV class three-phase combined optical voltage and current transducer (NXVCT). The operation principle of this transformer is the same as previously described before in NxtPhase papers. Dielectric performance of this transformer was tested in HV laboratory. IEC 60044-7, 60044-8, IEEE C57.13, IEEE C37.92 standards were used to test the transformer.

The effect of temperature and vibration on the accuracy of the combined optical VT and CT was tested. The results of this temperature study results show that the device meets the accuracy requirements of IEC 0.1% class voltage transformers when the temperature is in the range of – 40 ^{o}C to + 60 ^{o}C. The device also maintains 0.1% class accuracy when subjected to vibration. This study was performed with a reduced voltage of 35 kV, and the current was varied between 3 A and 2250 A.

J.N Blake and A.H. Rose [21] tested an OCT and OPT with a Landis-Gyr class 2 MAXsys 2510 power meter.

The thermal rating of the OCT was tested using 63 kA for a few cycles. The mechanical integrity of the CT was tested using 171 kA peak dynamic current.

The accuracy of the CT was tested using a calibrated NIST traceable active three-winding wire wound CT made by JAMB Industries. The applied current was 0.01% to 150% of the CT rated current.

The metering performance of the optical system was tested using an OCT and OPT which supplied a Landis-Gyr class 2 MAXsys 2510 power meter.

The current was varied between was 0.01% to 150% of the CT rated current and the voltage was kept constant.

Figure 2.26 shows the NXCT and power meter error versus rated current test results. The results show that the NXCT performance is better than the IEC or IEEE standard requirements. For rated currents the accuracy is less than 0.1 %. The high accuracy even at currents below 1% of rated (below energy meters' rating) is partially due to the white noise and dithering of the optical CT, allowing the meter to be more accurate by exercising more significant bits of its input analog-to-digital converter. This is an actual benefit of white noise.

A mechanical test was also performed and the performance of the CT was not affected.

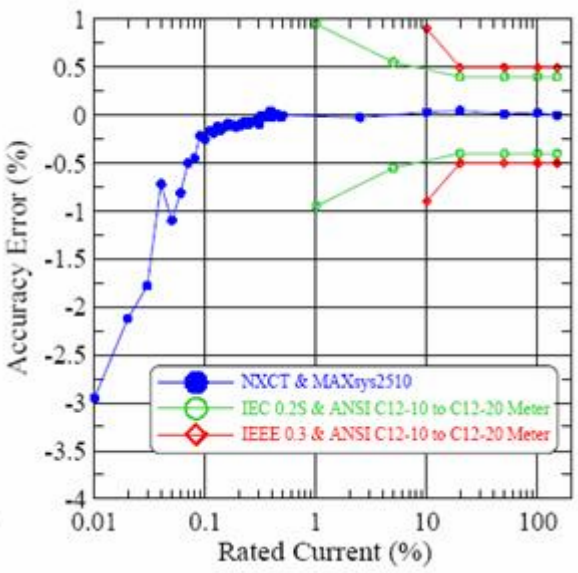

Figure 2.26 NXCT and Maxsys 2510 power meter accuracy error versus rated current (100% = 1 A secondary) [21]

2.3 Literature Review of Optical Voltage Transformers

In previous chapters, optical current transformers based on the Faraday Effect have been examined. In this chapter, optical potential transformers based on the Pockels effect are explained and discussed.

The **Pockels effect** is the electrical field-produced birefringence of polarized lights in crystals that lack inversion symmetry, such as lithium niobate or gallium arsenide. The electrical field changes the crystal's refraction index, which results in the splitting of the polarized light into two polarized light beams. Figure 2.27 illustrates the phenomena.

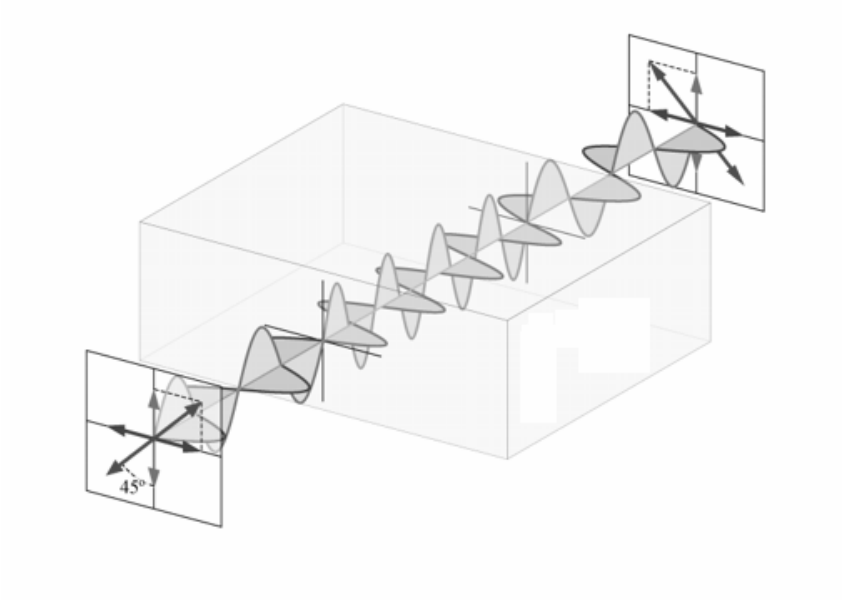

Figure 2.27 Illustration of the Pockels effect (half-wave plate) [41]

Linearly polarized light entering a crystal is split into two waves, parallel (shown as green) and perpendicular (blue) to the optical axis of the crystal. The parallel wave propagates slightly slower than the perpendicular one. In this case the length of the crystal is half the length of the wave. Consequently, at the far side of the crystal (plate), the parallel wave is exactly half of a wavelength delayed relative to the perpendicular wave. The combination of the two waves (red) results an orthogonally polarized wave compared to its entrance state. Figure 2.27 shows a half-wave plate [41]

Depending on the wave-length different phase shifts can be achieved. The electrical field varies the amplitude of the two waves and generates a phase shift depending on the field.

The birefringence is proportional with the electric field intensity. The Pockels effect is similar to the Kerr effect observed mainly in liquids. The difference is that the birefringence is proportional to the electric field in the case of Pockels effect, and it is quadratic in case of the Kerr effect. Friedrich Carl Alwin Pockels discovered this effect in 1893 [41].

Many publications deal with the development of a Pockels effect-based optical sensor. Most of them are focused on crystal sensor development and the material aspect of crystals, as well as the problem of the temperature sensitivity of these crystals. This literature review summarizes the power system applications of the Pockels effect and discusses Nxtphase Company publications related to the optical voltage transformers. Nxtphase supplied an optical PT for this project.

2.3.1 General Literature Review

In 1986, T.W. Cease, Judy G. Driggans and Scott J. Weikel [22] developed an optical voltage sensor using the current sensing method. This current sensing method has been used before to develop a magneto-optic current transducer (MOCT) for SCADA and protection systems in ref [23]. The tests of this MOCT proved that it is stable, reliable, and accurate. The main difficulty with using this current transformer for the voltage-sensing was that the MOCT is sensitive only to magnetic fields, not electric fields. The solution to this problem is to measure a current that is proportional to the voltage to be measured. This yields an optical sensor, which provides the benefits of optical sensing. The designed magneto-optic voltage transducer can be seen in Figure 2.28. The current flowing through the series-connected capacitors is proportional with the voltage. The MOCT measures this current; consequently, the output of the MOCT is proportional to with the voltage.

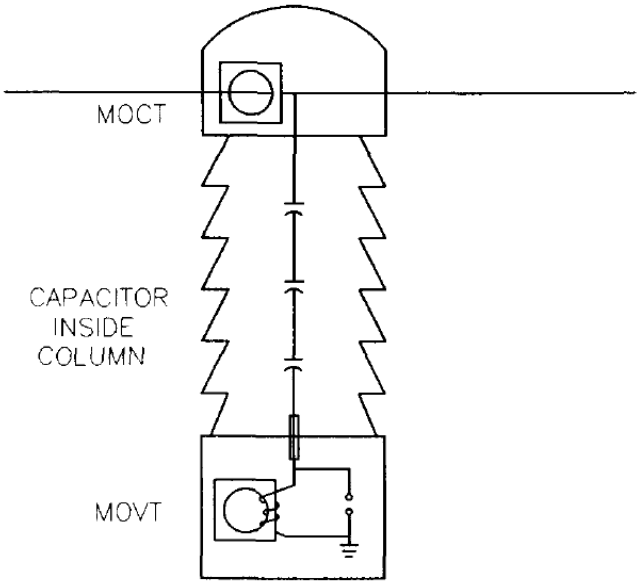

Figure 2.28 MOCT based Optical PT [22]

The paper describes the different tests performed on the new device. The most important is the comparison of the accuracy of the new device with a magnetic PT. The result shows less than 0.8% deviation.

K. Bohnert, P. Gabus, and H. Brändle [24] of ABB in Switzerland developed an optical current and voltage sensors for high-voltage substations. The electro-optic voltage transducer (EOVT) utilizes the Pockels effect. The full line-to-neutral voltage is applied on a BGO crystal (Bi4Ge3O12), and the light beam is used to measure the voltage. An additional temperature sensor was used to compensate for the temperature dependence of the Pockels effect. Figure 2.29 shows the combined voltage and current sensor.

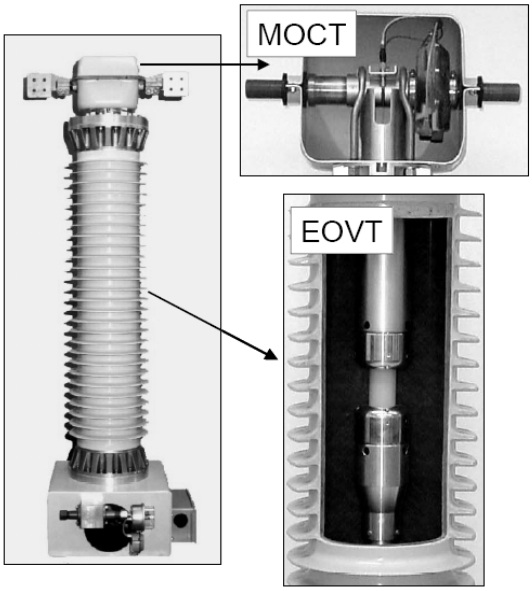

Figure 2.29 Current and voltage transducers [24]

The insulator supporting the EOVT is filled with a soft polyurethane resin instead of the usual SF_6 gas.

Valery N. Filippov, Andrey N. Starodumov and others [25] proposed a novel design for optical voltage sensor based on the $Bi_{12}TiO_{20}$ crystal. As a phase-retarding element, a glass back-reflecting prism is used instead of quarter-wave plate. The main advantage to using this method is that no additional temperature control channel is needed. This study focused on the investigation of temperature effects on optical sensors, and attempts minimize this effect by utilizing different techniques.

In 1995, Lars Hofmann Christensen [26] designed a prototype 132-150 kV optical voltage transformer (OVT). This transformer is based on Pockels effect in $Bi_4Ge_3O_{12}$ and it was designed without using any capacitor divider. Two electrodes were used to create the electric field. This passive OVT does not require any power supply to operate. OVT has only 25 components, including the optical modulator. Temperature dependency and voltage output accuracy have been tested. The ratio of transformer can be adjusted by changing the shape of one of the electrodes.

Peter Bauerschmidt and Reinhard Lerch [27] proposed an optical voltage sensor based on a quartz resonator. This transformer has frequency-modulated signal transmission instead of intensity-modulated transmission. A quartz resonator has been used as a voltage/frequency (V/f) converter, which converts electrical voltage or electric field strength into a proportional frequency shift. The Pockels effect-based resonator cannot withstand high voltage. A capacitive voltage divider has been used to reduce the effects of voltage on the resonator. The block diagram of the optical voltage transformer can be seen in Figure 2.30.

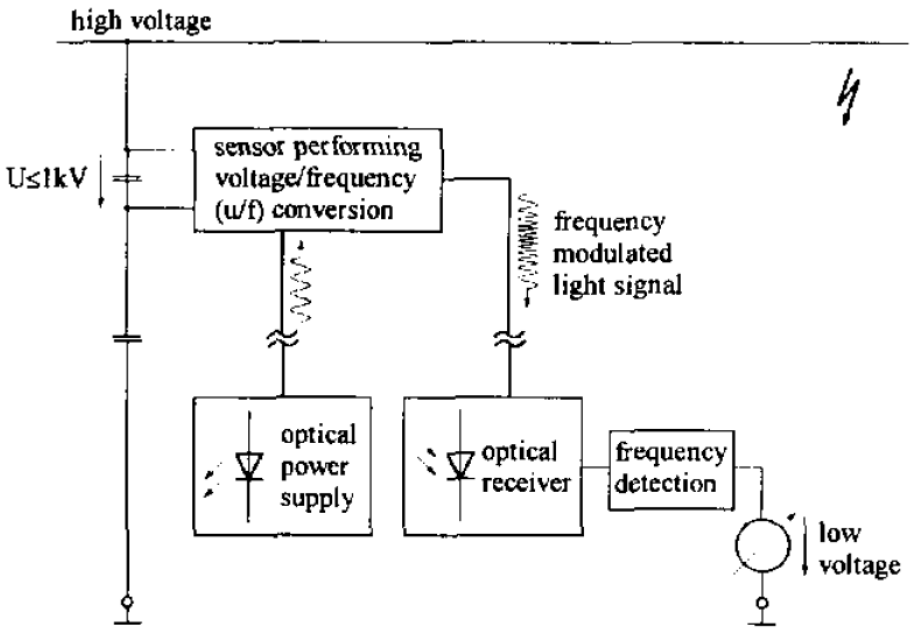

Figure 2.30 Block diagram of optical voltage transformer [27]

Josemir Coelho Santos, M. Cengiz Taplamacioglu, and Kunihiko Hidaka [28] developed a new high-voltage measurement technique for up to 400 kV of voltage and 0 to 30 MHz wide bandwidth. A prototype of the transformer uses Pockels crystals, super luminescent diode, and a special optical fiber link. AC and DC voltage tests, impulse voltage tests, and step voltage tests were performed successfully on the prototype transformer.

In 2005, Changsheng Li and Xiang Cui [29] presented a new optical voltage and current sensor with an electrically-switchable quarter wave-plate. This method was used to reduce the difficulties with the multiple light paths, which are used in the combined voltage and current sensing system. $Bi_4Ge_3O_{12}$ (BGO) crystal was used as a sensor. The paper describes the principles of system operation principles, which is a new application of polarization multiplexing technology for the measurement of multiple variables. The presented experimental results proved the feasibility of the proposed combined optical current and voltage sensor.

K.Kurosawa, S.Yoshida, E.Mori, G.Takahashi, and S.Saito [30] developed and tested an optical voltage transformer for DC voltage measurement. The authors have already developed optical voltage instrument transformers for AC voltage measurement in gas insulated switchgears. Pockels effect is not suitable for DC measurement. The authors developed a method which overcomes these problems. The developed DC voltage measurement system has been described, and a series of tests that examined ratio error and temperature characteristics have been performed. Figure 2.31 shows the schematic diagram of the optical DC measuring.

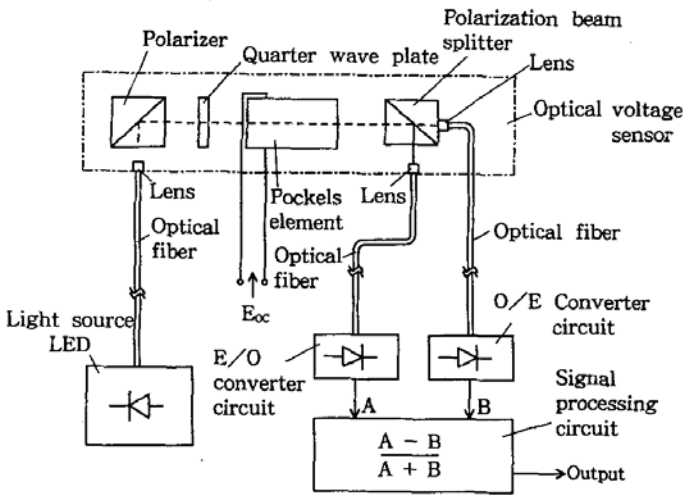

Figure 2.31 Schematic diagram of an optical DC voltage measuring system [30]

Peng-Gang Zhang and Irvine-Halliday [31] described a fiber-optic based high-voltage sensor that which uses the Pockels effect. A capacitive voltage divider supplies the sensor head with reduced voltage. The sensor uses ($Bi_{12}SiO_{20}$) crystals to generate a light signal proportional with the voltage. Fiber-optic cable transmits the sensor-generated signal to the ground level, where photodiodes convert the light signal to an electric signal. The paper describes the operation in detail, and presents test results proving the feasibility of the presented method.

2.3.2 NxtPhase Company's Publications

Farnoosh Rahmatian, Patrick P. Chavez, and Nicolas A. F. Jaeger [32] described the design and testing of 138 kV and 345 kV optical voltage transducers (OVTs). These transformers are suitable for both metering and protection applications in power systems, and they do not require special insulation. Pockels effect is used for the voltage measurement. To use the Pockels effect electric field sensors efficiently, a quadrature method has been applied to obtain voltage from electric field measurements. This method is used to define the needed number of sensors, as well as their positions. The stray field-caused errors are minimized to acceptable levels by a novel shielding technique and the multi-sensor quadrature method. The high-voltage-produced electric field is measured by three miniature optical field sensors placed in side the column.

One 138 kV OVT and one 345 kV OVT were constructed and tested [32]. An opto-electronic chassis is connected to the sensors through fiber-optic cables. The signal processing unit is used to calculate the voltage. Accuracy of the OVTs are tested according to the IEC 60044-2 (1997) and IEEE C57.13-1993 standards. The developed OVT units meet the 0.2 class (IEC) and the 0.3 class (IEEE) revenue metering requirements.

It is known that OVTs have 40 kHz bandwidth, but it is tested only for 3 kHz due to the difficulties of generating high-voltage high-frequency signals. A standard capacitive divider and a step-up power transformer were used as a harmonic source to test the bandwidth. Table 2.1 shows the test results.

Table 2.2 Measurement of harmonic content [32]

Harmonic No.	Reference (% of fundamental)	OVT (% of fundamental)
1 (fundamental)	100	100
2	0.05	0.03
3	4.31	4.37
4	0.02	0.02
5	2.75	2.76
6	0.21	0.21
7	0.96	0.96
8	0.04	0.04
9	0.51	0.53
10	0.03	0.03
11	0.16	0.17
12	0.01	0.01
13	0.13	0.13
14	0.01	0.01
15	0.04	0.04

To test the accuracy of transformers under severe contamination, fog pollution tests were conducted. The pollution test proved that the pollution does not affect the accuracy.

Insulation performances of the OVTs were tested, and a 650 kV peak lightning impulse test as well as 750 kV peak chopped impulse test were applied to the 138 kV class OVTs. A 345 kV OVT was also tested with a switching impulse under wet conditions. Partial discharge tests were also performed on both OVTs. All units performed satisfactorily under tests.

Rahmatian, Patrick P. Chavez, and Nicolas A. F. Jaeger [33] reported on an early design of a 230 kV optical voltage transducer using a similar design method that was described in ref [32]. In addition to the study in ref [32], the quadrature method is tested for different situations and conditions. It was found that three sensors are able to accurately measure the voltage, and it was used in 230 kV OVT. N_2 gas was used for insulation, and the OVT weight is around 220 kg. The transformer ratio is 70,000:1 V where the 140 kV corresponds to 2 V. Lightning impulse testing, wet testing, power-frequency resistance testing, partial discharge testing, chopped impulse testing, mechanical testing, and linearity testing were conducted for three transformers. The accuracy of the transformers met with the standards, and each transformer has a 0.95 degree phase delay due to signal

processing. These three OVTs were installed as a three-phase voltage measurement system at BC's Ingledow substation in Surrey, BC, Canada.

The accuracy of optical voltage transducers under pollution and other field distributions was tested by Farnoosh Rahmatian, P. Chavez, and Nicolas A. F. Jaeger [34]. The operation principle of this transformer is the same as the transformer design described in ref [32]. It is known that the outside perturbations can affect the electric field distribution inside an OVT. To avoid any impact on accuracy, resistive shielding has been used in NXVTs. In this study, a series of tests were conducted to test the performance of the shielding. Two OVTs were placed very close to each other. The sensing head of one of the OVTs was grounded, and the other OVT was energized with 50 kV. This situation represents the worst-case scenario in a substation. The output voltage of the grounded transformer was zero. It was observed that the neighboring 50 kV-produced electric field did not affect the grounded transformer output and accuracy.

Moisture on polluted insulators can also affect the electric field distribution. To simulate various dry-banding conditions, aluminum foil was used to simulate a low-resistance pollution layer for different locations of the insulator. Table 2.2 shows the location of the aluminum foil in the OVT, and the percentage ratio errors. In all these extreme cases the error is less than 0.2%, which meets with the standards.

Table 2.3 Accuracy measurement under various drybanding (DB) [34]

Perturbation Type	**Ratio Error (%)**
Middle DB	0.18
Middle DB, one side	0.11
Top DB	0.12
Top DB, one side	0.13
Bottom DB	0.12
Bottom DB, one side	0.10
Middle wet band	-0.09
Top DB on one side and bottom DB on the other side	-0.08

The bandwidth of the NXVT optical voltage transformer is about 40 kHz where the conventional voltage transformer has a bandwidth of 1.5 kHz. The bandwidth of the transformer was tested as in ref [32] by using a step up transformer and a standard capacitive divider. Results show that OVT output and the reference divider voltage match almost perfectly.

F. Rahmatian, D. Romalo, and others [35] also studied the effect of electrical field distribution on an older version of the OVT and its effects. To simulate the neighboring electric fields, a grounded metallic plane was used to disturb the electric field close to the NXVT. The OVT was energized to 170 kV, which is 120% of rated voltage and the introduced error was less than 1% in this extreme case.

The field distribution is also affected by rain and water flow. Wet-without-water flow and wet-with-water flow conditions were tested, and the introduced error was again less than 1% on this early prototype OVT.

Farnoosh Rahmatian, P. Chavez, and Nicolas A. F. Jaeger [36] tested the 138 kV OVT under severe dynamic field disturbances, including salt-clay pollution. The dielectric performance of voltage sensors was also verified by high-voltage dielectric tests. The tests included a lightning impulse test, chopped impulse tests and a partial discharge test. The voltage sensors are placed in a hollow-core composite insulator filled with low-pressure dry nitrogen. In the earliest studies, the affect of melting ice was investigated in this paper. The results were similar to the previous studies. The linearity and accuracy of the OVT is not affected by pollution and melting ice.

2.4 Market Survey of Optical Instrument Transformers

The companies manufacturing optical (and some other non-conventional) current and voltage transformers were identified using a web-based search, and the descriptions of products were obtained. This provides valuable information on the status of optical instrument transformer applications in the present world. The information provided is directly taken from the websites and other marketing material without any judgments or verification on the correctness of this information. Especially, cost and feature performance comments in this section are as claimed by the manufactures and do not represent the educated option on this report.

The products along with their manufacturers are listed as follows:

2.4.1 Digital Optical Instrument Transducers (ABB)

(ABB) Instrument Transformers

Source of information: www.abb.com

ABB developed optical voltage and optical current transformers as well as a combined unit for 72 kV – 800 kV transmission system.

The Digital Optical Current Transducer (DOCT) contains a magnetic current transformer, which supplies a burden resistor. The voltage drop on this resistor is proportional to the primary current. This voltage drop is digitized and the signal is transported to ground-level through a fiber-optic cable. A polymer insulator supports the current transformer, which has a weight of 50 kg. The DOTC can be mounted directly on the bus. The photo of the device is shown in Figure 2.32.

The Digital Optical Voltage Transducer (DOVT), measures the secondary voltage of a capacitor voltage divider. The measured value is digitized and transmitted by optical fiber to the metering and protection units.

The combined unit contains both systems. The polymer insulator of the DOVT supports the head of DOCT. The optical fiber is integrated in the polymer insulator body. The

digital output from the combined unit can be used both for measuring and relay protection. The major advantages are lower installation and transport costs, and reduced space and inspection requirements.

Figure 2.32 Digital Optical Instrument Transducers

2.4.2 Magneto-Optic Current Transducer (MOCT)

(ABB) Instrument Transformers

Source of information: www.abb.com

The MOCT system uses light to accurately measure current on high-voltage systems. Its modal of working is almost similar to the DOCT. As in DOCT, a magnetic current transformer measures the primary current. The secondary current supplies a burden resistor. The voltage drop on this resistor is proportional to the primary current. This voltage drop is transported to the ground level through a fiber optic cable embedded in the supporting polymer isolator.

The MOCT has an accurate metering current range of 5 A to 2000 A using the same sensor and is suitable for outdoor application.. Metering accuracy exceeds class 0.2 per IEC 60044-1 over a wide metering range. For relaying applications, the system provides accurate waveform reproduction through 100 kA. The unit has significantly smaller size and lighter weight than oil or SF_6 insulated equipment.

2.4.3 Electro-Optic Voltage Transducer (EOVT)

(ABB) Instrument Transformers

Source of information: www.abb.com

This device consists of an optical sensor supplied by the total line to neutral voltage. A light signal is sent from the ground-level electronic control module through the sensor. The electronic module processes the returned light signal and produces an analog output proportional to the supply voltage. The optical sensor is placed in a SF_6 insulated composite bushing. The bushing is built with a fiberglass tube covered by silicon rubber sheds.

The nominal out put voltage is 120 V; the accuracy of the device is class 0.2 for metering. The EOVT is lighter and smaller than conventional oil-filled voltage transformers. The elimination of oil/paper insulation provides enhanced safety and reduced maintenance costs.

2.4.4 Fiber Optic Current Transducer (FOCT)

ABB Australia branch

Source of information: www.abb.com

The FOCT is the result of a development project led by ABB in co-operation with TransGrid and the Australian Photonics Cooperative Research Centre based at the Australian Technology Park in Sydney.

The transducer measures the current produced by magnetic field generated by phase shift of a light beam. The obtained light signal is digitized and transmitted to the measuring or protection instruments.

The configuration of the sensor coil minimizes the interfering environmental effects of temperature and vibration. Because of the wide dynamic range of the FOCT, one transducer can be used for all applications - protection, control and metering. The device is compact, light and easily integrated with other high-voltage equipment.

The pre-commercial version of the FOCT was installed at a TransGrid substation in July 2001 for testing.

2.4.5 SEECO Current Sensor

Southern Electrical Equipment Company Inc.

Source of information: www.seecoswitch.com

The SEECO SENSE digital current and voltage sensor is used to generate current and voltage outputs in metering, relaying, and fault detection applications. It is light weight device due to composite insulator being used. Compared to conventional oil-filled transformers, SEECO SENSE units are extremely light-weight, with a compact size. Its

compact size facilities are used in stations or on pole structures where space or mounting applications are restricted.

SEECO SENSE units are available in current-only, voltage-only, and combination current and voltage configurations. Ratings range from 7.5 - 500 kV, with current ratings of 600, 1200, and 2000 amp, and fault ratings of 3000, 6000 and 10000 A.

For revenue metering, the accuracy of the current sensors exceed IEEE class 0.3% accuracy. The current sensors have broad dynamic metering ranges, and the device is perfectly linear down to 1% of rated current. The major technical data:

- CT is 600, 1200 and 200 A, +/- 1.5% accuracy. BIL 95 kV-1470 kV
- VT 7.5 - 500 kV (line to line), +/- 0.5%, BIL 95 - 1470 kV

Figure 2.33 shows the current and voltage sensors.

Current Sensor Voltage sensor

Figure 2.33 SEECO Current and Voltage Sensors

2.4.6 AREVA Instrument Transformers

AREVA T&D

Source of information: www.areva-td.com

AREVA T&D offers the following instrument transformers:

Current related instruments:
CTO (Current Transformer with Optical sensor)
BMO (Bus- or Breaker-Mounted Optical current sensor)
Voltage related instruments:
VTO (Voltage Transformer with Optical sensor)
Combined instruments:
CMO (Combined Measurement with Optical sensors)

Electronics & Interface:
CVCOM (Current & Voltage COM an electronic rack)

The Current Transformer with Optical sensor (CTO) measures the current of High Voltage Lines, used for both metering and protection applications.

Table 2.4 Technical Data

SUMMARY OF PERFORMANCE: CTO, BMO, VTO, CMO		
PRIMARY RATED VOLTAGE		100 kV to 800 kV other voltages : refer to factory
PRIMARY RATED CURRENT		40 A to 4000 A other currents : refer to factory
SECONDARY RATED CURRRENT	Amplified metering output Low level metering output Low level protection output Digital output	1 A ; 0.5 VA 4 V ; burden higher than 10 kOhms 150 mV ; burden higher than 10 Ohms IEC ; 60044.8
SECONDARY RATED VOLTAGE	Amplified metering output Low level metering output Low level protection output Digital output	69 V ; 0.5 VA 4 V ; burden higher than 10 kOhms 2 V ; burden higher than 10 kOhms IEC ; 60044.8
DYNAMIC AND ACCURACY	Metering current Protection current Metering voltage Protection voltage	IEC ; Class 0.2 IEC ; Class 5P20 IEC ; Class 0.2 IEC ; Class 3P
ENVIRONMENT	Operating temperature Outdoor equipment Indoor equipment	- 40°C ; + 40° C (Celsius degrees) - 40°F ; + 104°F (Fahrenheit degrees) - 25°C ; + 50° C (Celsius degrees) - 13°F ; + 122°F (Fahrenheit degrees)

The Figure 2.34 shows the system components.

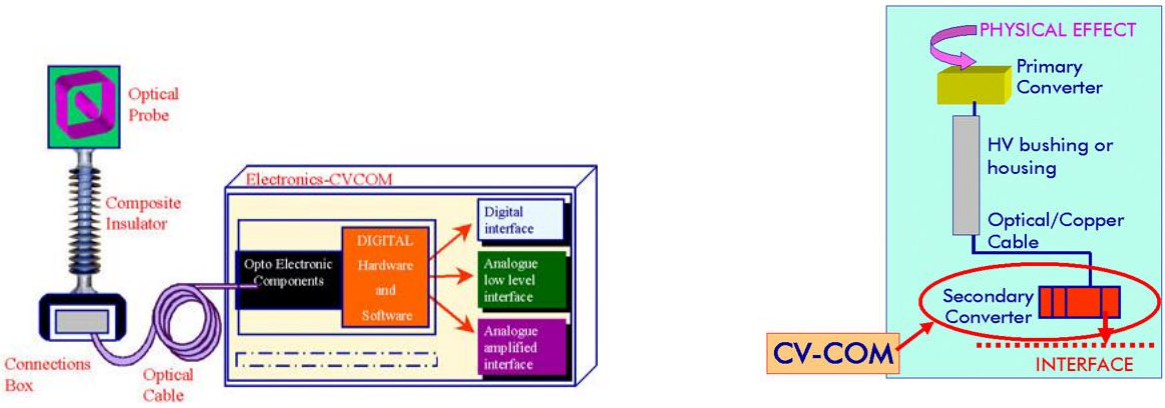

Figure 2.34 AREVA Instrument Transformer system components

The components of the CTO are:

Head with the primary optical sensor: In this device the Faraday polarization modulation is converted into a light intensity modulation with the use of two polarizes crossed at 45^{o}. It uses "ring glass" material, which is a solid element, drilled for the conductor pass, with machined and polished edges on the perimeter. The light is internally reflected in a closed loop around the measured conductor.

Composite insulator with embedded optical fibers. It holds the head and provides HV insulation.

Base, It includes junction box for fibers and optical cables connecting the unit to the electronic platform.

A modular electronic platform, (CVCOM): This unit processes the light and provides a signal proportional with the current

2.4.7 AIRAK Optical Current Transducer

AIRAK Inc.

Source of information: www.airak.com

Airak, Inc. offers low-cost and easy to install fiber-optic current and / or temperature sensor.

The sensor uses the Faraday Effect and measures the current induced magnetic field produced by light changes, which caused by the rotation of the plane of polarization. The system arrangement is shown on the Figure 2.35.

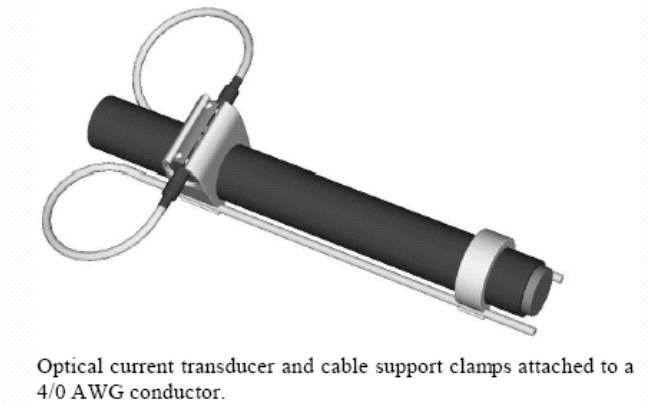

Optical current transducer and cable support clamps attached to a 4/0 AWG conductor.

Figure 2.35 Optical Current Transducer

This is a low-voltage device designed for monitoring load currents or the temperature of conductors in electrical distribution lines. It can be used for electrical distribution, automation, and for monitoring the current of actuators in avionic, land, and naval

vessels. The sensor can be used for monitoring emergency power (UPS) systems, high-power AC-DC converters, and high-power DC-AC converters.

The technical data of the offered current and temperature sensor is listed below.

Table 2.5 Optical Current Transducer Specifications

Dynamic Range	60 dB minimum
Frequency Response	5 Hz- 20 kHz Standard; Wider possible
Full-Scale Measurement Range	30-30,000 A
Voltage Isolation	Greater than 11,300 V_{pk-pk}
Absolute Error (w/out flux concentrator)	Less than +/- 3.5% f.s
Standard Error (w/out flux concentrator)	Less than +/- 1.0% f.s
Sensitivity/Resolution	Better than 0.01% f.s
Repeatability	Better than 0.1% f.s
Sensor Drift	Less than 2% / 1000 Hr
Temperature Range (uncompensated)	19^oC to 33^oC
Temperature Range (compensated)	-40^oC to 70^oC
Sensor Weight (w/out flux concentrator)	28 grams

2.4.8 NxtPhase T&D Optical Voltage and Current Transformers

NxtPhase T&D Corp.

Source of information: www.nxtphase.com

NxtPhase T&D Corp. offers optical voltage and current sensors for high-voltage applications. These products are available at up to 800 kV class, and are used in metering, protection, monitoring, and other applications in HV substations. A novel version of the fiber optic CT from NxtPhase is also provided with flexible wrap-around sensing head cable, which is extremely convenient for retrofit applications (installed without breaking the current carrying bus), high-current generation applications, and industrial DC and AC applications. Since some of NxtPhase products are reviewed in detail in this report, we do not cover any particular product from NxtPhase in this section.

2.4.9 Optically Powered Current Transformer

Photonic Power Systems, Inc.

Source of information: www.photonicpower.com

The company offers current sensors for Series Capacitor and Thyristor Controlled Series Capacitor installations (FACTS), and High-Voltage Direct Current Systems (HVDC). The sensors systems themselves are not optical, but communication and powering of the electronics in high-voltage area is done via optical fibers.

A low-voltage CT with a burden resistor produces a voltage signal proportional to the current. This signal is fed into the Optically Powered Data Link (OPDL), which converts

the voltage signal to light signal and transmits it to the ground through a fiber optic link. The measuring head is supported by composite insulators with embedded fibers. The fiber optic link is terminated at the ground level in the second OPDL unit. The second unit is located in the control building. It converts the light signal to analog signal which supplies the metering and protection units. The OPCT system use laser technology. The photograph of a unit is presented on the Figure 2.36.
The OPDL system has two major components:

a) High voltage unit located in the measuring head

b) Local unit, located in the substation control room or an existing control enclosure.

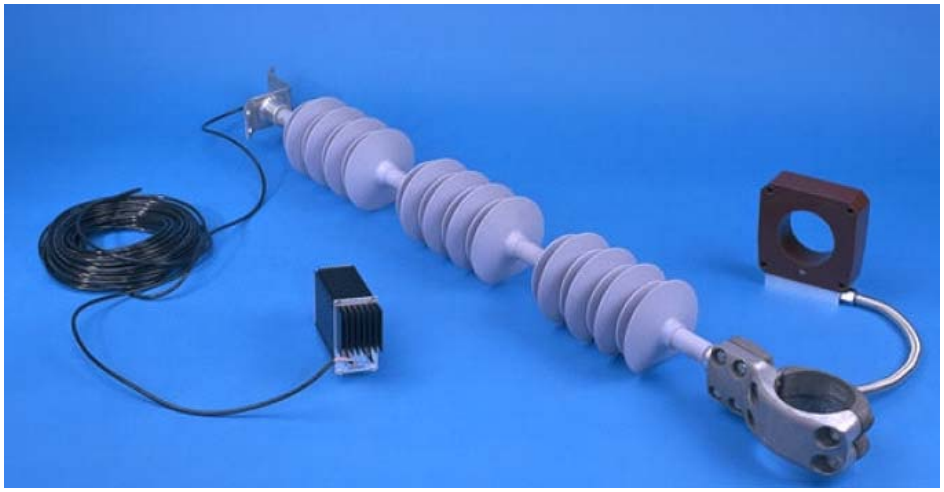

Figure 2.36 Optically-powered Current Transformer System

The local unit houses the laser with its associated laser driver and the data recovery circuitry. The laser can inject a maximum optical power of 1.5 Watts into the fiber link. A self-check function supervises all vital functions of the OPCT. An alarm is initiated long before the laser reaches the end of its lifetime, indicating necessary maintenance.

This unit can provide:

- a digital serial output,
- Voltage output +/- 10 Volts (full scale)
- Current loop of 1 Amp (nominal) @ maximum 20 or 40 VA.

Two optical fiber links (a power link and a data link) connect the OPDLs high-voltage unit to the local unit. The power link provides the electrical supply to the high-voltage unit. The power link is supplied by a laser and connected to a photovoltaic power converter at the high voltage side. The conversion efficiency is better than 40%. The data link is supplied by an A/D converter, which provides two A/D channels with a sampling rate of 40 kHz each, corresponding to a bandwidth of 15 kHz (250 Harmonics @ 60 Hz system). The high voltage unit is shielded against any EMI or RFI noise and converts the voltage drop across the CT burden resistor into digital signals.

The accuracy of the system is better than 1% for protection purposes at nominal value and the metering accuracy and exceeds Class 0.2 requirements.

The current transformer is a dry outdoor unit rated for 600 V (10 kV BIL). The burden resistor and an input protection filter are housed together with the remote circuitry in a shielded enclosure in order to provide immunity against EMI and RFI disturbance. The unit is mechanically attached to the conductor and a short, mechanically protected fiber link connects the unit to the signal column.

2.5 Conclusion of Literature and Market Survey

The literature and market survey shows that several manufacturers produce optical instrument transformers. However, the majority of the products have been experimental and used for testing in utility environments. Typically, except for revenue metering applications, few units of each product are installed in substations in parallel with conventional instrument transformers. The operation of the two systems is monitored and the compared. We can conclude that the optical instrument transformer is a viable product, though not a mature product today.

The literature and market review showed that the optical current transformers are divided into two categories:

- Magneto-optical units, which use a traditional magnetic CT and transmit the CT output to the ground through an optical link
- All-optical units, which have all-dielectric construction and use the Faraday Effect to measure the current.

Mostly the all-optical units were considered in this study. Several turns of special proprietary optical fiber were wound around the current carrying bus bar. The current-generated magnetic field changes the polarization angle of the light passing through the fiber-optic. The change of the polarization angel is proportional with the current. An opto-electronic circuit measures the change of the polarization angle.

The optical potential or voltage transformers operation is mostly based on the Pockels effect. The sensing element can be BGO crystal (Bi4Ge3O12) or other electro-optic materials. These crystals are supplied by the full voltage or by reduced voltage. Many manufacturers use capacitive voltage dividers to generate the reduced voltage. The electric field produces birefringence of the polarized light wave passing through the crystals. An electronic circuit converts the light waves to an electric signal proportional to with the voltage.

The major advantages of the optical instrument transformers are:

- Light-weight with a small footprint that reduces installation cost
- High dielectric strength due to all dielectric construction

- No saturation and wide range of operation
- High accuracy
- Relatively broad frequency band (60 Hz ~ 20 kHz)
- No need for SF_6 gas for insulation (in some OVTs, SF_6 is still used)

The emerging challenges are:

- Understanding of noise level and any possible impact on the application
- Temperature sensitivity if not compensated properly
- Electronics needed to convert the light signal to the analog signal
- Cost position in some cases (albeit a rapidly changing factor).

The literature presents large numbers of technical data, but only a few papers are dealing with the comparison of the optical to the magnetic system.

3 Task #2 Analysis of the Measurement and Protection System Operation

NxtPhase supplied an Optical CT and a combined Optical CT and PT for this project. Salt River Project donated a 69 kV magnetic CT and a 69 kV (line-to-line) magnetic PT to ASU. These units were used to compare the performance of the new optical system with the traditional magnetic system. The tests were performed in ASU's high voltage laboratory.

3.1 Study of Optical CT Operation

The objective of the study is to compare the performance of the NxtPhase Optical CT with a conventional CT donated by Salt River Project. The experimental work requires the building of a high-current generator as well as understanding of the operation of the NxtPhase OCT.

3.1.1 NxtPhase Optical Current Transformer

NxtPhase is one of the companies that manufacture Optical Current Transformers. The company provided a CT marked NXCT to ASU for these tests. The NXCT uses the Faraday Effect, but in a different architecture than the better-known polarimetric technique. The NXCT uses a fiber-optic current sensor that works on the principle that the magnetic field, rather than the rotation of a linearly polarized light wave, changes the velocities of circularly polarized light waves within a sensing fiber that is wounded around the current-carrying conductor. The current is measured via an interferometric technique, making the NXCT performance immune to vibration. The operation of the NxtPhase OCT is described in the manufacture's data sheet and reference [4], and reproduced here.

The optical circuit of the NXCT is shown in Figure 3.1. As can be seen from the figure, light from a Light source, mainly Light Emitting Diode (LED), enters into an optical fiber polarizer. In the polarizer, it is polarized and then splits into two orthogonally polarized light waves. These two orthogonally polarized light waves pass through a modulator and then travel down a polarization maintaining (PM) fiber to the sensing head. A fiber optic quarter-wave plate converts the two linear orthogonal waves into circular waves-right- and left-hand polarized light waves, respectively. Once converted into circular waves, these two waves then travel through the sensing fiber, which is wound an integral number of times around the current carrying conductor.

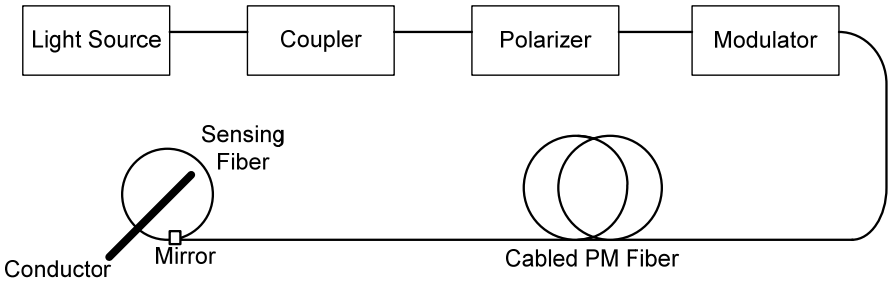

Figure 3.1 NXCT Optical Circuit [4]

The two waves travel at different speeds through the sensing fiber. The difference in speeds is proportional to the strength of the magnetic field aligned with the sensing fiber. After completing its journey in the sensing region, the two waves reflect off a mirror. The reflection causes a swapping or reversal of circular polarization of the two waves and the two waves now travel in the opposite direction with respect to the magnetic field. While traveling in the opposite direction, the two waves continue to maintain their velocity difference for the return trip through the sensing fiber.

During its return journey, once the light has retraced its way through the sensing region, the two waves again encounter the quarter-wave plate which converts them back to linear polarization states. This produces a change of states for the two linearly polarized lights. Now, the light that traveled outbound in the PM fiber as x-polarization returns in the y-polarization state, and vice-versa. According to the Figure 3.1, the path followed by the two waves during its entire journey can be pictorially depicted as follows:

Light Wave 1:

Forward Path:

X-Polarized outbound in PM Fiber > Right-hand Circular outbound in sensing fiber

Reverse Path:

Left-hand Circular inbound in sensing fiber > Y-Polarized inbound in PM Fiber

Light Wave 2:

Forward Path:

Y-Polarized outbound in PM Fiber > Left-hand Circular outbound in sensing fiber

Reverse Path:

Right-hand Circular inbound in sensing fiber > X-Polarized inbound in PM Fiber

Magnetic field on the sensing head is the only physical quantity that affects the time-of-flight difference between the two light waves. This is based on Faraday Effect. Thus, a measurement of the time-of-flight difference between the two waves yields an accurate measurement of the current flowing in the wire passing through the sensing head.

Figure 3.2 depicts the NXCT physically. As can be seen, NXCT is divided into three separable elements, the opto-electronics chassis, the fiber optic cabling, the sensor head and standoff. The opto-electronics chassis incorporates all the electronics as well as the light source and optical components up through the modulator. The opto-electronics chassis for a three-phase system, which includes the power supply, would be in the control room.

One interesting feature of the fiber current sensor is that the dynamic range of the sensor can be scaled to fit almost any application, simply by changing the number of fiber turns on the sensor head. Their first prototypes use four turns of sensing fiber, which allows the sensor to reliably detect currents over the range 100 mA to 100 kA. This range covers the vast majority of high voltage metering and relaying applications requirements.

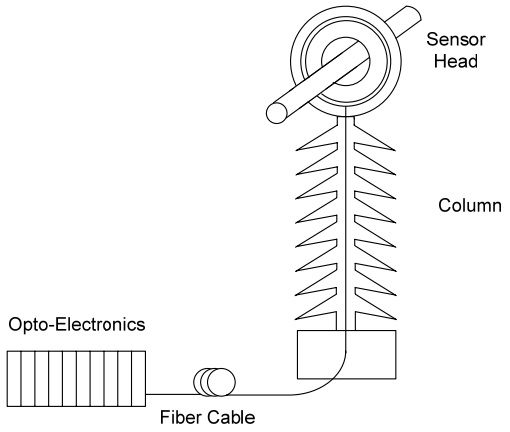

Figure 3.2 NXCT Optical Current Transducer [4]

3.1.2 Current Generator and Test Setup

ASU built test equipment in order to compare the operation of the optical and conventional magnetic current transformer. A current-generator, shown in Figure 3.3,

produces the high-current. The secondary coils of the three large magnetic current transformers are connected in parallel and supplied by a regulating transformer. An insulated conductor forms a short-circuited loop as the primary conductor.

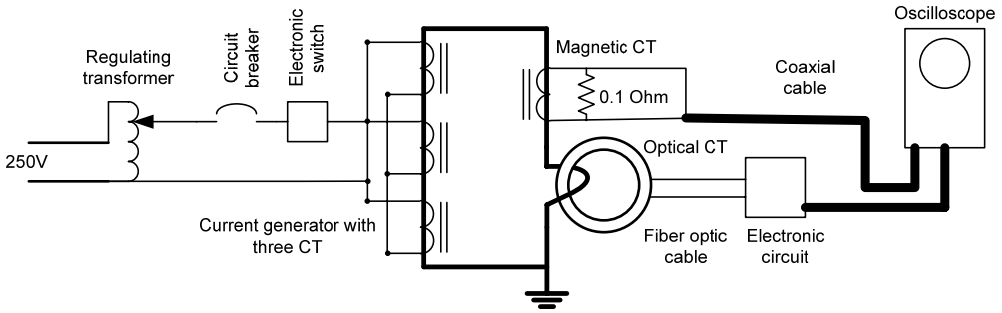

Figure 3.3 Experimental test setup connections diagram

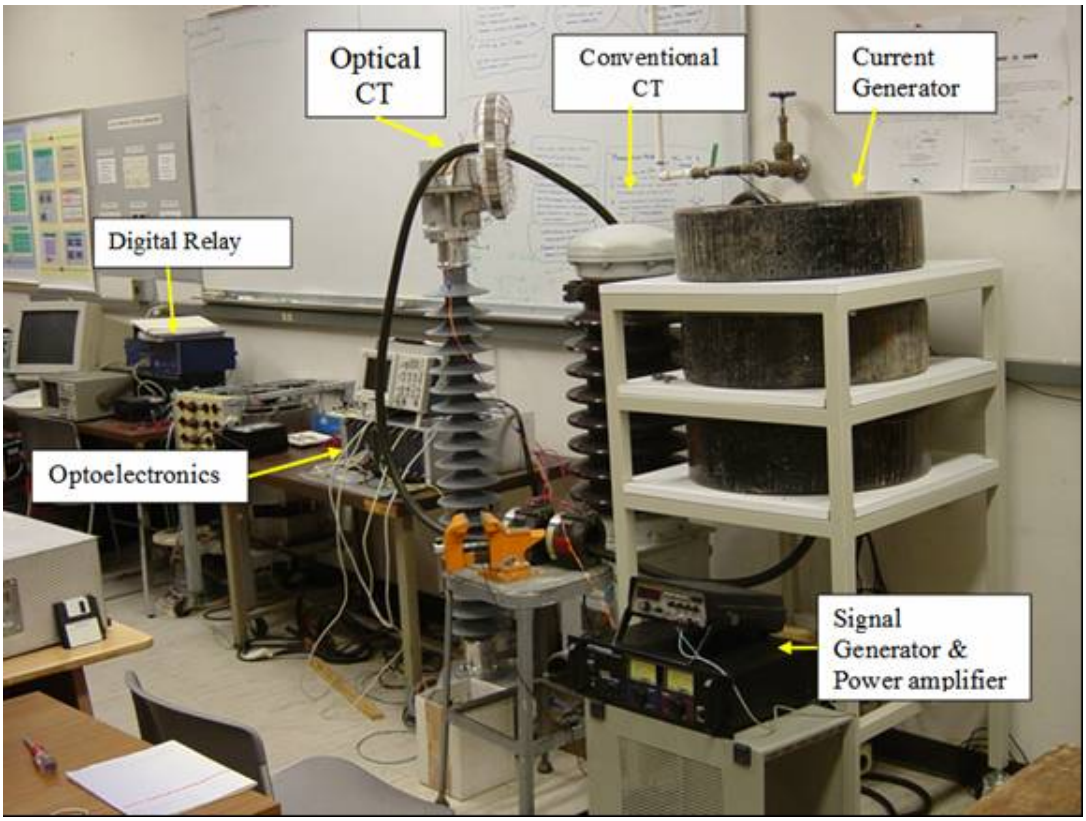

Figure 3.4 Experimental test setup

Optical and magnetic current transformers are supplied by this loop, as shown in Figure 3.4. The maximum current of the system without the load is 1200 A. Impedance of the magnetic current transformer that is being tested limits the current.

A mechanical switch is used to energize the system, and an electronic switch is used to switch on the system at a selected point on the voltage sine wave, such as zero voltage or maximum voltage. A block diagram of the electronic switch is shown in Figure 3.5 below. All tests are performed at room temperature.

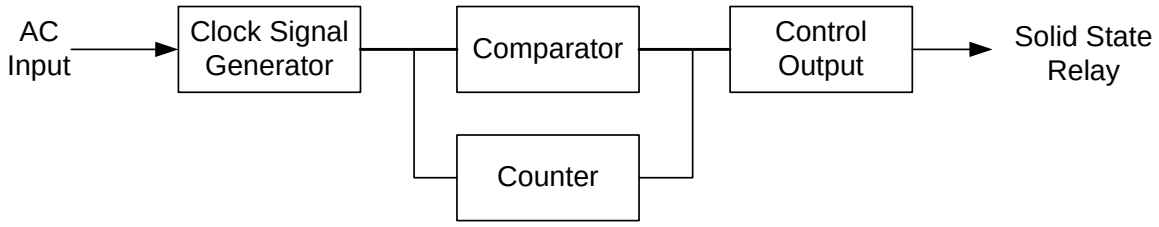

Figure 3.5 Electronic Switch Block Diagram

The current is measured by a conventional magnetic CT, donated by Salt River Project and an OCT supplied by NxtPhase.

The traditional CT is manufactured by General Electric Co. The CT specifications are:

- Voltage 69 kV, BIL 1000 kV
- Current 800 A / 400 A /5 A
- ASA Accuracy Classification 0.3 B-0.1, B-0.2, B-0.5, B-2 at 60 Cycles
- B- 0.1 class 2.5 VA, PF= 0.9, Z=0.1 Ω

Accuracy Classification 0.3 represents the percent of allowable error and B-0.1, B-0.2, B-0.5, and B-2 values represent burden in ohms for a 5 A rated output. The accuracy of metering depends on the burden. Table 3.1 and Table 3.2 show the standard burden and accuracy classes [37].

Table 3.1 ASA Accuracy Classes for Metering Current Transformers [37]

ACCURACY CLASS	LIMITS OF RATIO CORRECTION FACTOR AND TRANSFORMER COORRECTION FACTOR				Limits of Power Factor (Logging) of Metered power Load
	100% RATED CURRENT		10% RATED CURRENT		
	MIN	MAX	MIN	MAX	
1.2	0.988	1.012	0.976	1.024	0.6-1.0
0.6	0.994	1.006	0.988	1.012	0.6-1.0
0.3	0.997	1.003	0.994	1.006	0.6-1.0
0.5	0.995	1.005	0.995	1.005	0.6-1.0

Table 3.2 ASA Standard Burdens for Current Transformers at 60 Cycles [37]

Designation of Burden	Burden Characteristics		Secondary Burden at 60 Cycles and 5 Amperes Secondary Current		
	Resistance Ohms	Inductance Millihenry's	Impedance Ohms	Volt-amperes	power Factor
B-0.1	0.09	0.116	0.1	2.5	0.9
B-0.2	0.12	0.232	0.2	5	0.9
B-0.5	0.45	0.58	0.5	12.5	0.9
B-1	0.5	2.3	1	25	0.5
B-2	1	4.6	2	50	0.5
B-4	2	9.2	4	100	0.5
B-8	4	18.4	8	200	0.5

A 0.1 ohm calibrated resistor was connected as a load to a conventional current transformer, and a Tektronix TDS3052 Scope measured voltage across this resistor. The 0.1 ohm resistor corresponds to a burden of 0.1 ohm x 5 A x 5 A = 2.5 VA at full load, which is equal to the specified maximum value. For the first test series, the CT was set at 800 A / 5 A setting. This resulted in a scale of 1 V equivalent to 1600 A.

A current loop was threaded through the OCT to apply current as an input for OCT. The OCT output is an analog voltage signal. This analog signal was used as a scale of 1 V which is equivalent to 1000 A. This signal was produced by the LEA output of the OCT.

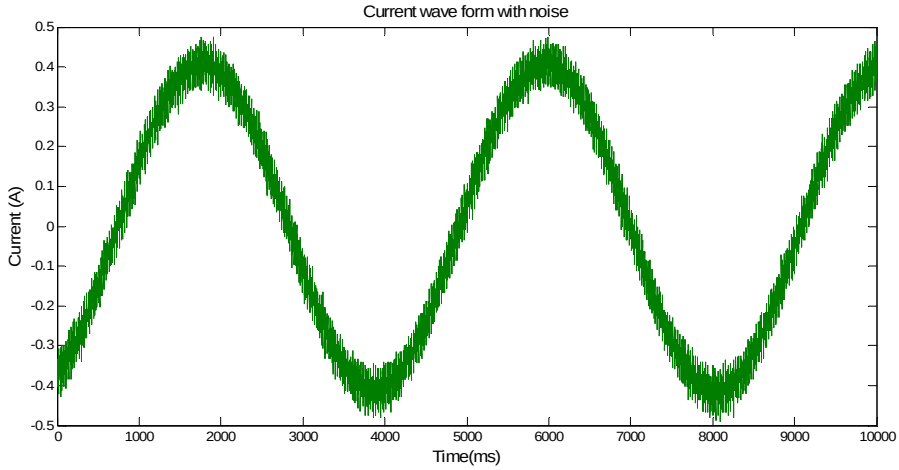

Figure 3.6 Sample Current waveform with noise

The preliminary test indicated that the OCT output voltage has ≈25% white noise at less then 5 A current as shown in Figure 3.6. The manufacturer specified noise level is 18% at the same low current level. All optical and/or electronic systems have some kind of inherent noise; however in this case, because the scope used for capturing signal was not floating, it was effectively grounding one side of the LEA, and injecting differential noise

into the measurement. Using a simple differential amplifier for isolating (buffering) the signal reduced the noise (by eliminating most of the noise injected by the scope). OCT output voltage is applied as an input for the differential amplifier, and the output voltage of the amplifier is connected to the input of the digital scope. The typical output voltage of the system is shown in Figure 3.7. It can be seen that the white noise is reduced significantly.

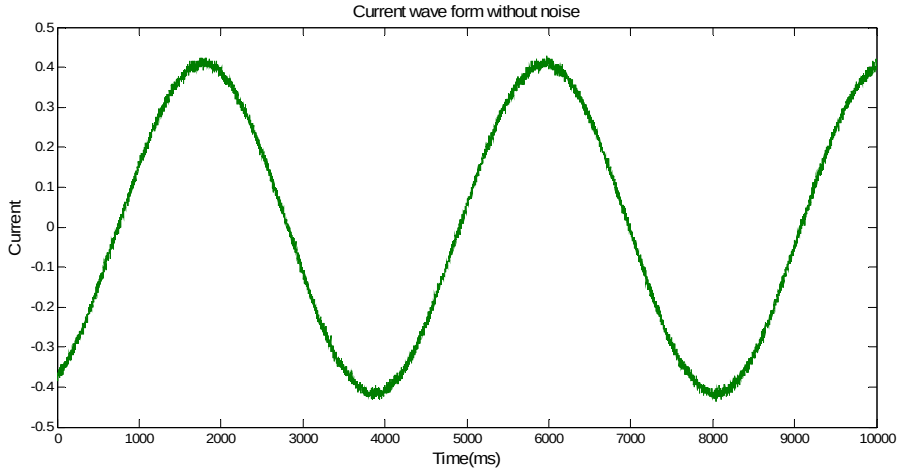

Figure 3.7 Sample Current waveform without noise

A calibrated Tektronix TDS3052 digital oscilloscope was used to measure the two output voltage signals of the two transformers. The oscilloscope measured the voltage signals simultaneously. At each measurement the waveform was recorded and the RMS voltage value was read from the output of the scope. Specifications of this scope are given below:

- Bandwidth: 500 MHz
- Sample Rate: 5 GS/s
- Vertical Accuracy: ±2%
- Time Base Range: 1 ns-10 s/div
- Time Base Accuracy: 20 ppm

NxtPhase NXCT-138 Optical Current Transformer specifications are below:

- Max System Voltage: 145 kV
- BIL: 650 kV
- One minute withstand voltage (wet): 275 kV
- Rated frequency: 60 Hz
- Weight: 152 lbs
- Rated max thermal current: 3000 A

- Rated Short-circuit current : 63 kA
- 1C Accuracy (relaying): n/a
- 2C Accuracy (metering): 0.15

A calibrated Westinghouse AC voltmeter was used to measure the output voltage of the regulating transformer, which supplied the current-generator. Specifications of this voltmeter are given below:

- Model: PA-151
- Voltage range: 3, 15, 75, 150, 300, 750 V
- Permissible error: ±2%
- Measurement uncertainty: ±0.5% rdg + 0.001 V

A calibrated Weston AC ammeter was used to measure the control circuit current and CT secondary side current. Specifications of this voltmeter are given below:

- Model: 904
- Ampere range: 2, 5, 10, 20 A
- Permissible error: ±2%
- Measurement uncertainty: ±0.06% of output +100 μA

The effect of external magnetic fields on the accuracy of OCT was also tested. One turn of cable was passed through the OCT, and the outgoing cable was placed adjacent to the sensor head. The cable touches the outside cover of the sensor-head. The magnetic field produced by the adjacent conductor does not affect the OCT output. There was no difference between the current measurements. This test proved that the OCT is not affected by the exterior magnetic field generated by other conductors.

3.1.3 Comparison of Steady State Performance of the Magnetic and Optical CT in Protection Mode

The Optical CT was set up for protection mode. The magnetic transformer used 0.1 ohm burden resistance. This assures metering accuracy.

The current generator output current was controlled by a regulating transformer as shown in Figure 3.3. The tests were conducted for 5 different input voltage levels of the regulating transformer. These voltage levels are proportional with the output current of the current-generator. The voltage levels were set in an ascending order starting from 45 V. For each voltage level, 5 measurements were performed and readings were manually recorded. The input voltage was adjusted to the desired level and the electronic switch was switched on. The waveform begins with a transient and gradually reaches its steady state. When the current reaches the steady state, the value oscilloscope was stopped and then the electronic switch was switched off. The scope measure the RMS value of the

steady state current when is it is stopped. The RMS values of the two voltages measured by the oscilloscope are recorded manually. Once this reading is completed, the switch is turned on again and the process repeated five times.

The RMS voltage reading of the oscilloscope for the conventional CT is the voltage across the burden resistor and that of the OCT is the opto-electronics voltage output. The minimum measured current was about 145 A, the maximum about 756 A. This maximum current is limited by the impedance of the magnetic current transformer. The results of the test are shown in Table 3.3.

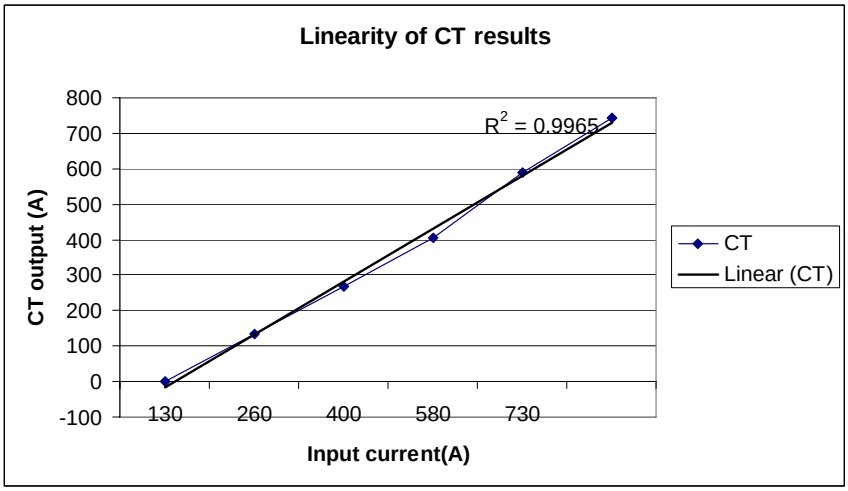

CT

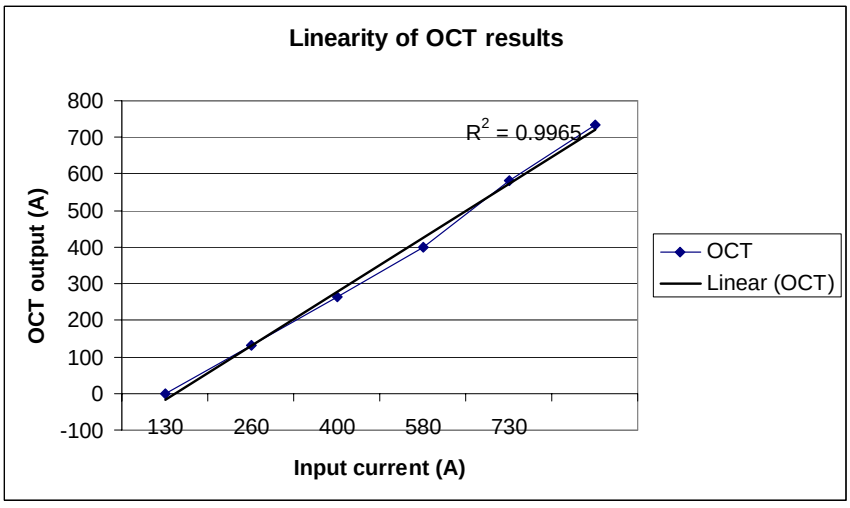

OCT

Figure 3.8 Linearity of results

The average of five readings at each voltage level has been calculated and plotted on Figure 3.8. The figures represent the input-output relationship of the conventional CT and

the optical CT. Both the figures follow an almost linear pattern that supports the findings of the literature review. Thus, it signifies the validity of readings recorded for both conventional CT and OCT. Please note that the accuracy of the scope used for the readings is specified as 2%, and readings for all measurements are within this level.

Table 3.3 Test results

Input (V)		OCT (mV)	(A)	Group avg.	Stdv	CT(mV)	(A)	Group avg.	Stdev A	Diff. A	Max & Min (A)	Average diff (A)	Error % CT based	Error % OCT based
45	45	132	132	132	0	84	134.4	134.24	0.11	2.4	2.4	2.24	1.79	1.82
45		132	132			83.9	134.24			2.24	2.08		1.67	1.70
45		132	132			83.9	134.24			2.24			1.67	1.70
45		132	132			83.8	134.08			2.08			1.55	1.58
45		132	132			83.9	134.24			2.24			1.67	1.70
90	90	262	262	263	1	167	267.2	267.2	1.13	5.2	5.2	4.2	1.95	1.98
90		264	264			167	267.2			3.2	3.2		1.20	1.21
90		264	264			168	268.8			4.8			1.79	1.82
90		262	262			166	265.6			3.6			1.36	1.37
90		263	263			167	267.2			4.2			1.57	1.60
140	140	402	402	401	2.54	254	406.4	405.76	2.67	4.4	5	4.76	1.08	1.09
140		403	403			255	408			5	4.4		1.23	1.24
140		403	403			255	408			5			1.23	1.24
140		400	400			253	404.8			4.8			1.19	1.20
140		397	397			251	401.6			4.6			1.15	1.16
200	200	580	580	580.2	2.77	368	588.8	588.8	2.99	8.8	9.8	8.6	1.49	1.52
200		579	579			368	588.8			9.8	7.6		1.66	1.69
200		579	579			367	587.2			8.2			1.40	1.42
200		578	578			366	585.6			7.6			1.30	1.31
200		585	585			371	593.6			8.6			1.45	1.47
250	250	730	730	732.6	1.67	462	739.2	741.76	1.43	9.2	10.4	9.16	1.24	1.26
250		734	734			464	742.4			8.4	8.4		1.13	1.14
250		734	734			464	742.4			8.4			1.13	1.14
250		732	732			464	742.4			10.4			1.40	1.42
250		733	733			464	742.4			9.4			1.27	1.28

In Table 3.3, the last two columns give the percentage differences, or errors, between the magnetic CT and optical CT. The maximum CT-based percentage difference is 1.95%, the minimum is 1.08%, and the average difference 1.42%. The maximum OCT-based percentage difference is 1.98%, and the minimum is 1.09%, and the average difference is 1.44%. The obtained values show that the error is less than 1.5%.

According to the manufacturer, the magnetic CT burden was less than 2.5 VA, which should assure 0.2% accuracy. The optical CT was in protection mode, and we used an additional differential amplifier for noise reduction. The accuracy of the OCT, combined with the differential amplifier in this arrangement is estimated to be around 2%. The comparison of the experimental results with the manufacture provided data shows the less than 1.5% deviation which is acceptable.

Figure 3.9 shows the optical CT measured output currents versus the magnetic CT output current. The figure shows that the differences are small, and the relation is nearly linear.

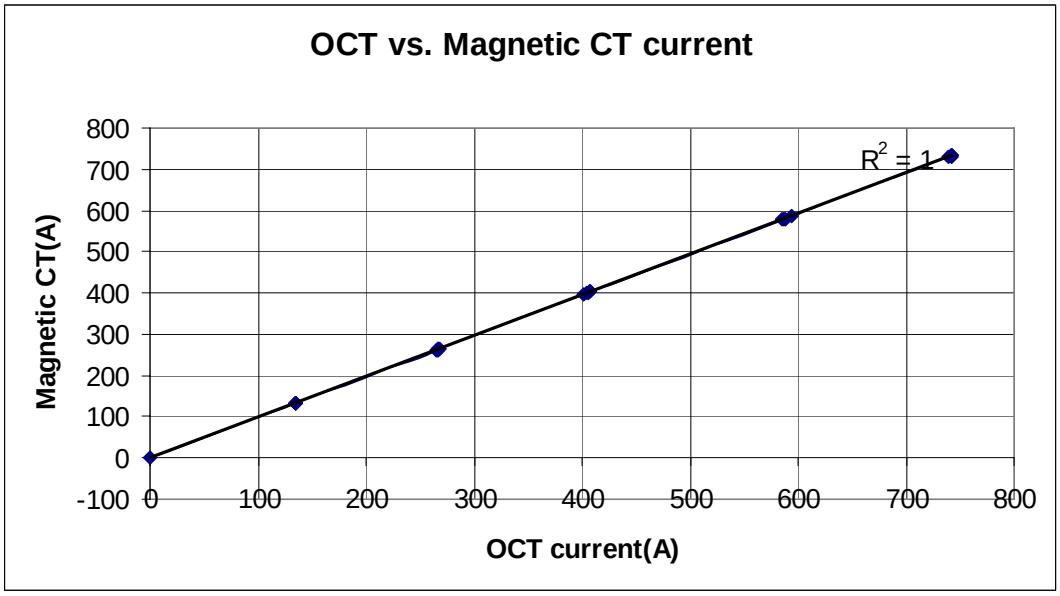

Figure 3.9 OCT current vs. Magnetic CT current

Figure 3.10 shows the OCT-based percentage errors or differences versus those of the OCT current. The figure stipulates that the error is basically a calibration off-set between the OCT and the conventional CT, and is not dependent on the current level. The scale factor of the OCT (calibration) had been performed without the isolation amplifier in place; accordingly, up to a few percent of off-set due to this isolation amplifier is expected. The real purpose of this test was to show linearity, as opposed to absolute calibration, and Figure 3.9 shows that the relative linearity is nearly perfect between the two CTs.

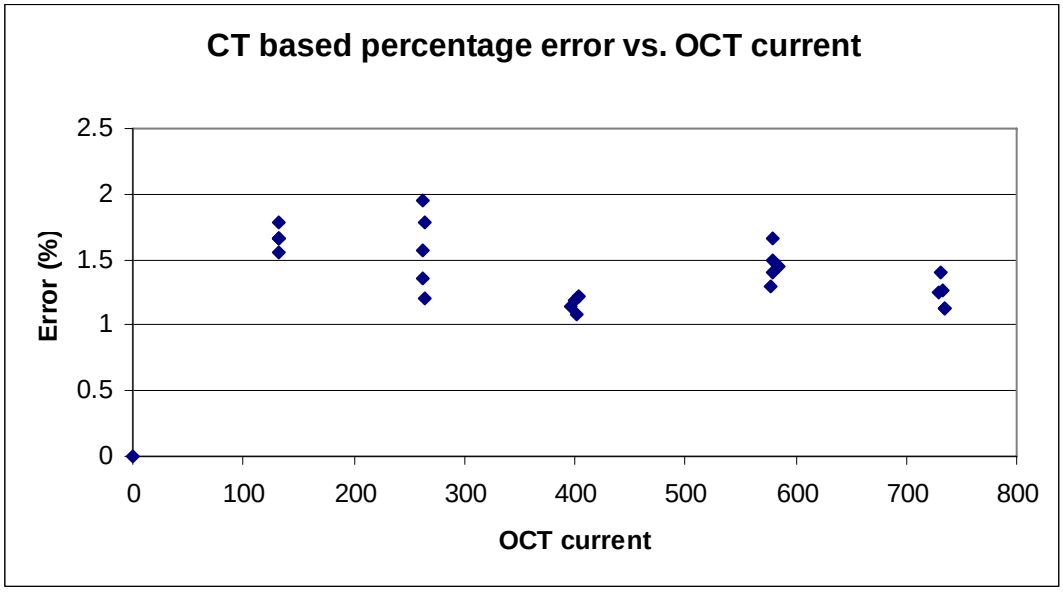

Figure 3.10 CT based percentage error vs. OCT current

The test was repeated using a calibrated analog ampere meter instead of a burden resistor across the conventional CT. The ammeter accuracy was 2% and its setting was 5 A, which corresponds to an 800 A primary current. OCT output was measured with a scope as before, as well as with a Fluke digital voltmeter with accuracy of 0.4%. In addition, we measured the primary current using a precision current transformer made by JAMB Inc. The JAMB CT has been certified by NIST to maintain 100 ppm accuracy over a range of primary currents from 10 to 1000 amps [5]. This CT was loaded by a precision 1 ohm resistance with 0.1% accuracy. A Fluke multimeter calibrated to 0.5% measured the voltage across this resistor, for a total accuracy of 0.6%.

Table 3.4 Repetition of current measurement using precision CT and ampere meters

	Input current (A)	OCT Output (A)	Magnetic CT (A)	% Difference Input Current vs. OCT	% Difference Input Current vs. magnetic CT	% Difference magnetic CT vs. OCT
1	130.83	128.20	128.00	2.01	2.16	0.15
2	260.6	256.10	256.00	1.72	1.76	0.03
3	401.58	393,5	392.00	2.01	2.38	0.37
4	582.70	570.8	571.20	2.04	1.97	0.06
5	736.00	721.1	729.60	2.02	0.86	1.15

The current was increased to the desired level by regulating transformer, and the output of the precision CT, magnetic CT and optical CT were recorded. The protection output of the OCT with a noise reduction amplifier was used. Results are shown in Table 3.4.

The results indicate around 2% deviation between the OCT and precision CT input current. Similar deviation was found between the output of the magnetic CT and precision CT. However, the differences between the OCT and magnetic CT output are much less. These results are better than those recorded on Table 3.3. And again, all agreements are within the amounts allowed within this metrology set up.

3.1.4 Comparison of the Magnetic and Optical CT Wave Shape

The current sine waves generated by the magnetic and optical CTs were recorded in a steady state condition, and the differences of the two sine waves were calculated. Figure 3.11 shows the recorded current sine waves and the current difference when the primary current was 730 A RMS.

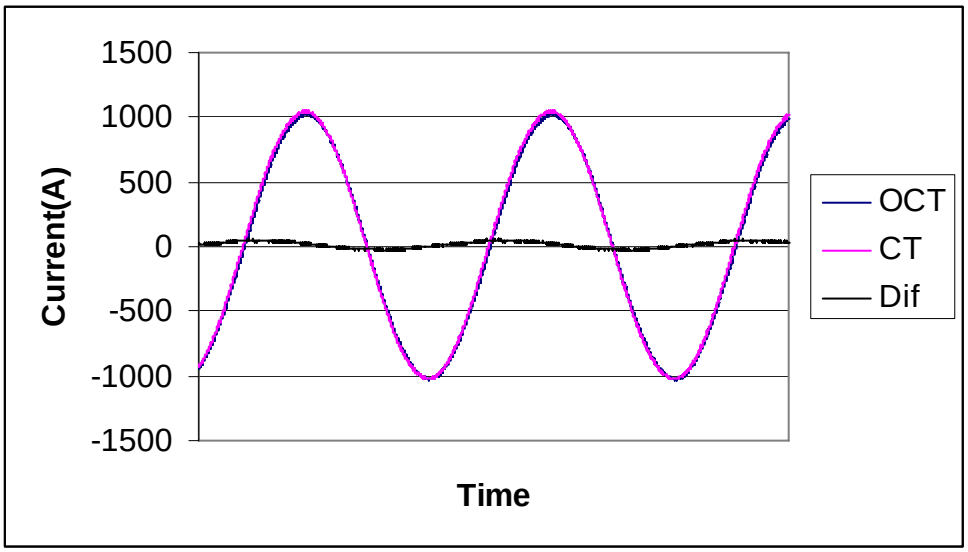

Figure 3.11 OCT and Magnetic CT currents and difference between them, when the primary current is 730 A

The figure shows that the amplitude difference is less then 5%. The phase difference is less then 2.77 degrees (around 128 μs) which is significantly higher than the manufacturer's data of 40 μs. It is expected that the additional delay is due to the differential amplifier used in this case. Detailed investigation of the results shows that both the OCT output and the magnetic CT output have small DC bias as observed on the scope. We assume that this negligible bias is due to measuring error and most likely associated with the oscilloscope used. Again, all results are within specifications of devices under test and test equipment.

Figure 3.12 shows the percentage difference of the two sine waves when the primary current is 109 A RMS. The percentage difference was calculated using the peak value of the OCT current. The figure shows that the maximum error is less than 5% at the current's peaks. If we ignore the impact of noise the peak error is about 3%, and the rms

error is less than 2%, consistent with data taken using the same equipment and reported in the previous section Tables 3.3.

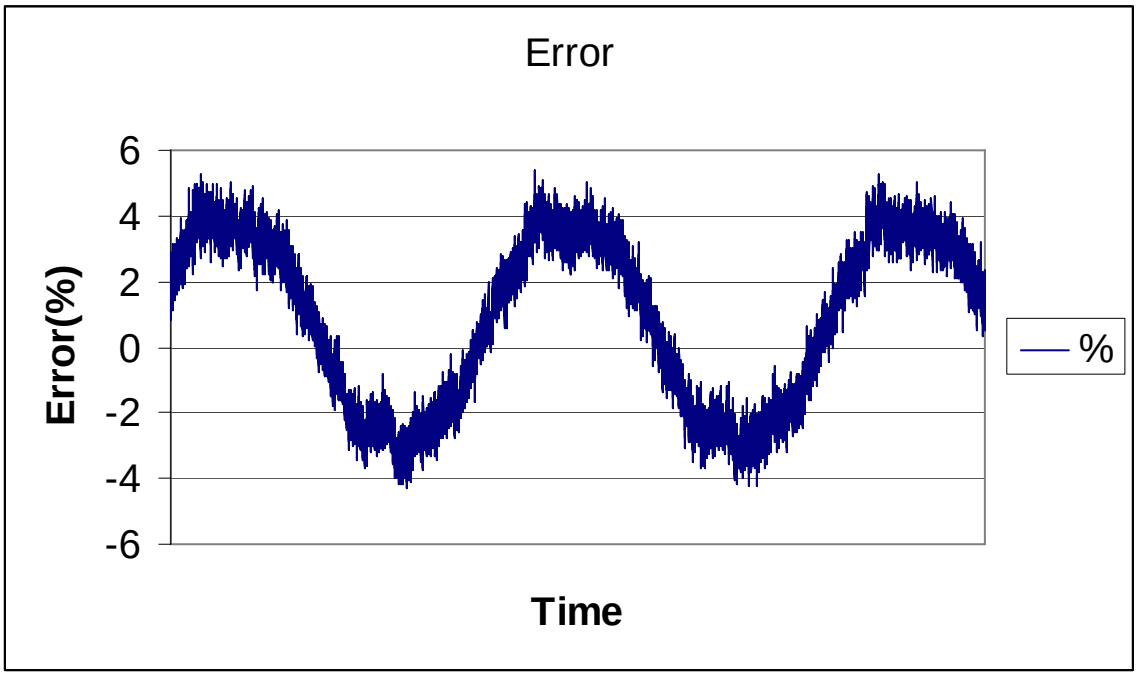

Figure 3.12 Sine wave differences at steady state between them when the primary current is 109 A.

The figure shows that the positive and negative peaks are different. The analysis of the OCT and magnetic CT produced sine waves shows less than 0.1% DC bias at the magnetic CT, and less than 0.7% DC bias at the OCT output. The negligible 0.1 % bias at the magnetic CT is most likely due to measuring error. We assume that the 0.7% bias is the product of the isolation output amplifier. Nevertheless, the accuracy of the scope is specified as 2%, which implies that the DC off-set error caused by the scope used for the measurement can account for all the offsets observed.

The figure shows a noticeable component of white noise. This is expected due to the small signal and the settings of the OCT. The noise is on the order of 1 or 2 A rms primary, and has no impact on energy measurement (averages to zero) or typical protection applications (filters out and is very small).

The measured phase shift at 109 A (60 Hz) was about 2.25 degrees which corresponds to 104 μs delay.

The comparison of the two sine waves shows less than 5% instantaneous amplitude (including noise), and less than 3 degrees phase shift. These values may appear to rather large when compared with the specifications of the optical and conventional CTs under test, but they are within acceptable range when considering all test equipment and set-up used. Particularly, oscilloscopes are generally a weak link in accuracy comparisons;

Oscilloscopes are great for getting waveform and timing information, but they absolute accuracies (both DC and AC) in amplitude are typically limited (<2%), they can cause ground loops and affect measurements, the usually provide a path for significant amount of noise to enter into the data recorded.

3.1.5 Comparison of the Current Transformers Accuracy in Metering Mode

The optical CT was set in metering mode, and the amplifier reducing the noise was removed. The magnetic CT burden (0.1 ohm, 2.5 VA) corresponded to the metering mode. The system accuracy was tested using a precision magnetic CT. The paper [5] recommends the measuring technique.

The concept is that the output of the CT is compared with the output of precision calibration CT using differential amplifier. Figure 3.13 shows the test set up. A 1000:1 active precision CT produced by JAMB Inc. has been used to make the comparison. The JAMB CT has been certified by NIST to maintain 100 ppm accuracy over a range of primary currents from 10 to 1000 amps [5].

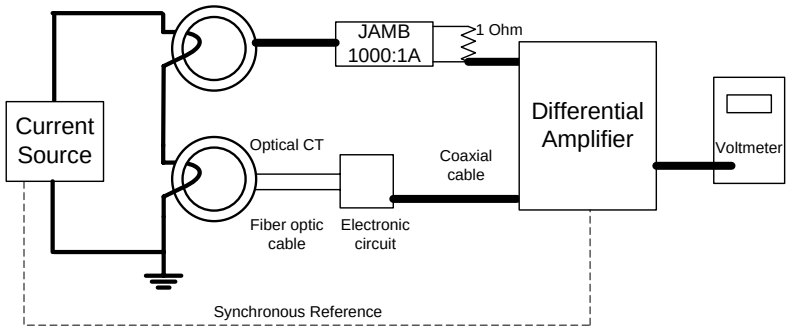

Figure 3.13 OCT measurement test setup

The JAMB CT output is connected to a 1 ohm calibrated resistor and the voltage across this resistor has been used as an input 1 for the differential amplifier. The input primary current was measured using a voltmeter connected across the 1 ohm resistance. When the voltage across the resistor was 1 V, the current was 1000 A.

The OCT output was input 2 for the differential amplifier. The OCT output was 1 V when the primary current was 1000 A. The voltmeter shows the voltage difference between the voltage across the resistor and OCT output voltage. This method allows us to find the error signal of OCT output.

Table 3.5 shows the test results for this experiment. The applied current has changed from 250 to 760 A. Eight different current values were tested and the corresponding voltmeter readings were recorded. 'A' represents the output voltage of OCT and 'B' represents the voltage across the resistor of 1 ohm. A-B is the voltage difference of these two readings. As an example the 0.4 V in the first row means that the difference between the two current readings is 0.4 A which is 0.16%.

Table 3.5 Test results

App. Current(A)	A-B (V and A)	Diff (%)
248	-0.4	-0.16129
313	-0.7	-0.22364
390	-0.8	-0.20513
466	-0.8	-0.17167
543	-0.6	-0.1105
619	-0.6	-0.09693
688	-0.4	-0.05814
762	-0.2	-0.02625

The test results show that the accuracy of the optical CT in metering mode is less than 0.2% in all cases but one. The CT meets with the standard requirements.

By using the JAMB precision current transformer, the magnetic CT was also tested. The test setup can be seen in Figure 3.14.

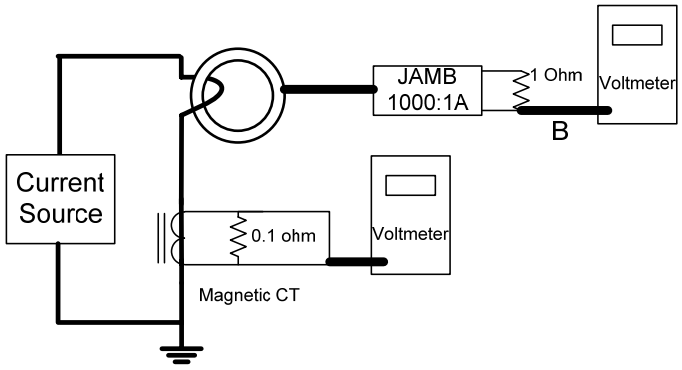

Figure 3.14 CT measurement test setup

A 0.1 ohm of calibrated resistor has been connected to the secondary side of the magnetic CT and the voltage across this resistor recorded for the current readings. This voltage represents the secondary current of CT and it has been converted to the primary current using the turn ratio of 800 A / 5 A.

The 1 V of the voltage across the resistor connected to the output of JAMB transformer represents the 1000 A current flowing through the conductor. The readings of voltage across the 1 ohm resistor have been converted to the primary current. These two calculated primary currents have been compared in Table 3.6.

Table 3.6 Primary current vs. magnetic CT output

App. Current(A)	V_R (mV) [B]	Current (A)	V_{CT}(V)	Current(A)	Diff(A)	%
248	248.66	248.66	1.55	248	-0.66	-0.26613
313	313.4	313.4	1.95	312	-1.4	-0.44728
390	389.6	389.6	2.45	392	2.4	0.615385
466	466.3	466.3	2.91	465.6	-0.7	-0.15021
543	543.3	543.3	3.4	544	0.7	0.128913
619	619.2	619.2	3.87	619.2	0	0
688	688.3	688.3	4.33	692.8	4.5	0.65407
762	762.4	762.4	4.79	766.4	4	0.524934

The results show that the magnetic CT, with 0.1 ohm burden resistance has accuracy better than 0.65%, which is higher than the expected 0.2%

The results of the optical and magnetic CT's were combined in Table 3.7.

Table 3.7 shows that the difference between the optical and magnetic CT test is less than 0.9%. This value is rather large because the CT's accuracy class is 0.2%.

Table 3.7 CT comparisons

OCT-JAMB (A)	CT-JAMB (A)	OCT-CT (A)	OCT –CT %
-0.4	-0.66	0.26	0.10484
-0.7	-1.4	0.7	0.22364
-0.8	2.4	-3.2	-0.82051
-0.8	-0.7	-0.1	-0.02146
-0.6	0.7	-1.3	-0.23941
-0.6	0	-0.6	-0.09693
-0.4	4.5	-4.9	-0.71221
-0.2	4	-4.2	-0.55118

3.2 Study of Optical PT Operation

The objective of the study is to compare the performance of the NxtPhase Optical PT with a conventional PT donated by Salt River Project. The experimental work requires a high voltage test system and the understanding of the operation of the NxtPhase OPT.

3.2.1 NxtPhase Optical Potential Transformer

NxtPhase voltage transformer (NXVT) is one of the optical transformers in the market today. NxtPhase provided to ASU one of the combined optical voltage and current transformer (NXVCT) to conduct the experiments. Only the voltage transformer part of NXVCT was used for the voltage transformer tests. NXVT uses a fiber optic voltage sensor based on the principle that the electric field changes the light's circular

polarization to an elliptical polarization. The operation of the NXVT is described in the manufacturer's data sheet and referenced in a detailed way.

NXVT sensors are placed in a post type high voltage composite insulator. The post insulator is built with a fiberglass tube, which is covered outside by rubber sheds. Inside the insulator tube is a smaller tube, which is a hollow cylindrical resistor used for shielding. Three Pockels cell-based sensors are placed in the inner tube. Dry nitrogen is used for insulation. Two electrodes are placed at the ends of this structure: a high voltage electrode at the top (connected to the line) and a ground electrode at the bottom [32, 36].

The voltage on the line creates an electric field between the line and the ground. This field is used by Pockels cells based sensors to measure the voltage. The effect of the external field is eliminated by the resistive inner tube providing permittivity shielding [38].

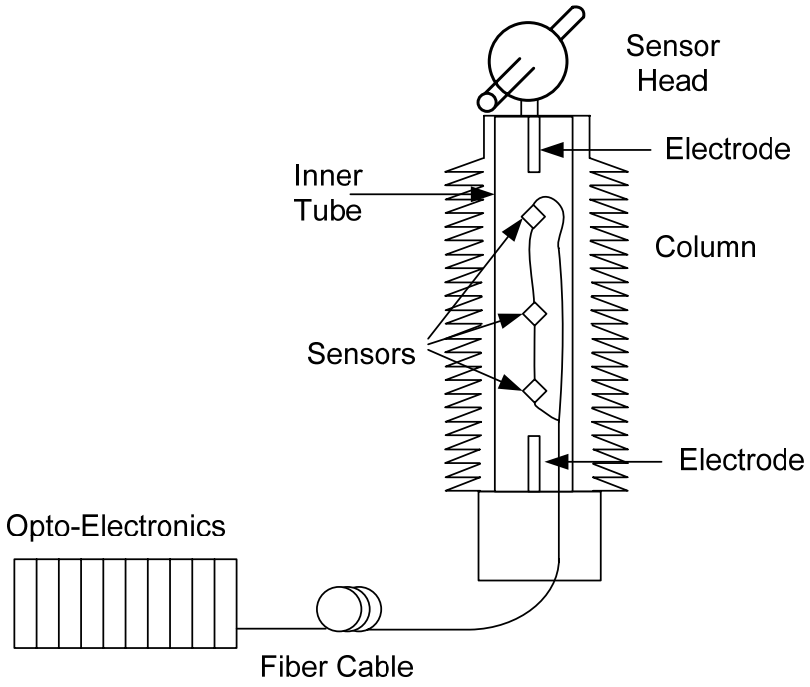

Figure 3.15 NxtPhase Voltage Transducer

Three electric field sensors are located in the inner tube: one in the middle, one near the high voltage, and one near the ground electrode. These sensors are connected to the opto-electronic system by fiber optic cables through the inner tube. The location of these sensors has a crucial importance to the accuracy of voltage measurement. A numerical integration formula (Quadrature Method) is used to define the sensor locations. This method also minimizes the stray field effect for the electric field sensors, caused by the external electric field. The number of electric field sensors is optimized and defined as three for NXVT. Both resistive shielding and the Quadrature method help to reduce the electric field effect caused by neighboring phase voltages. Consequently, the accuracy of OVT becomes more reliable [34, 39].

The light signal from a light emitting diode is sent from the NxtPhase opto-electronics through the fiber optic cable. The light signal travels up the unit's column. Light enters sensors (Pockels cells) that are located halfway between the electrodes and the other two sensors, which are located above and below the middle sensor. While light passes through the sensors, the electric field, created by line-to-ground voltage, changes the polarization of the light from circular to elliptical. These changes at the three sensors are collected and processed by electronics to calculate the line-to-ground voltage of the line [32, 42].

Detected sensor signals are connected to opto-electronic in the control room through a fiber optic cable. These signals are processed, and analog and digital outputs are generated as a NXVT output signal. There is a 40μs time delay as a result of this signal processing. At 60 Hz, digital phase compensation was used to set the phase displacement to 0 degrees [32].

The NXVT has three outputs

- Digital output
- Low voltage analog output (4 V)
- High voltage analog output (69-115 V) [40]

Transformer ratio is dependant on the voltage rating of transformer. For the 138 kV OVT, 1200:1 or 700:1 and for the 345 kV OVT it is 3000:1 or 1800:1 [32].

Conventional voltage transformers have bandwidth less than 1.5 kHz. However, the NXVT has a bandwidth of 40 kHz, which provides better transient response. This can improve the performance of protection relaying and provide better power quality measurements [32, 34, 40].

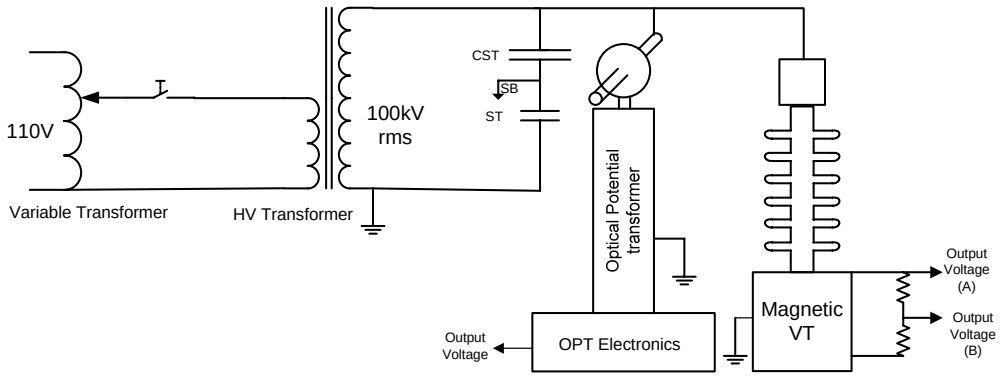

Figure 3.16 Connection diagram for the AC test of optical and magnetic PT

3.2.2 High Voltage Test Setup

The optical PT was tested at ASU's High Voltage Laboratory. A 100 kV, 5 kVA high voltage transformer and 200 kV impulse generator has been used to compare the magnetic Voltage Transformer (VT) and Optical Potential Transformer (OPT) performance. Figure 3.16 shows the connection diagram of the test system.

Optical and magnetic potential transformers are connected in parallel and supplied by the high voltage transformer. The voltage was varied by a regulating transformer. The maximum applied voltage was 100 kV, which is more than the rated voltage of the transformers. The over-excitation is permitted in the investigation of the transformer's saturation effect on the measured voltage. The applied voltage was measured with a capacitive voltage divider. The accuracy of this divider system is only 5%. This divider was used to adjust the test voltage to an approximate value.

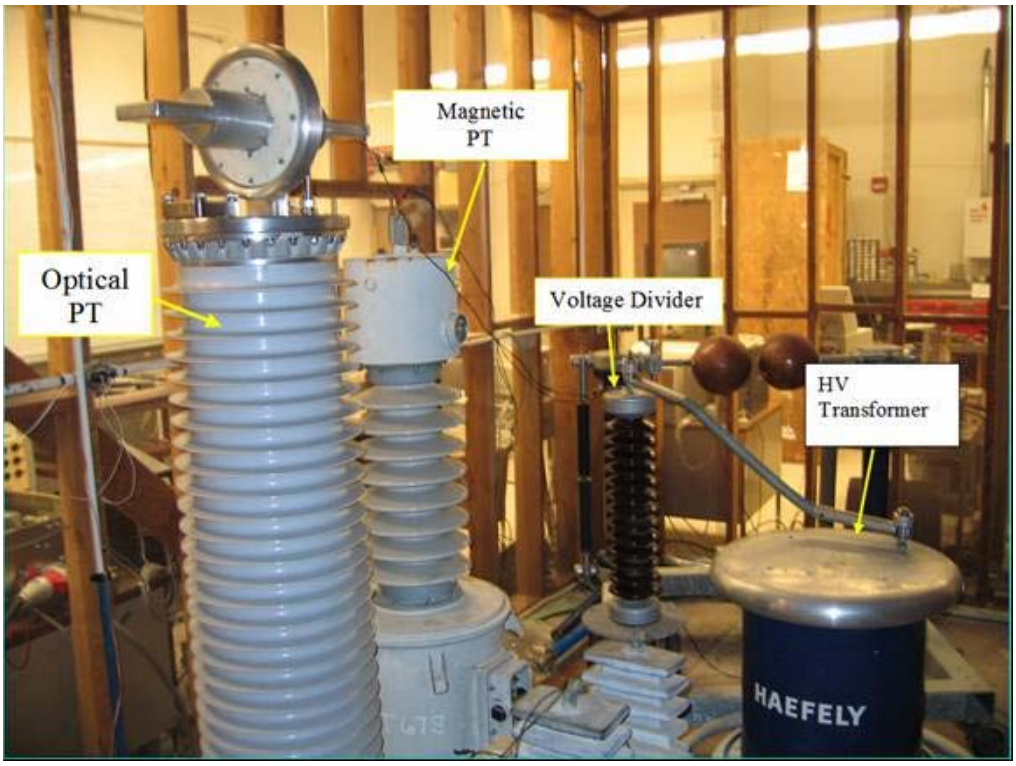

Figure 3.17. Experimental test setup

The output of the magnetic transformer has been connected to a resistive voltage divider in order to make the voltage ratios of the magnetic PT equal to the optical PT voltage ratio. Outputs of the potential transformers were connected to the digital oscilloscope, which recorded the wave shape and calculated the RMS. value of the voltage. The photo of the test set up is shown on Figure 3.17.

The traditional outdoor substation class VT is manufactured by Associated Engineering Company. The VT specifications are:

- Voltage 69 kV, BIL 350 kV
- Pri Volts/ Sec Volts 40250 V / 115 V
- Thermal Rating 6000 VA

The magnetic PT used in W mode has accuracy 0.3% when it supplies relays. This is the protection mode when the burden is 115.2 ohm.

The high energy analog (HEA) output of the optical PT was compared with the output voltage of the magnetic PT. A voltage divider has been connected to the secondary side of the magnetic VT to make the output voltage equal with that of OPT. The OPT output voltage is 1 V when the primary voltage is 700 V. However, magnetic VT has 2 V output voltage for 700 V primary voltage. Two 5 M ohm resistor have been connected in a series and the voltages across the resistors have been used to compare the outputs. In Figure 3.16 'Output voltage A' corresponds to the 2 V at 700 V primary voltage and 'Output voltage B' corresponds to the 1 V at 700 V primary voltage. During the test, both output A and B were used.

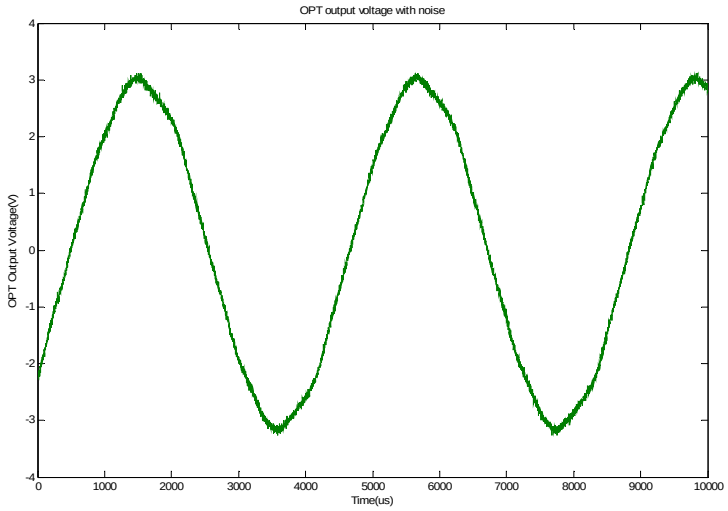

Figure 3.18 Sample OPT output voltage waveform with noise (most of noise is expected to have been caused by the oscilloscope's connection)

The preliminary test indicated that the OPT output voltage has about 4.16 % white noise as shown in Figure 3.18. Although this noise is less than the noise of output voltage of OCT, it can be disturbing. The noise was reduced to an acceptable level (estimated less than 0.1%) by using the average function of the digital oscilloscope

A calibrated Tektronix TDS3052 digital oscilloscope was used to measure the two output voltage signals of the two transformers. The oscilloscope measured the voltage signals simultaneously. At each measurement the wave form was recorded and the RMS. voltage

value was read from the output of the scope. The same digital oscilloscope was used for the current transformer test.

NxtPhase NXVCT-138 Combined Optical Potential and Current Transformer specifications are:

- Max System Voltage: 145 kV
- BIL: 650 kV
- One minute withstand voltage (wet): 275 kV
- Rated frequency: 60 Hz
- Weight: 152 lbs
- Rated max thermal current: 3000 A
- Rated Short-circuit current: 40 kA
- 1C Accuracy (relaying): IEC 0.5/5P
- 2C Accuracy (metering): 1.2-30 A 0.30% , 30-600 A 0.30%
- Voltage accuracy missing: IEC class 0.2, IEEE class 0.3

In addition to the digital oscilloscope, a Fluke 189 True RMS multimeter was used to measure the output voltage of transformers. Specifications of this multimeter are given below:

- Model: 189
- Voltage range: 2.5 mV to 1000 V- 100 kHz bandwidth
- Frequency: 0.5 Hz to 1000 kHz
- Accuracy (Basic DC V): 0.0025%, (Basic AC V): 0.4%

3.2.3 Comparison of Steady State Performance of an Optical and Magnetic PT

The voltage on the parallel connected optical and magnetic transformer was increased in nine steps between 5 kV and 80 kV. Regulating transformer voltage was adjusted to the desired voltage level. After this the main switch on the control box was closed and the PTs were energized. This generated transient voltage, which was recorded by a digital oscilloscope. The waveform begins with a transient and gradually reaches its steady state value. The digital oscilloscope provided the RMS. value of the two output voltages in steady state condition. The obtained values were recorded manually. This process was repeated 5 times at each voltage level. The HEA output was used on the optical PT and the A output at the magnetic PT.

Table 3.8 gives the measured values.

Table 3.8 Test results

Applied (V)		OPT (V)	(V)	Group avrg (V)	Stdv	PT (V)	(V)	Group avrg (V)	Stdev	Diff.	Max & Min	Average diff	% PT based	%OPT Based
4900	4900	0.7	4900	4922.4	14.34	1.41	4935	4956	19.17	35	49	33.6	0.709	0.714
4900		0.703	4921			1.41	4935			14	14		0.284	0.284
4900		0.703	4921			1.42	4970			49			0.986	0.996
4900		0.705	4935			1.42	4970			35			0.704	0.709
4900		0.705	4935			1.42	4970			35			0.704	0.709
9800	9800	1.4	9800	9800	0	2.82	9870	9870	0	70	70	70	0.709	0.714
9800		1.4	9800			2.82	9870			70	70		0.709	0.714
9800		1.4	9800			2.82	9870			70			0.709	0.714
9800		1.4	9800			2.82	9870			70			0.709	0.714
9800		1.4	9800			2.82	9870			70			0.709	0.714
24500	24500	3.5	24500	24556	31.30	7.04	24640	24696	31.30	140	140	140	0.568	0.571
24500		3.51	24570			7.06	24710			140	140		0.567	0.570
24500		3.51	24570			7.06	24710			140			0.567	0.570
24500		3.51	24570			7.06	24710			140			0.567	0.570
24500		3.51	24570			7.06	24710			140			0.567	0.570
35000	35000	5	35000	34970.6	37.17	10	35000	35000	0	0	70	29.4	0.000	0.000
35000		4.99	34930			10	35000			70	0		0.200	0.200
35000		5	35000			10	35000			0			0.000	0.000
35000		4.99	34930			10	35000			70			0.200	0.200
35000		4.999	34993			10	35000			7			0.020	0.020
40250	40250	5.72	40040	40096	31.30	11.5	40250	40250	0	210	210	154	0.522	0.524
40250		5.73	40110			11.5	40250			140	140		0.348	0.349
40250		5.73	40110			11.5	40250			140			0.348	0.349
40250		5.73	40110			11.5	40250			140			0.348	0.349
40250		5.73	40110			11.5	40250			140			0.348	0.349

Table 3.8 Test results (Cont)

Applied (V)		OPT (V)	(V)	Group avrg (V)	Stdv	PT (V)	(V)	Group avrg (V)	Stdev	Diff.	Max & Min	Average diff	% OPT based	%PT Based
50000	50000	7.04	49280	49294	31.30	14.2	49700	49700	0	420	420	406	0.845	0.852
50000		7.04	49280			14.2	49700			420	350		0.845	0.852
50000		7.05	49350			14.2	49700			350			0.704	0.709
50000		7.04	49280			14.2	49700			420			0.845	0.852
50000		7.04	49280			14.2	49700			420			0.845	0.852
60000	60000	8.56	59920	59948	38.34	17	59500	59500	0	-420	-420	-448	-0.706	-0.701
60000		8.56	59920			17	59500			-420	-490		-0.706	-0.701
60000		8.57	59990			17	59500			-490			-0.824	-0.817
60000		8.57	59990			17	59500			-490			-0.824	-0.817
60000		8.56	59920			17	59500			-420			-0.706	-0.701
70000	70000	10	70000	70000	0	19.8	69300	69300	0	-700	-700	-700	-1.010	-1.000
70000		10	70000			19.8	69300			-700	-700		-1.010	-1.000
70000		10	70000			19.8	69300			-700			-1.010	-1.000
70000		10	70000			19.8	69300			-700			-1.010	-1.000
70000		10	70000			19.8	69300			-700			-1.010	-1.000
80000	80000	11.5	80500	80500	0	22.4	78400	78120	156.5248	-2100	-2100	-2380	-2.679	-2.609
80000		11.5	80500			22.3	78050			-2450	-2450		-3.139	-3.043
80000		11.5	80500			22.3	78050			-2450			-3.139	-3.043
80000		11.5	80500			22.3	78050			-2450			-3.139	-3.043
80000		11.5	80500			22.3	78050			-2450			-3.139	-3.043

Figure 3.19 compares the response of the two PTs and presents the error bars caused by 5 times repetition of each test. This figure shows slight deviation between the two curves above 60 kV. Accordingly, the magnetic CT began to saturate above 60 kV. However, the OPT output voltages vary linearly with the applied voltage in the 5-80 kV range.

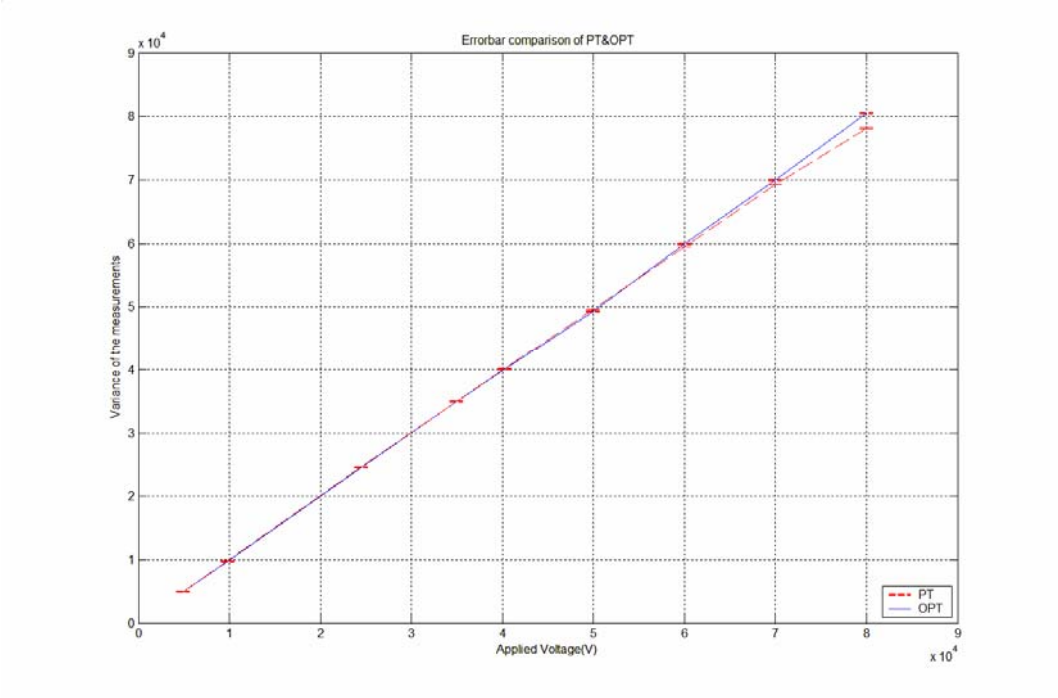

Figure 3.19 Error bar analysis of magnetic PT and OPT

Figure 3.20 shows the OPT output voltage vs. magnetic PT output voltage. The figure shows a highly linear relation between the two outputs.

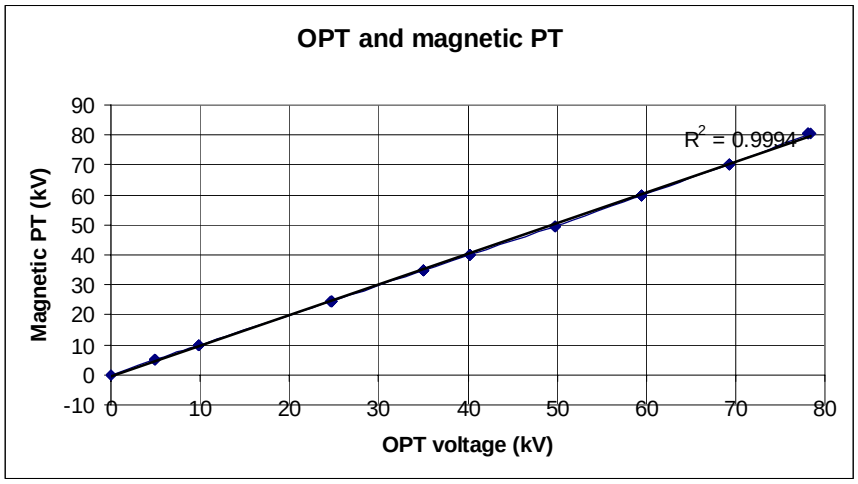

Figure 3.20 OPT output voltage vs. magnetic PT output voltage

Figure 3.21 shows the PT-based percentage difference, referred to here as error, between the magnetic and optical PT output voltages. The figure shows that the deviation is less than 1% under the rated voltage but the saturation increases the deviation rapidly to more than 3%.

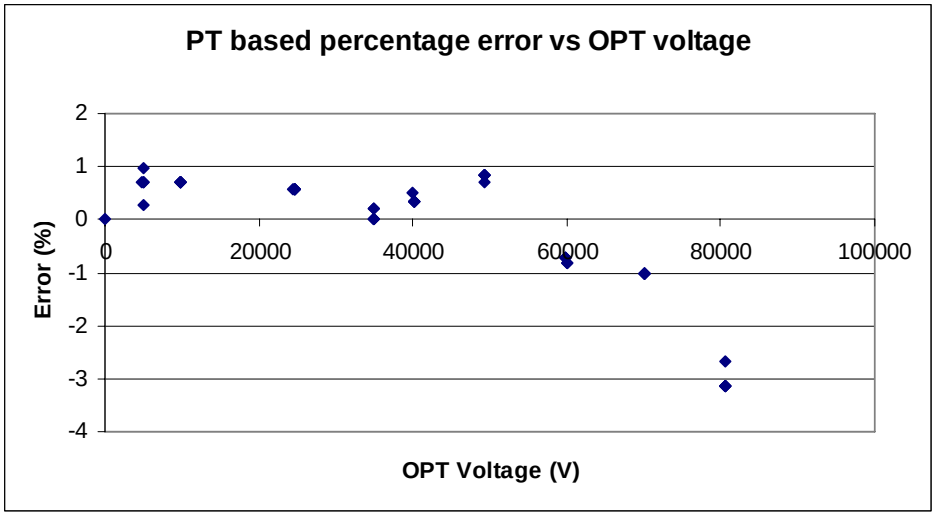

Figure 3.21 Difference between the magnetic and optical PT output voltages

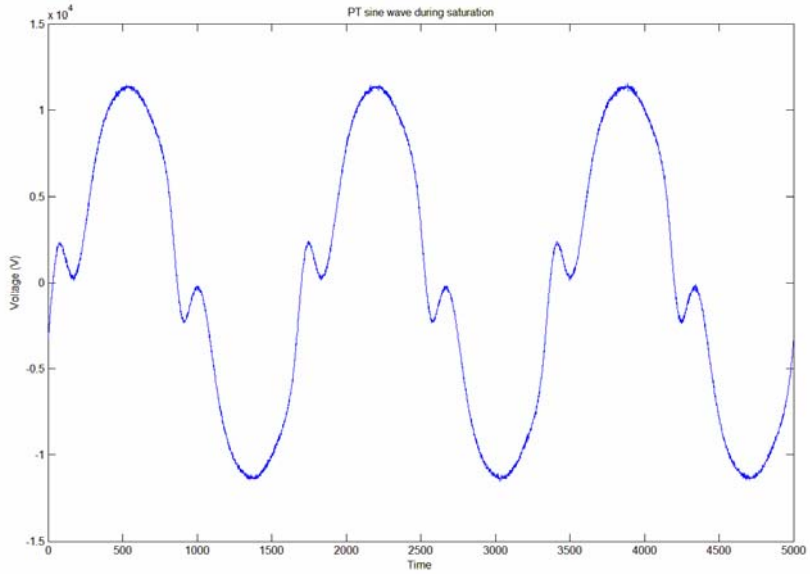

Figure 3.22 Saturation caused distortion of magnetic PT output voltage at 80 kV applied voltage

The saturation distorted the magnetic PT-produced output voltage. Figure 3.22 shows the magnetic PT distorted output voltage when the applied voltage was 80 kV. However, the

output voltage (not shown) of the optical PT remained sinusoidal, because the optical PT does not saturate.

The effect of the voltage coupling due to adjacent high voltage conductors was investigated by energizing only one of the PTs and measuring the output voltage of both the energized and the floating PT. The distance between the two PTs is approximately 50 cm. Figure 3.23 shows that the energization of the magnetic PT alone generates output voltage on the non-energized optical PT. The voltage picked up by the neighboring OPT was around 10%~15% of the applied voltage to the PT. Since the OPT is floating and it has basically a high impedance/low capacitance insulation, it is expected that the HV electrode of the OPT when floating (not grounded) will floating to some voltage between the nearby voltage (PT and source) and ground.

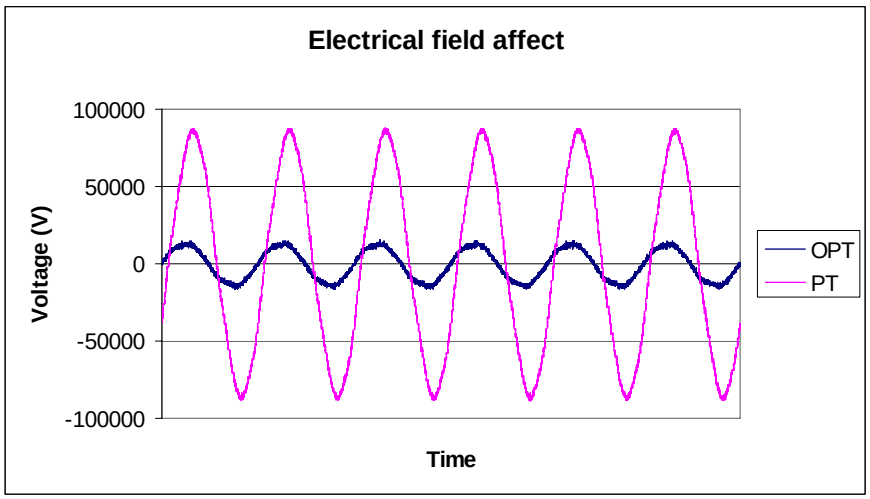

Figure 3.23 Electrical field coupling effect; Magnetic PT energized, OPT floating

Similarly the energization of the optical PT alone produces small output voltage on the floating magnetic PT. The voltage picked up by the neighboring PT was around 10%~15% of the applied voltage to the OPT. Again, since the PT is floating and it has basically a high impedance/low capacitance insulation (and significant inductance), it is expected that the HV electrode of the magnetic PT when floating (not grounded) and its windings will floating and pick up some voltage between the nearby voltage (PT and source) and ground.

The presented results serve as a warning that the adjacent electric field can disturb the operation of a PT. However, the severity of this disturbance must be investigated using a well-defined and measured electric field. In our test the electric field was not measured, which prevents firm conclusion.

3.2.4 Comparison of the Magnetic and Optical PT Wave Shape

The voltage sine waves generated by the magnetic and optical CT was recorded in steady state condition and the difference of the two sine waves were calculated. Figure 3.24

shows the recorded voltage of the sine waves and the voltage difference between them, when the primary voltage was 70 kV.

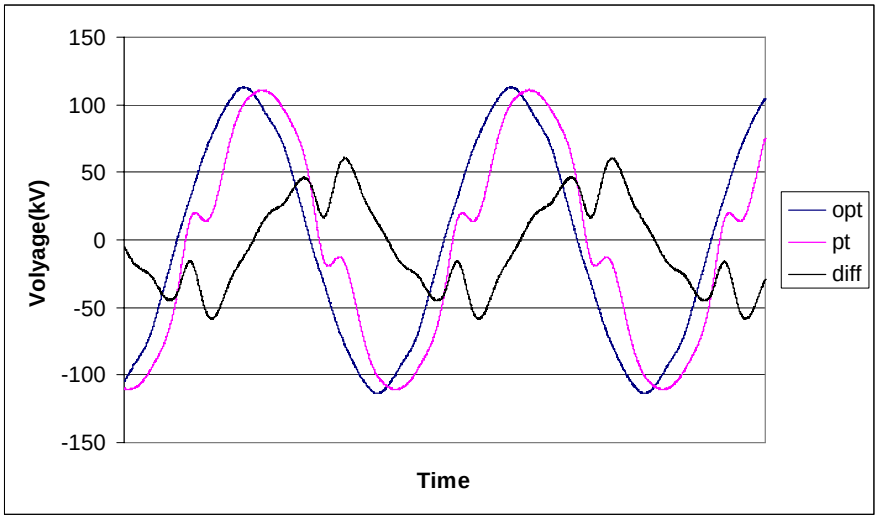

Figure 3.24 OPT and Magnetic PT voltages and difference between them when the primary voltage is 70 kV

The figure shows that the sine wave of the magnetic CT is badly distorted, as a result of saturation. Simultaneously, the OCT output is sinusoidal and not distorted. The difference is more than 54%.

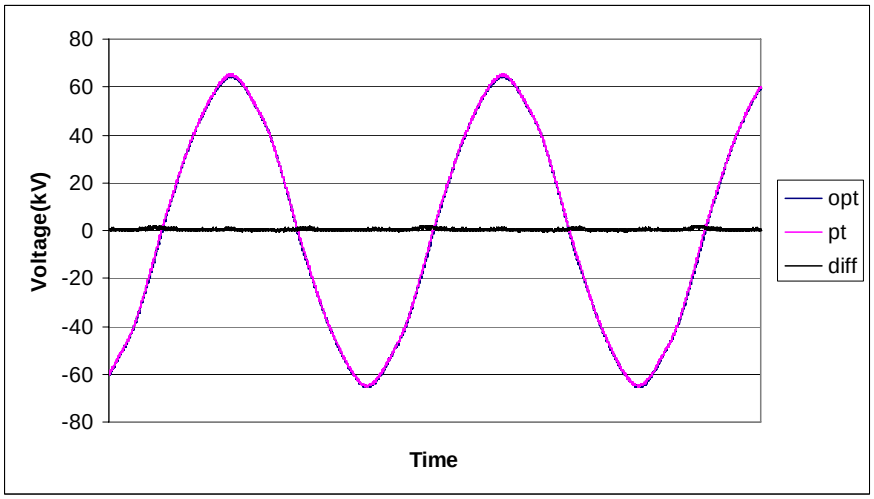

Figure 3.25 OPT and Magnetic PT voltages and difference between them when the primary voltage is 40 kV

Figure 3.25 shows the recorded voltage sine waves when the primary voltage was 40 kV. It can be seen that at low voltage two sine waves are almost identical and no wave distortion can be observed on the figures.

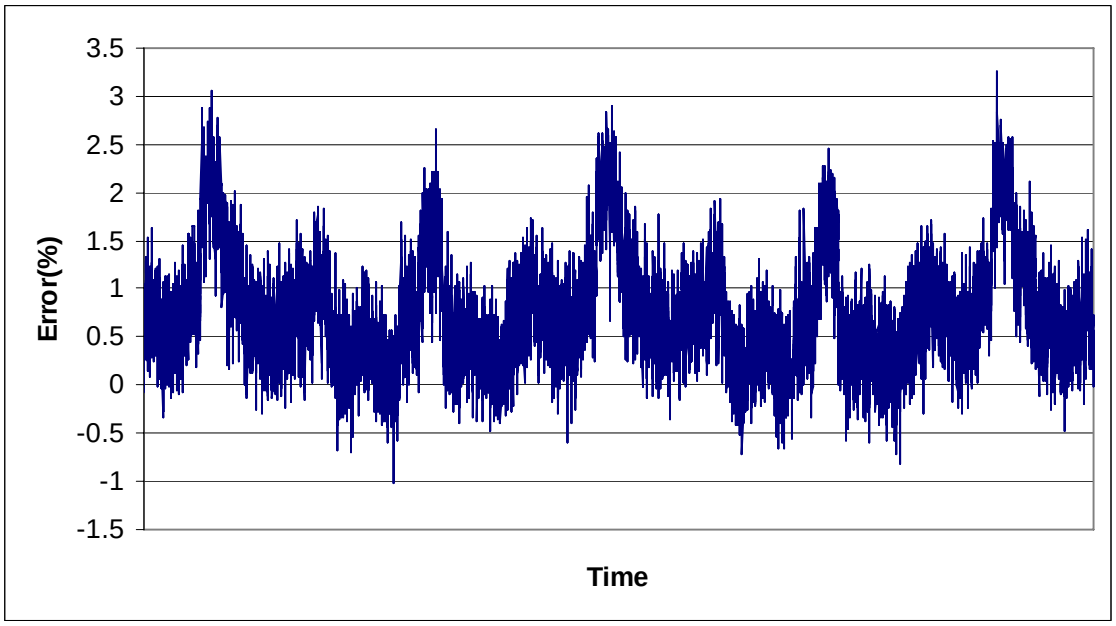

Figure 3.26 Error between magnetic PT and OPT at rated voltage

Figure 3.26 demonstrates the difference or error between the magnetic and optical CT output at rated voltage of 40 kV. The amplitude error is less then 3.5%. The phase difference is 42 μs, which corresponds to 0.9 degrees. The phase shift is acceptable, but the amplitude difference is relatively large.

4 Task #3: Investigation of the Steady State and Transient Response of the Two System

In order to evaluate the transient performance of the optical instrument transformers, tests have been performed at ASU's high voltage laboratory using separate voltage and current source. Short-circuited current transformers that are supplied by a regulating transformer at the low current side generated the high current. This circuit supplied the optical current sensor or CT with high current. The switching of the circuit simulated transients is caused by a short circuit.

A high voltage test transformer supplied voltage to the optical voltage sensor or the PT. The switching of this circuit simulated the voltage transients generated by a short circuit.

AEP installed a magnetic and optical system on the Corridor Substation. This system operated for two years. The performance of the optical system in the field was evaluated by analyzing the system performance during faults. The data measured by both systems were downloaded and analyzed.

4.1 Transient Response of Current Transformers

The optical and magnetic CTs were supplied by a simulated short circuit current with DC bias in order to compare the responses of the two systems. The effect of DC bias was

simulated by switching the DC current to the OCT. The frequency response of the OCT was also determined.

4.1.1 Reproduction of Short Circuit Current

The true reproduction of the short circuit current with its DC component is very important for the proper operation of the network protection relays. A solid state relay switched on the current generator to produce transient current is similar to the short circuit produced current.

The transient short circuit current was recorded simultaneously using both magnetic CT and optical CT. The obtained current waves were scaled using 1 V= 1600 A for magnetic CT and 1 V=1000 A for OTC. The optical CT was in protection mode.

Figure 4.1 shows the recorded magnetic and optical CT short circuit currents, and the difference of the two currents when the switch operated at the maximum voltage (90 degree phase shift).

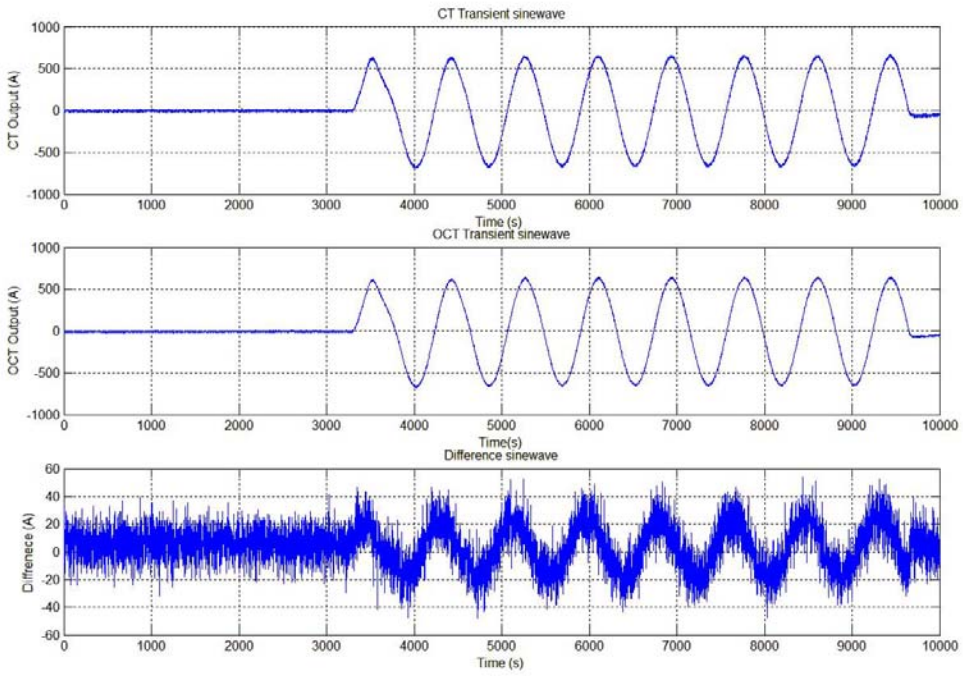

Figure 4.1 Transient short circuit current when the switching occurred at 90 degree voltage

The DC component on Figure 4.1 is relatively small.

Figure 4.2 shows the same waves, when the switching was initiated at zero voltage.

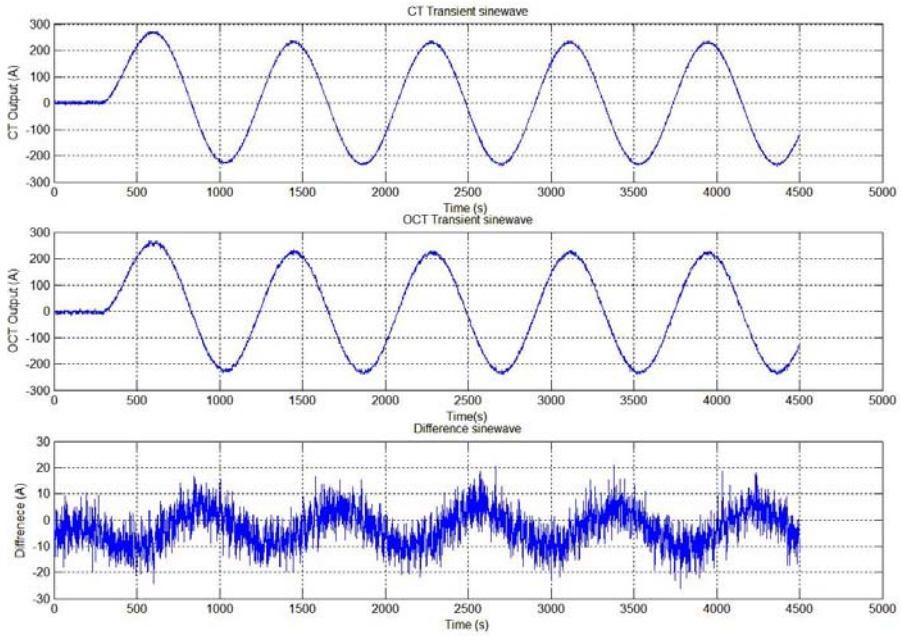

Figure 4.2 Transient short circuit current when the switching occurred at voltage zero

The comparison of magnetic and optical CT recorded peak short circuit currents shows that for zero crossing switching, the maximum current for magnetic CT is 272 A (I_{max}) and for optical CT it is 266 A (I_{max}). This difference is 1.1%.

The comparison of the two curves shows small phase difference between the magnetic and OCT measured current.

For 90^0 switching, the maximum current level for magnetic CT is 672 A (I_{max}) and for OCT it is 648 A (I_{max}). This difference is 2.3%.

Figure 4.3 shows the actual short circuit current on the American Electric power system. This current was recorded on 2005 January 11 at 20.00 hours. Load current was around 120 A; the fault increased the current five times, and the peak current was around 600 A. The figure shows a fast attenuating DC current component. In the first cycle the positive peak is around 600 A and the negative peak is around 250 A.

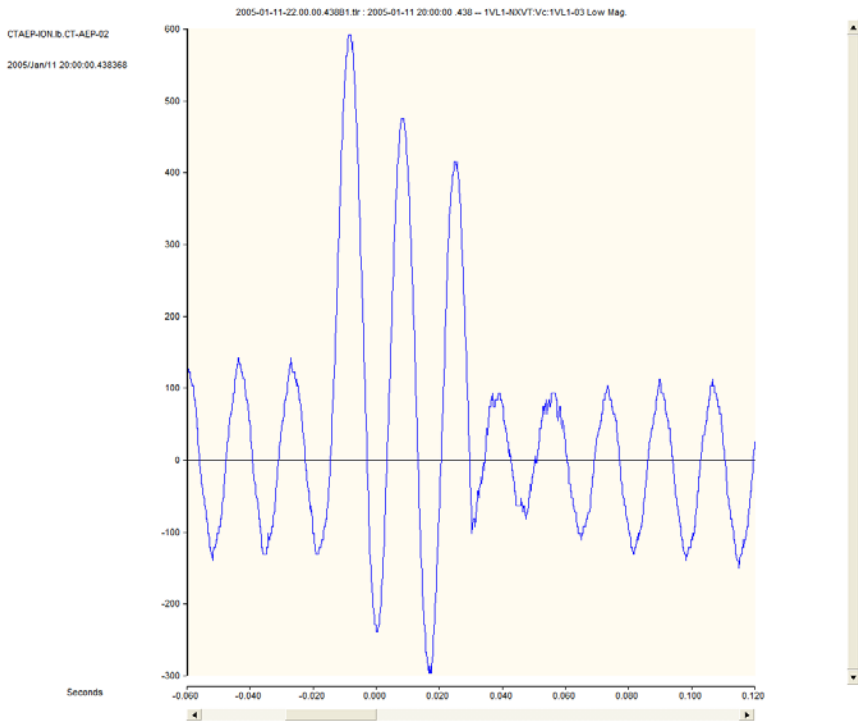

Figure 4.3 Typical recorded fault current

The comparison of Figure 4.1, Figure 4.2 and Figure 4.3, shows that our simulated waveform is different. In order to improve the simulation the current generator was modified by adding a second current injection circuit.

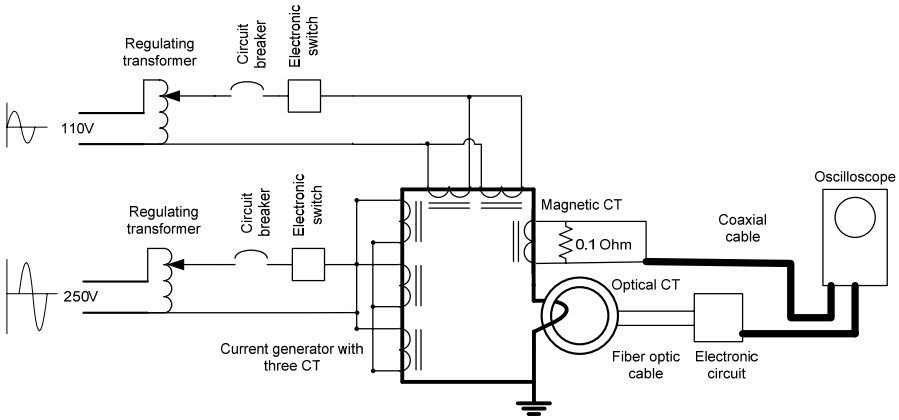

Figure 4.4 Short circuit simulation test setup

Figure 4.4 shows the modified circuit. In this circuit two 800 A / 5 A current transformers and three 600 A / 5 A current transformers are supplied by a regulating transformer in order to generate current over the close loop conductor. The two 800 A / 5 A current transformers produced the 50 A load current. This current always flows in the circuit after the electronic switch is closed. The three 600 A / 5 A current transformers are

connected also parallel but supplied by 250 V line to line voltages. These transformers generate the fault current, which has a phase shift from load current. The closing of the manual switch initiates the load current; the operation of the electronic switch produces the fault current. The duration of the fault current can be adjusted by the electronic switch between 2 to 20 cycles. After the desired duration, the electronic switch switches off the fault current, but the load current flows continuously.

Figure 4.5 shows the recorded currents from the test setup. Load current was 50 A while the fault current was 300 A.

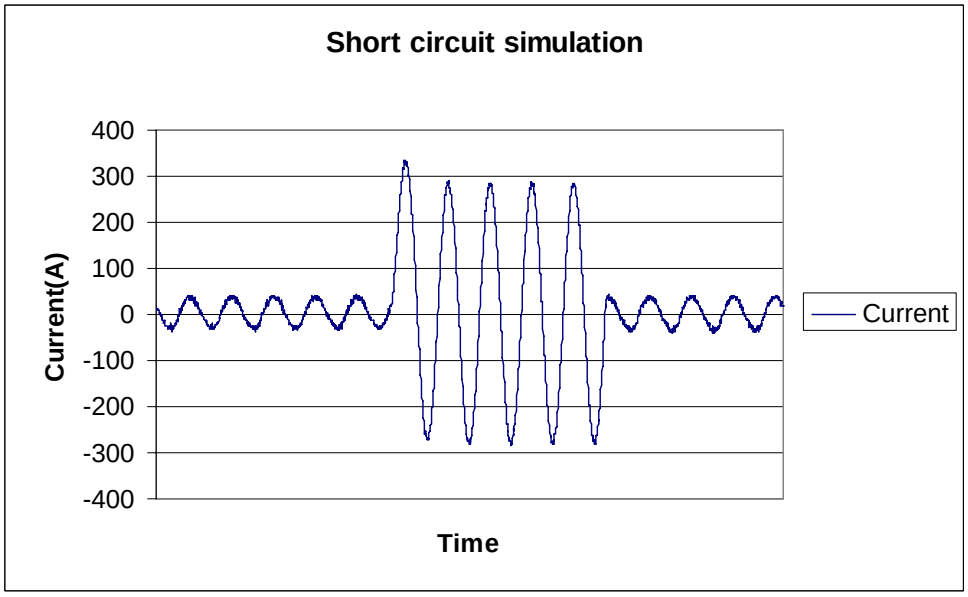

Figure 4.5 Simulated fault current

The comparison of Figure 4.3 and Figure 4.5 shows similarity although the DC component in Figure 4.5 is less than in Figure 4.3.

Both CTs were tested using the circuit in Figure 4.4. Around 50 A load current and around 600 A (peak-to-peak) short circuit current have been generated, and OCT output voltage and the voltage across the 0.1 ohm resistor connected to the secondary side of magnetic CT were recorded. A typical result is shown in Figure 4.6.

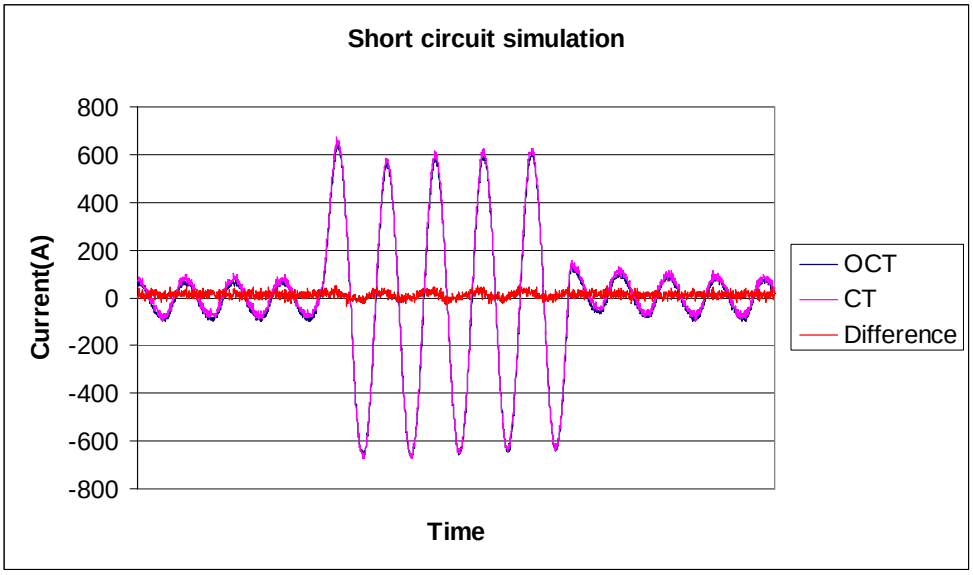

Figure 4.6 Short circuit simulations for CT and OCT

Results show that there is a small difference between the outputs. The magnetic CT output is slightly less than the optical CT output. The output of the OCT has more noise then the magnetic CT output. Table 4.1 shows the difference between the positive and negative peak currents. The measured 5% difference is not expected.

Table 4.1 Difference between peak currents

CT	Max: 640	Min: -668
OCT	Max: 672	Min:-672
Difference	Max: 5%	Min: 0.59%

4.1.2 Low Voltage DC Impulse Test

The reproduction of the short circuit generated DC current component is important; this initiated the testing of the OCT using low voltage DC current pulses. Figure 4.7 shows the test circuit.

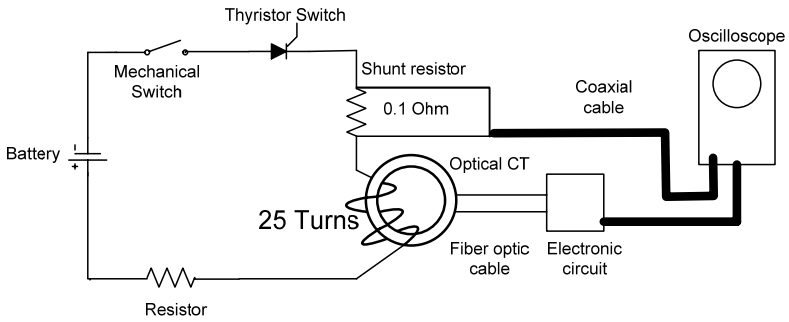

Figure 4.7 DC impulse test setup

A thyristor switch connected a 12 V battery to the OCT circuit. The current was measured using a 0.1 ohm shunt. This generated a 2.5 A current pulse. To increase the current effect, 25 turns of conductor was thread through the OCT sensor head. The equivalent OCT current was 62.5 A. The test was repeated 5 times, for both polarities. A typical test result is shown in Figure 4.8.

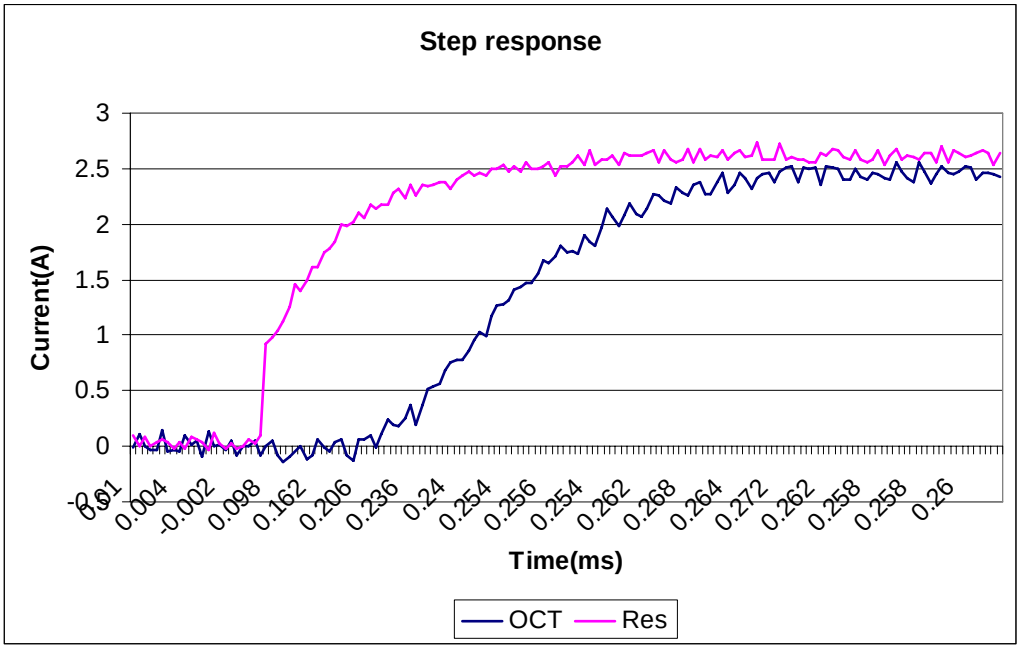

Figure 4.8 DC test results

Figure 4.8 shows that the OCT delays the current impulse by 68.67 µs and increases the rise time of the pulse from 74.99 µs to 96µs. The raise time is defined as the time required for the pulse to increases from 0.1 I_{max} to 0.9 I_{max}.

The current was increased to 20 A, which is equivalent to 500 A in the OCT. The results were similar. No saturation was observed.

The magnetic CT was not tested because the literature indicates that even small current produce saturation.

4.1.3 Temperature Effect

The literature survey showed that the Faraday Effect is temperature sensitive and the manufacturers of OCTs compensate for the temperature effect by the electronic circuit. The OCT sensor head was heated with an electric heater. The temperature was recorded using thermocouples. The system was loaded by 392 A. The load current was maintained constant. The temperature was increased and the output voltage of the OCT was recorded at different temperature values.

The results were tabulated in Table 4.2 and plotted on Figure 4.9.

Table 4.2 Temperature effect on OCT

Temp (^{o}C)	OCT (mV)	OCT (A)
23.5	392	392
27.5	392	392
30	391	391
39.8	393	393
43.5	393	393
47.3	390	390

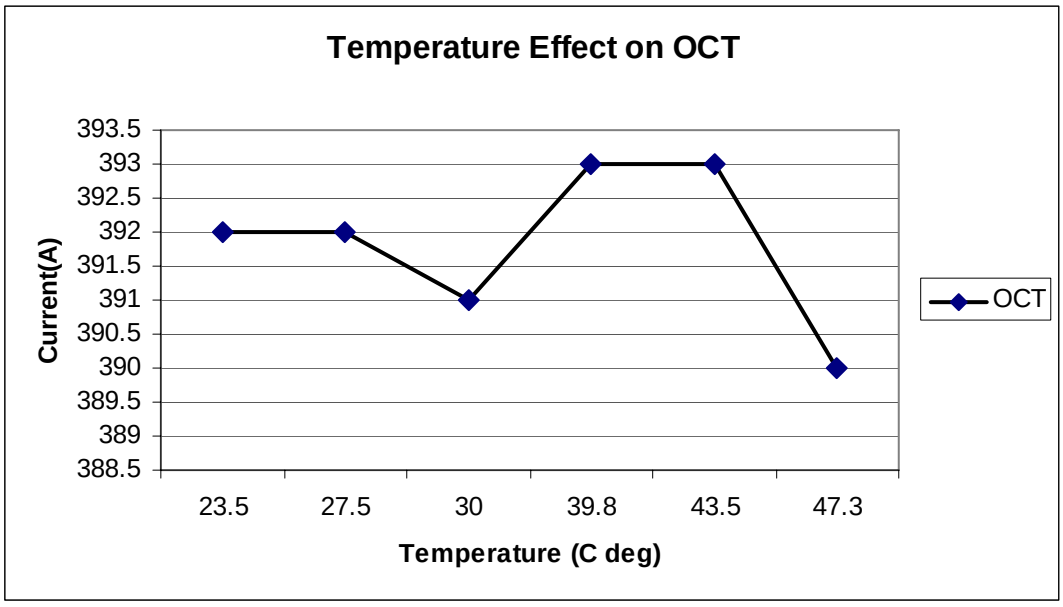

Figure 4.9 Temperature effect on optical CT reading

The result in case of OCT shows no consistent changes as a result of the temperature. The maximum deviation from the nominal 392 A is less than 0.55%, which is acceptable.

These cursory test results proved that the manufacturer applied an efficient temperature compensation technique.

4.1.4 Measurement of OCT Frequency Characteristics

One of the advantages of the OCT is that it has a better frequency response. According to the manufacturer, the OCT analog output has a built in 40 microsecond delay and a low pass filter with a cutoff frequency at 6 kHz. The OCT output above 20 kHz is almost zero. In order to verify the manufacturer specifications, the frequency response of the OCT has been measured. These measurement data are used for the development of the OCT analog electrical model.

The OCT was supplied by a variable frequency current. The input current and the output voltage were measured and compared. Figure 4.10 shows the experimental set up.

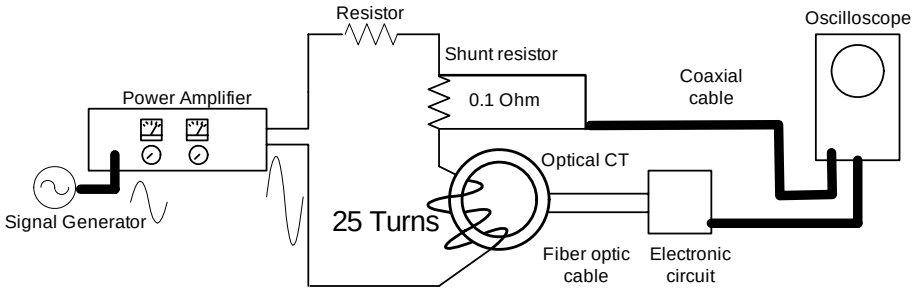

Figure 4.10 Frequency response experimental test setup

A signal generator, with 0 Hz to 1 MHz frequency range, has been used as a signal source. The variable frequency output voltage of the signal generator was amplified by a 1000 W stereo amplifier.

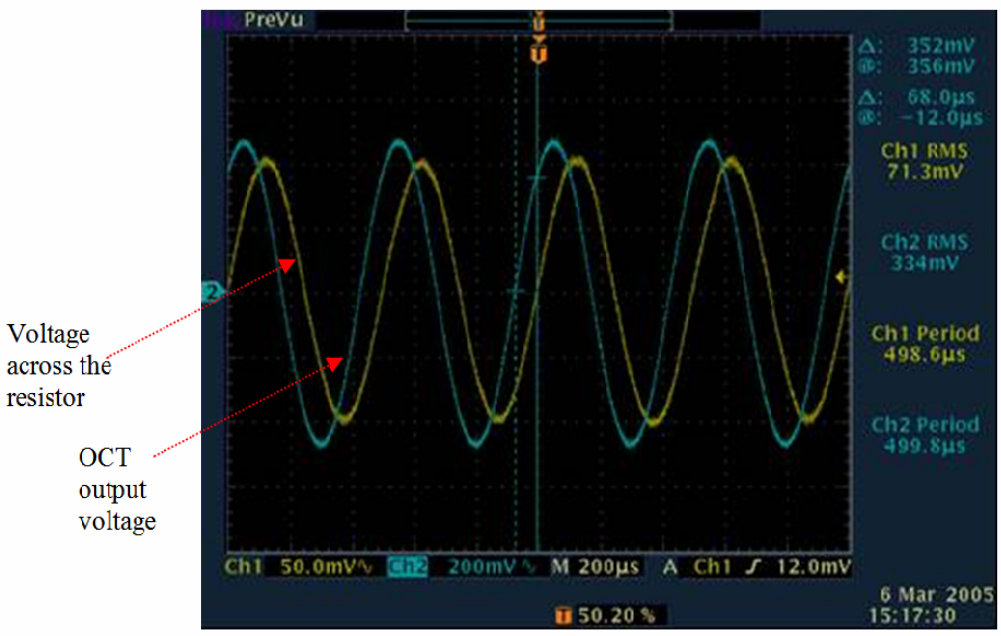

Figure 4.11 Current and OCT signals at 2 kHz

The stereo amplifier was set up to mono-mode and it supplies a current loop, which has 25 turns through the Optical Current Transformer. In addition, the loop contains a 4.8 ohm limiting resistance and a 0.1 ohm measuring resistance. The power amplifier drives around 4 A current through the loop, this corresponds to 25 x 4 ≅ 100 A. The frequency of the current was varied between 60 Hz ~ 16.8 kHz. Current in the loop was measured using voltage across the shunt resistance of 0.1 ohm as an input 2 of a Tectonics digital oscilloscope. The other channel input 1 has been used to measure the output voltage of the OCT. Figure 4.11 shows the input current and OCT output voltage at 2 kHz frequency.

The loop current was kept constant while the frequency was varied in steps of twelve. The waveforms of both signals were recorded simultaneously. The RMS values were manually recorded using the digital oscilloscope provided data. The phase difference corresponding to the time difference between the zero crossings of the signals were determined and converted to degrees. Figure 4.12 shows the signals at 4 kHz and demonstrates the method used for phase angle calculation. Digital oscilloscope noise filter has been used during this measurement to reduce the inherent output noise of the OCT signal.

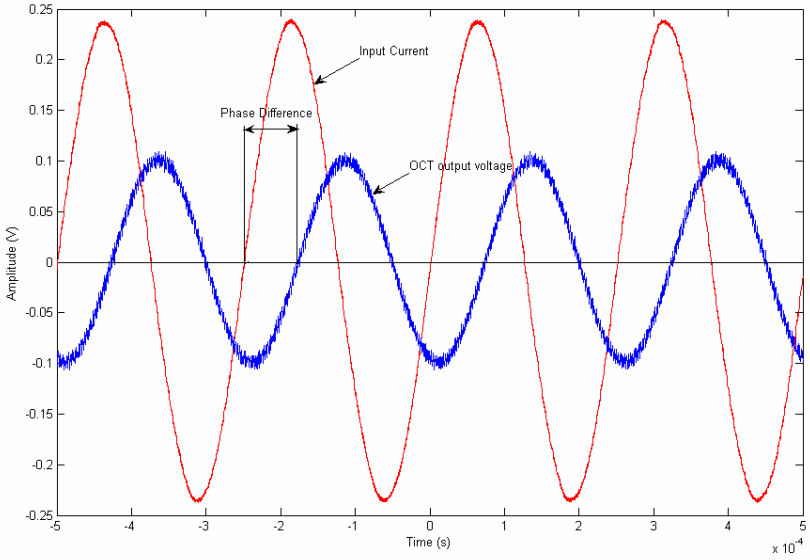

Figure 4.12 Input current and OCT output signals at 4 kHz

Figure 4.12 shows that the OCT output is lagging and the phase difference is 72.6 µs. This phase difference is converted to an angle by using the equation below

$$\frac{72.6\times10^{-6}\times360}{\frac{1}{4000}}=104.54^{0}$$

Table 4.3 shows the results of the measurements and calculated phase differences.

Table 4.3 Frequency characteristics of the OCT test results

Freq(Hz)	OCT (mV)	Current (A)	Resistor Voltage (mV)	Loop Current (A)	Normalized Amplitude	Phase Diff (µs)	Lagging	Phase (deg)
60	92.1	3.684	438	4.38	1	40	OCT	-0.86
300	91.37	3.6548	437	4.37	0.992074	72	OCT	-7.78
1000	89.64	3.5856	437	4.37	0.971343	70	OCT	-25.20
2000	85.13	3.4052	437	4.37	0.924321	72.8	OCT	-52.42
4000	70.47	2.8188	437	4.37	0.763616	72.6	OCT	-104.54
6000	55.53	2.2212	437	4.37	0.601726	69.2	OCT	-149.47
7670	43.44	1.7376	437	4.37	0.466982	65.6	Current	-181.13
8200	40.17	1.6068	435	4.35	0.435284	55.2	Current	-197.05
10000	30.92	1.2368	438	4.38	0.335722	38	Current	-223.20
12000	22.48	0.8992	438	4.38	0.242624	23.2	Current	-259.78
14000	16.68	0.6672	437	4.37	0.181836	11.6	Current	-301.54
16800	11.51	0.4604	436	4.36	0.137844	1	NO diff	-353.95

Using the data in Table 4.3, the normalized amplitude-frequency and phase angle-frequency characteristics of the optical CT have been plotted in Figure 4.13 and Figure 4.14 respectively.

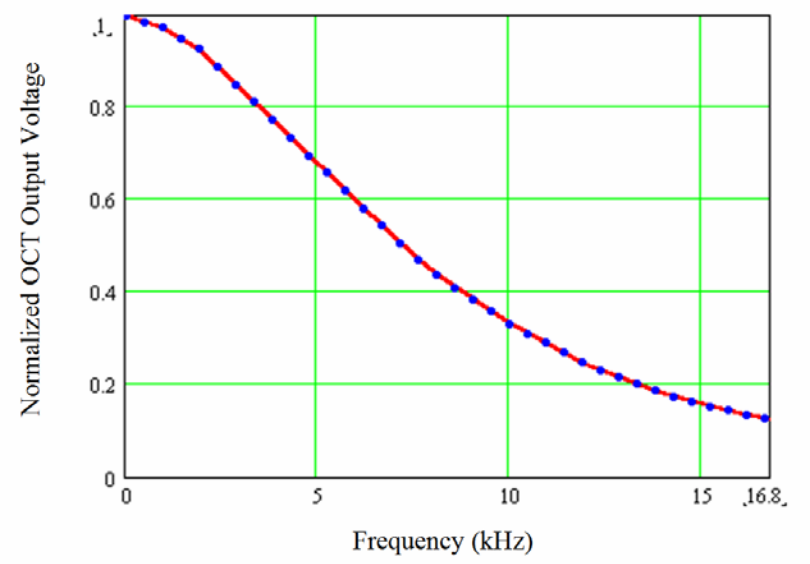

Figure 4.13 Normalized amplitude-frequency characteristics of OCT

The phase shift at 60 Hz was 40 μs, which corresponds to ~1 degree. According the manufacturer, 27 μs of 40 μs delay is due to the 6 kHz analog filter and 13 μs of 40 μs delay is due to the transit time of the light and the digital signal processing.

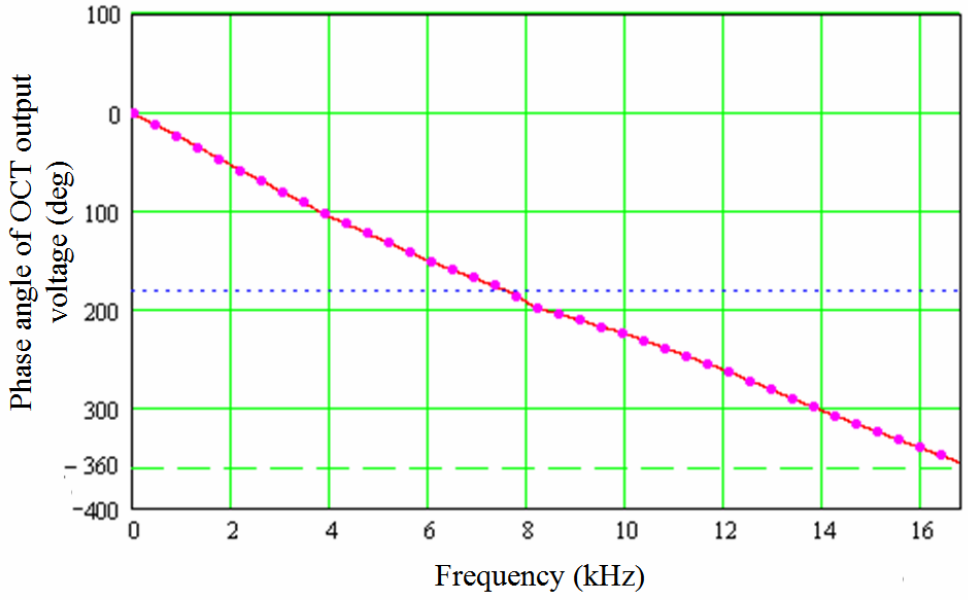

Figure 4.14 Phase angle-frequency characteristics of OCT

The observation of the amplitude-frequency characteristics suggests that the OCT frequency response can be duplicated by using a low-pass filter.

The observation of the phase angle-frequency characteristics suggests that the OCT frequency response can be duplicated by using a sixth order low-pass filter.

4.1.5 Electrical Circuit Model for OCT

The OCT input is the primary current and the output is a voltage signal. The scale is: 1000 A corresponds to 1 V. The required amplitude and phase angle frequency characteristics are shown in Figure 4.13 and Figure 4.14 respectively. We developed a circuit model for the optical CT. Figure 4.15 shows the connection diagram of the model.

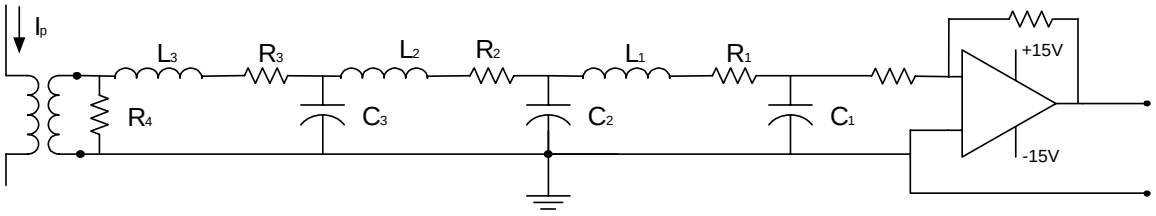

Figure 4.15 Electrical circuit model for OCT

An ideal transformer reduces the 1000 A input current to 1 A. The terminating 1 ohm resistance converts the 1 A current to 1 V voltage. This voltage supplies a six order low pass filter. The 1 ohm terminating resistance produces a low impedance source for the filter. The filter input impedance will be in the kΩ range. The operation amplifier permits the loading of the system with the appropriate burden résistance.

The performance of the model was analyzed by first calculating the circuit input impedance. This is followed by the calculation of the input current and the voltages across the shunt elements. Appendix 1 presents the analysis of the OCT electrical circuit model. The model operation was verified by PSPICE simulation program.

Figure 4.16 presents the amplitude-frequency characteristics and Figure 4.17 the phase angle-frequency characteristics of the model.

The performance of the model is compared with the measured values. Figure 4.16 shows the deviation between the measured and model-generated signals which is less than 5%.

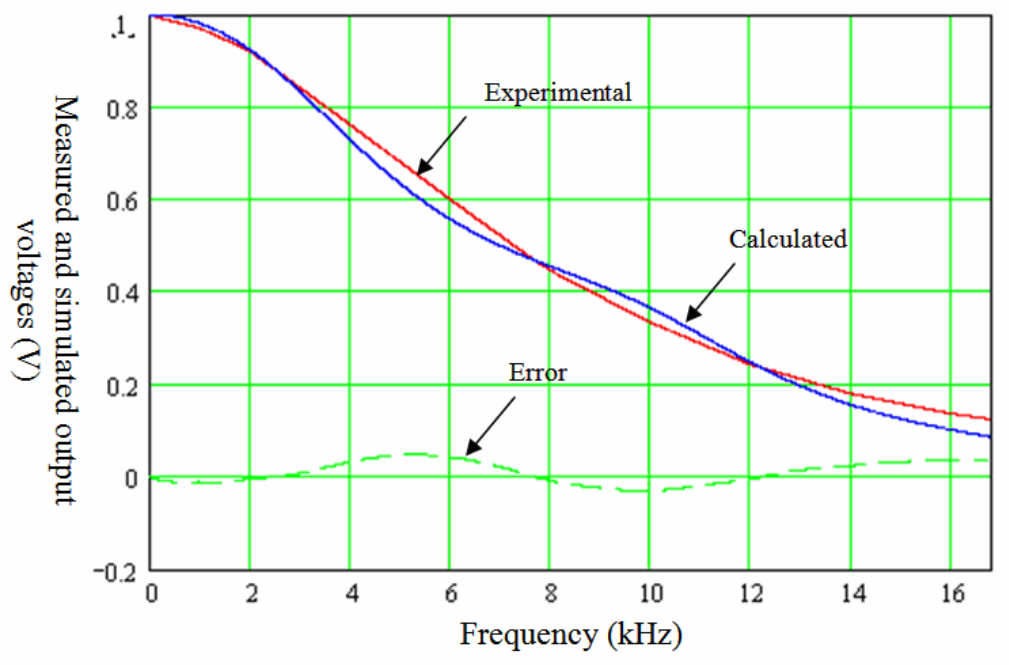

Figure 4.16 Comparisons of circuit model amplitude frequency characteristics with the measured values.

Figure 4.17 presents the phase angle-frequency characteristics of the model. The performance of the model is compared with the measured values. The figure shows that the system moves from inductive to capacitive at 180 degrees. During the transition, the error is infinite as a result because of division by zero or close to zero number. Disregarding the transition intervals, the error is less than 10%.

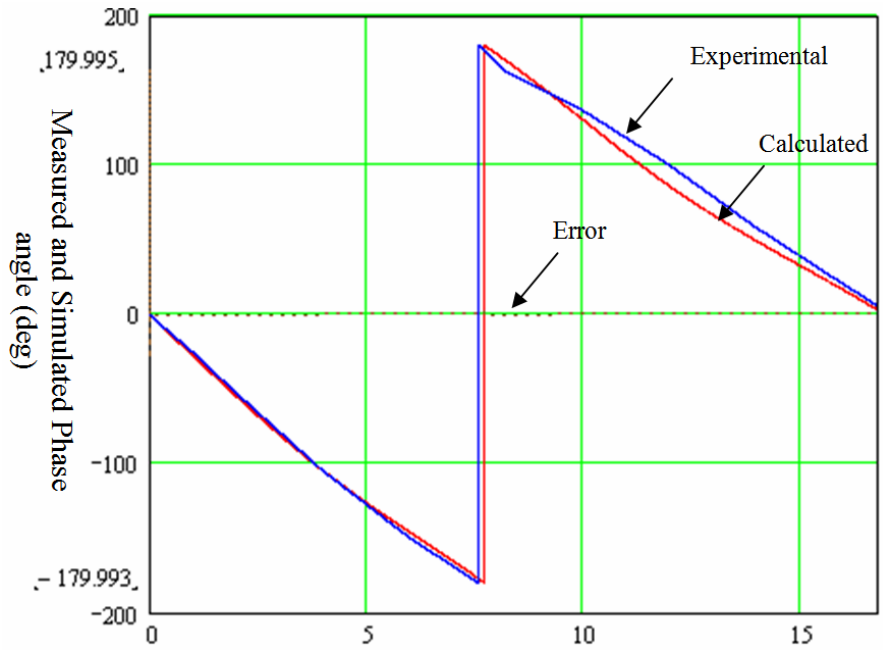

Figure 4.17 Comparisons of circuit model phase-angle frequency characteristics with the measured values.

The results proved that the developed model represents the optical current transformer with sufficient accuracy. It is visualized that the variation of model parameters permits the modeling of optical current transformers developed by other companies.

4.1.6 Verification of the Model by PSPICE Simulation

PSPICE simulation programs have been used to investigate the behavior of the electrical circuit model of the OCT in an analog electrical circuit. Figure 4.18 shows the circuit diagram that was used for the simulation. The ideal amplifier is not represented in this circuit.

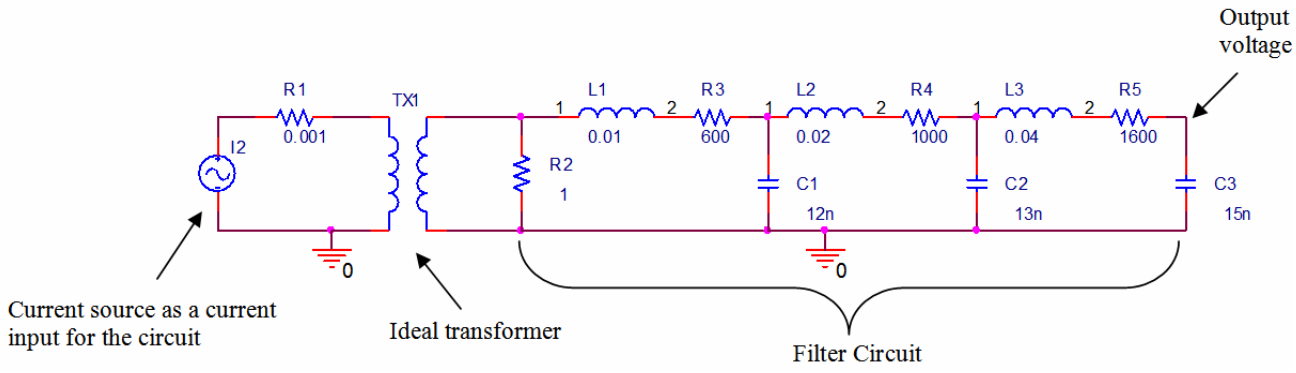

Figure 4.18 PSPICE circuit model

The circuit contains a current source, ideal transformer, and a low pass filter. The input current was 1000 A and the frequency changed stepwise from 60 Hz to 20 kHz. The output of the filter was not loaded.

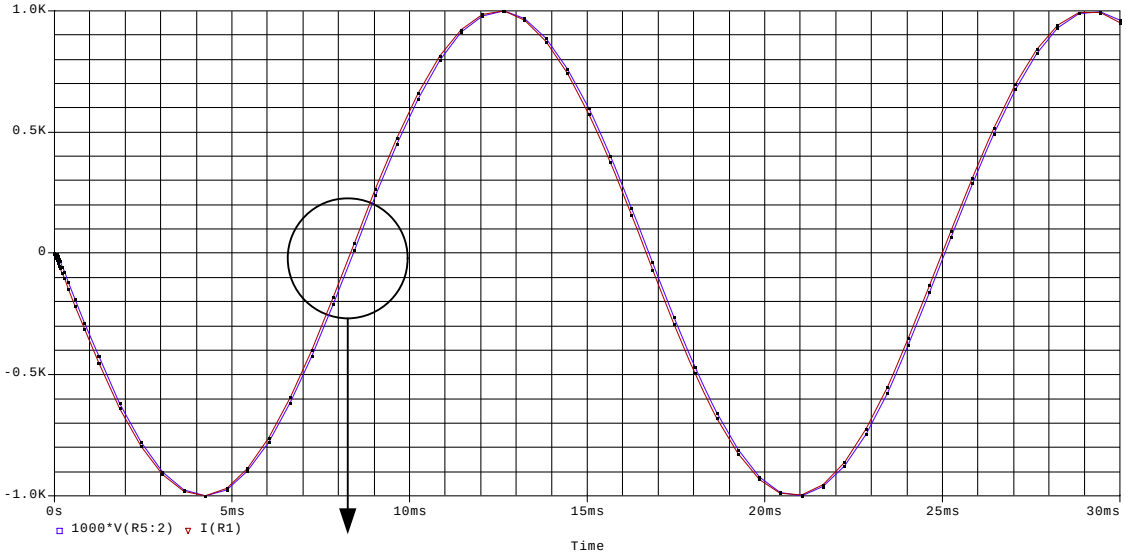

Figure 4.19 60 Hz Steady State

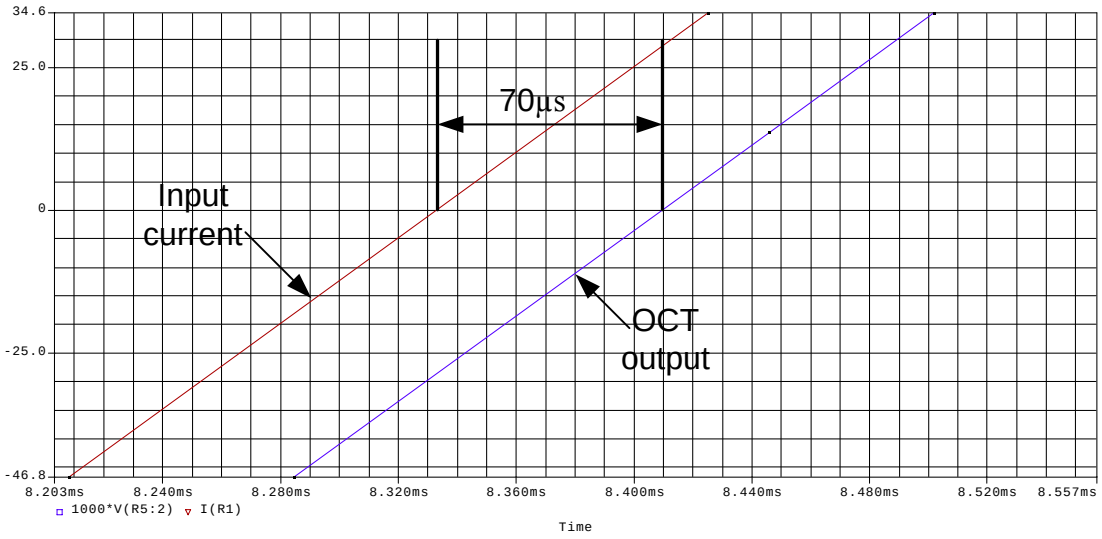

Figure 4.20 60 Hz Steady State phase difference

Figure 4.19 shows the input current and the simulated output voltage at 60 Hz. The peak amplitude error is zero, but a small phase shift can be observed on Figure 4.19. This was enlarged at Figure 4.20. The phase difference is 70 µs where the measured delay was 40 µs.

It can be seen that there is a difference between the two graphs which is negligible. This shows that the developed model can be used as an electrical model for OCT. The ATP model description and the results are also presented below.

ATP source data

```
BEGIN NEW DATA CASE
C --+----1----+----2----+----3----+----4----+----5----+----6----+----7----+----8
C DELTAT    TMAX    XOPT    COPT  EPSILN  TOLMAT
   .9E-5   3.E-2       0       0  1.0E-8  1.0E-8
C   IOUT   IPLOT  IDOUBL  KSSOUT  MAXOUT    IPUN  MEMSAV    ICAT  NENERG  IPRSUP
     10      20       1               1       0       0       1       0       0
C --+----1----+----2----+----3----+----4----+----5----+----6----+----7----+----8
C  TRANSFORMER
C Bus1->Bus2->Bus3->Bus4-><----R<----L<----C
    T1A   T2A            .001                                      3
    T3A   T4A             600.  10.                                3
    T4A   T5A            1000.  20.                                3
    T5A   T6A            1600.  40.                                3
    T3A                  1.                                        3
    T4A                        12.E-3                              3
    T5A                        13.E-3                              3
    T6A                        15.E-3                              3
C ..................... Saturable Transformer (Single Phase) .....................
C ----------->Bus3->Bus4-><----><--Iss<PhissBusSt><-Rmag<--------------------------->O
C TRANSFORMER             215.28 63.66FICBUS   0                          3
  TRANSFORMER            0.00010.0001FICBUS
C -------Current<-----------Flux Saturation Curve Data
  0.0001         0.0001
          9999
C --+----1----+----2----+----3----+----4----+----5----+----6----+----7----+----8
C Bus1->Bus2-><----------><---Rk<---Lk<VBase Winding Cards
 1   T3A                .00001.000011.E3
 2   T2A                .00001.000011.E0
BLANK card ends all branch cards
C  ****************************************
C  *      SWITCH CARDS                    *
C  ****************************************
C --+----1----+----2----+----3----+----4----+----5----+----6----+----7----+----8
C Bus1->Bus2->
C BUS0N1BUS0N2      -2.0   15.
C     S1A   T1A -2.0    10.            0.0
BLANK card ends all switch cards
C  ****************************************
C  *      SOURCE CARDS                    *
C  ****************************************
C --+----1----+----2----+----3----+----4----+----5----+----6----+----7----+----8
C Bus--><I<Amplitude<Frequency<--T0|Phi0<---0=Phi0         <----Tstart<----Tstop
C    BUS    VOLTAGE  FREQUENCY ANGLE(DEG                  TSTART
14   T1A-11000.      60.      0.0                        -1.0
BLANK card ending source cards
C ..................... Output Request Data .....................
C --+----1----+----2----+----3----+----4----+----5----+----6----+----7----+----8
C Bus-->Bus-->Bus-->Bus-->Bus-->Bus-->Bus-->Bus-->Bus-->Bus-->Bus-->Bus-->Bus-->
    T1A   T2A
    T1A   T2A   T3A   T4A   T5A   T6A
    T5A   T6A
BLANK end output variable requests
  PRINTER PLOT
BLANK card terminating plot cards
BLANK card data case
```

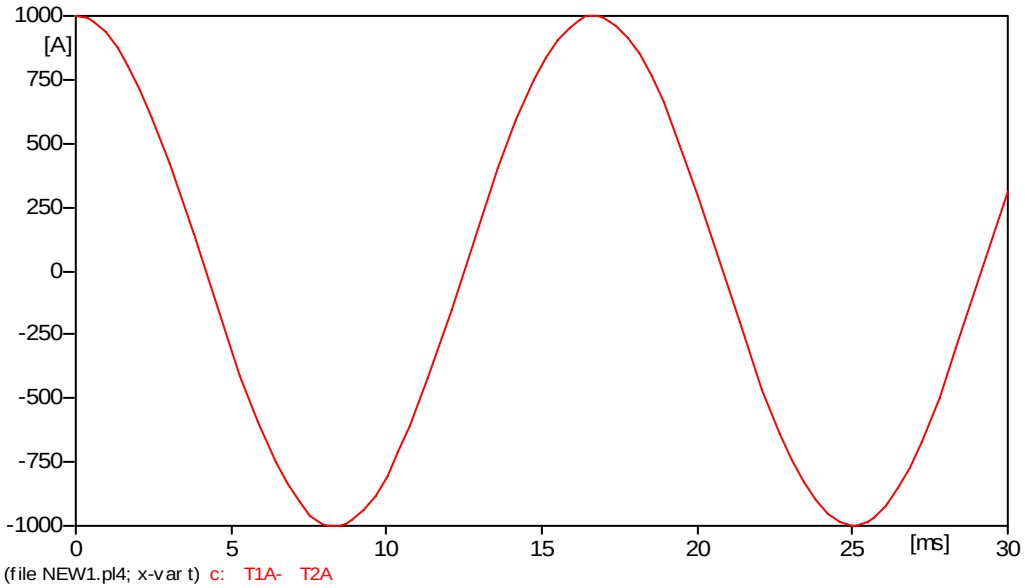

Figure 4.21 ATP simulation; input current

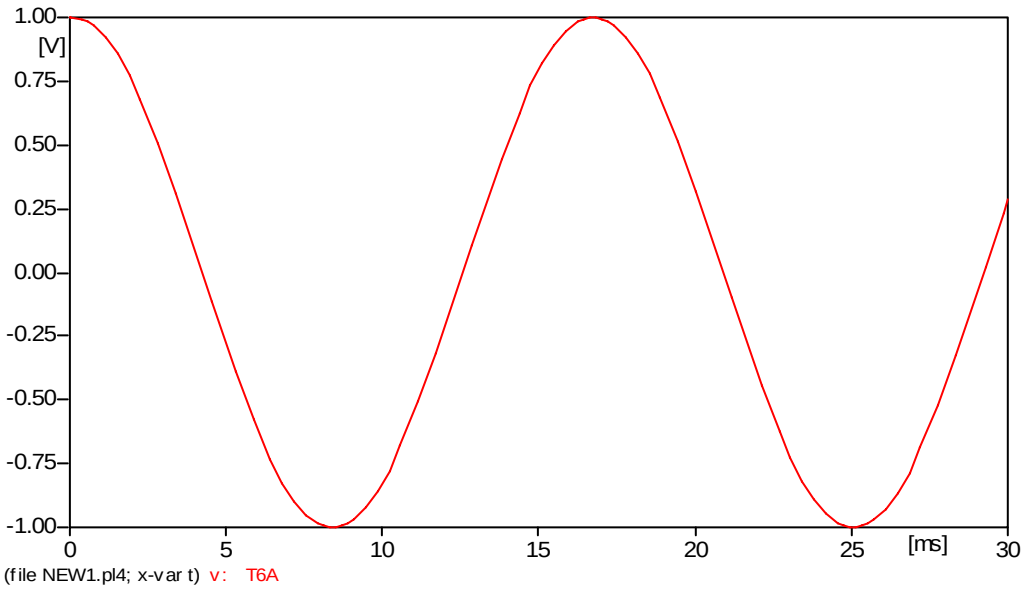

Figure 4.22 ATP simulation; output voltage

As shown in Figure 4.21 and Figure 4.22, ATP simulation also shows that the OCT electrical model has a 1 V output voltage for a 1000 A input current. However, the delay between input current and output voltage is 68 µs where the PSPICE simulation has 70 µs. This 2 µs difference can be negligible. Delay can be seen in Figure 4.23 below.

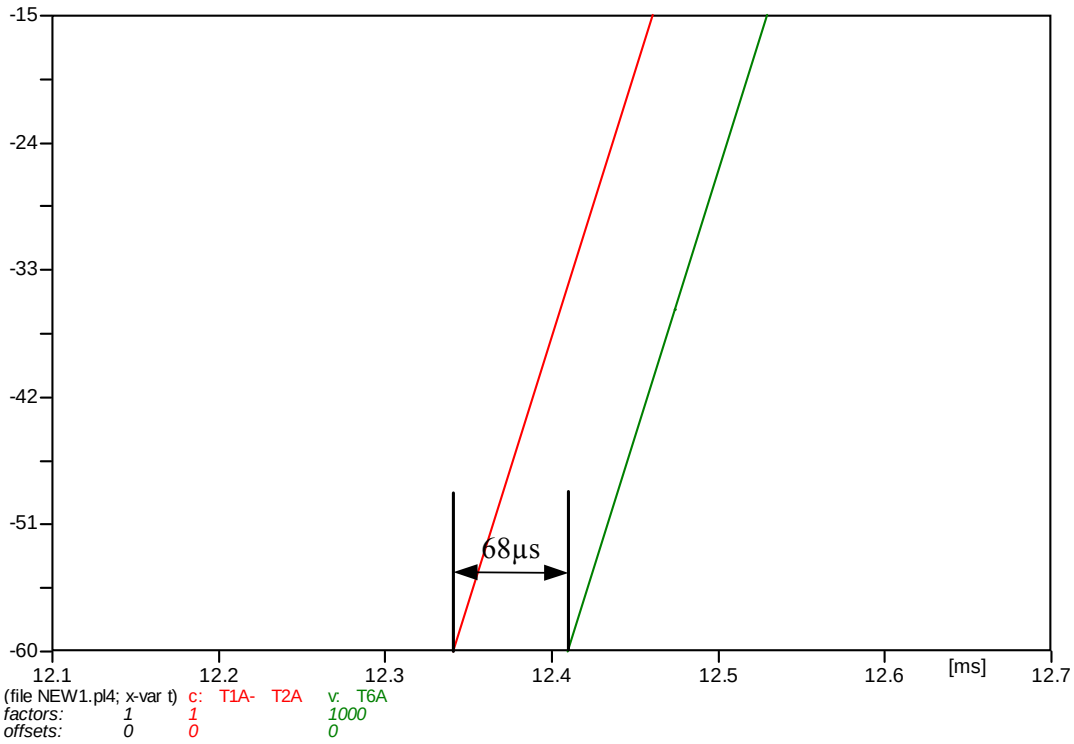

Figure 4.23 Phase delay

4.2 Transient Response of Voltage Transformers

NxtPhase provided a combined voltage and current transformer, and Salt River Project donated a 69 kV voltage transformer to ASU for the study. The response to transient impulse and switching type voltages were investigated.

4.2.1 Transient Analysis of PTs

The PT installed in the electric network is subjected to different transients. The most frequent is the lighting impulse generated during thunderstorms. The PT must withstand the lighting generated over voltages, but does not have to reproduce the voltage wave shape.

The switching on the network produces switching over voltages. The magnetic PT can not reproduce the switching type of over voltages accurately. The optical PT may be able to reproduce switching over voltages and this opens up new possibilities in the area of advanced network protection.

The short circuit in a network produces transient voltage dips. The results are distorted sine waves. The frequency band of these transients is few hundred Hz. The accurate reproduction of these transients is important because this voltage is used for network

time- varying impedance calculation and is utilized by the modern digital protection system.

The PTs response of fast varying voltages (lightning impulse) was investigated using an impulse test when the PT's response to the standard 1.2 µs /50 µs lighting impulse was measured. This was followed by the measurement of the frequency characteristic of the PTs.

4.2.1.1 Lightning Impulse Test of PT's

Standard 1.2 µs/50 µs impulse supplied the parallel connected magnetic and optical PTs. The impulse voltage was measured by an impulse voltage divider and digital oscilloscope. The response of the magnetic and optical PT was recorded with the same digital oscilloscope. The test was performed at 87 kV voltage level.

4.2.1.1.1 NXVT with HEA Output

Figure 4.24 shows the transient response of NXVT during the wave front. It can be seen that the fast-rising front of the lightning impulse produces a high frequency oscillation with peak amplitude over 250 kV. The actual voltage at the optical PT HEA output terminal was around 60 V. The electronic protection chopped the wave. This high-frequency, high- amplitude oscillation is expected to be due to the oscillation of the amplifier (including a wire-wound transformer) used to get HEA at high frequencies (fast rise time). The figure also shows that the lightning impulse rise time is around 1.2 µs.

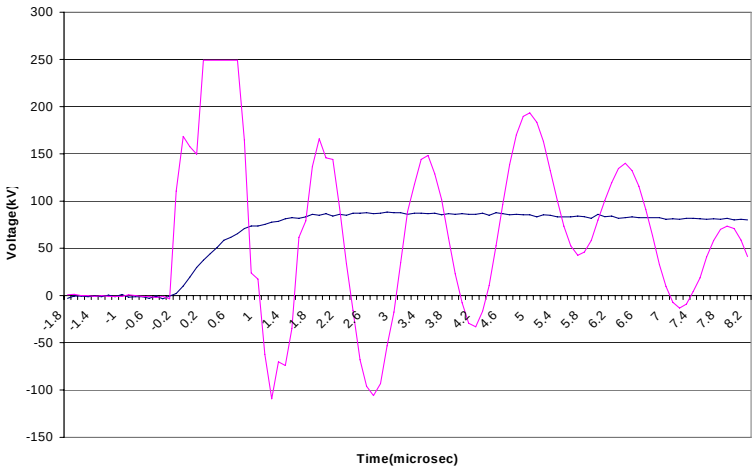

Figure 4.24 Optical PT response to lightning impulse HEA output

Figure 4.25 OPT impulse test HEA output shows the response of high energy (HEA) output on a longer time frame. It can be seen that the LEA output has large oscillation. We conclude that, as expected, this output does not reproduce the lightning impulse, which is a direct result of the frequency bandwidth of the HEA being restricted to 5 kHz.

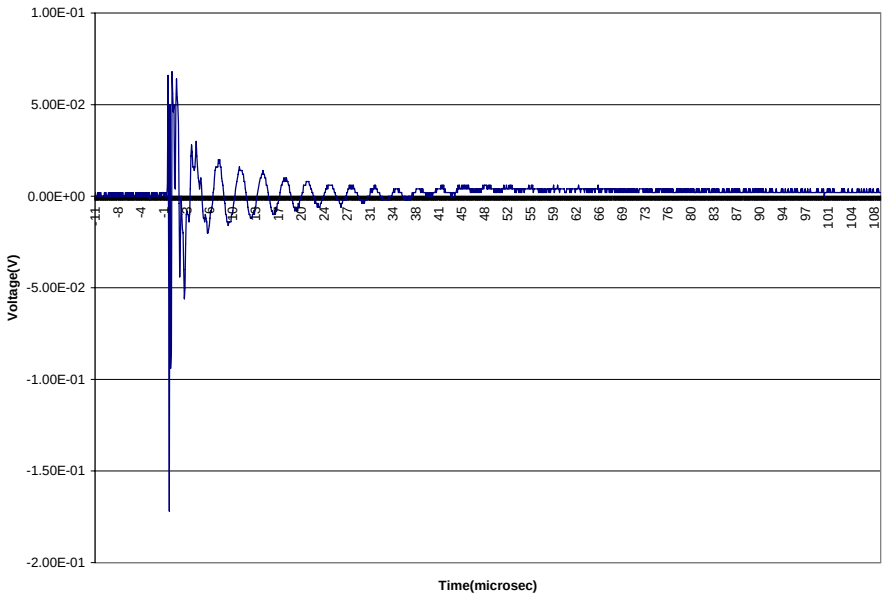

Figure 4.25 OPT impulse test HEA output

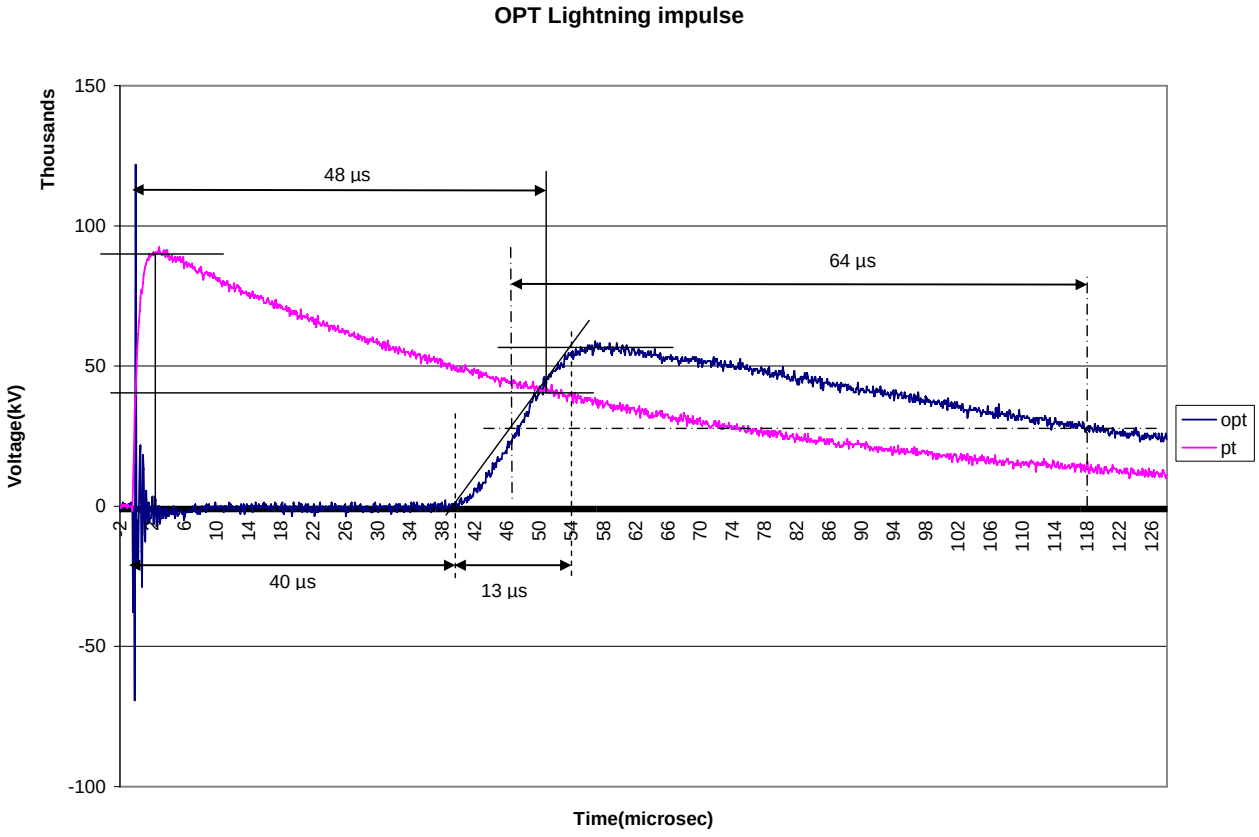

Figure 4.26 Optical PT lightning impulse test LEA output

4.2.1.1.2 NXVT with LEA Output

The test was repeated using the low energy analog (LEA) output of the NXVT. Figure 4.27 Lightning impulse test of magnetic PT shows that the optical PT delays the impulse by 40 μs as specified. A natural result of the bandwidth of the optical PT being 40 kHz is also that the rise time is increased from 1.2 μs to 13 μs. It can be seen that the half time of the pulse also increased from 50 μs to 68 μs. Considering the bandwidth of the optical PT electronics, it was not expected to reproduce the standard lightning impulse. Wider bandwidth electronics (>250 kHz) is required to capture the 1 μs rise time of the lightning impulse.

4.2.1.2 Magnetic PT Impulse Test

Figure 4.27 shows the magnetic transformer response to the 87 kV lightning impulse. The impulse produces large scale oscillation. No delay can be observed. The front time and half tine cannot be determined. In summary, as expected, the magnetic PT does not reproduce the impulse voltage.

The OPT has delay, as well as, but produces a lightning-type impulse with longer front and half time. This proves that the OPT bandwidth response is much better than the magnetic PT. The test results are consistent with equipment specification that the LEA output bandwidth is much greater than HEA output bandwidth and magnetic PT output bandwidth.

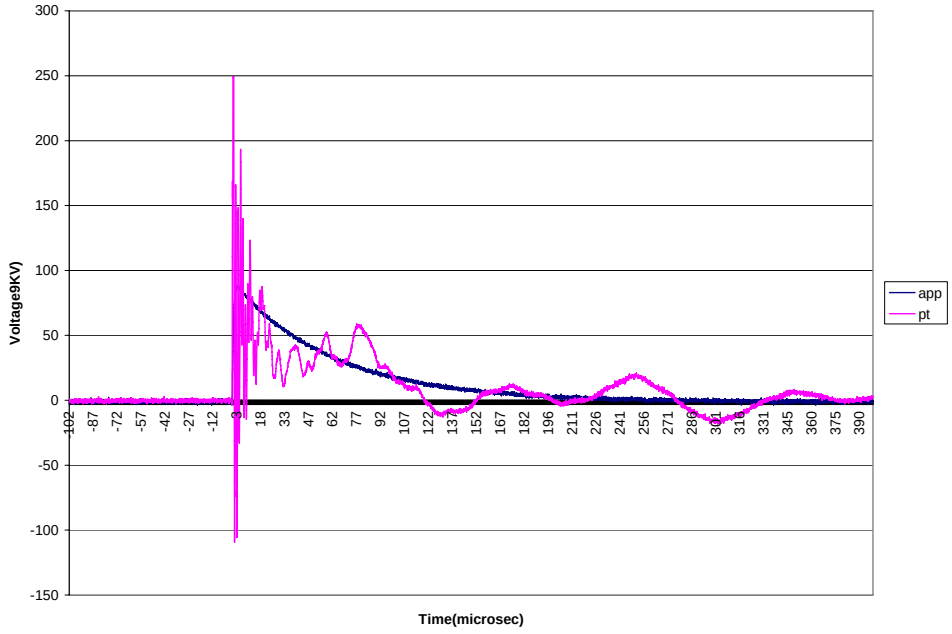

Figure 4.27 Lightning impulse test of magnetic PT

4.2.2 Frequency Characteristics of the PTs

According to the manufacturer and literature review, NXVT has a better frequency response than magnetic PT. Its bandwidth is 0.001 Hz to 40 kHz for LEA, and 20 Hz to 5 kHz for HEA, but it has a 40 microsecond delay. Digital phase compensation was used to set the phase displacement to 0 degrees at 60 Hz. In order to verify the specifications, frequency response of the NXVT has been measured at ASU's high-voltage laboratory. HEA output of the NXVT has been used for the test.

NXVT was supplied with a variable-frequency voltage. Applied voltage and NXVT output voltages were measured and recorded in order to make the comparison. The test setup can be seen in Figure 4.28.

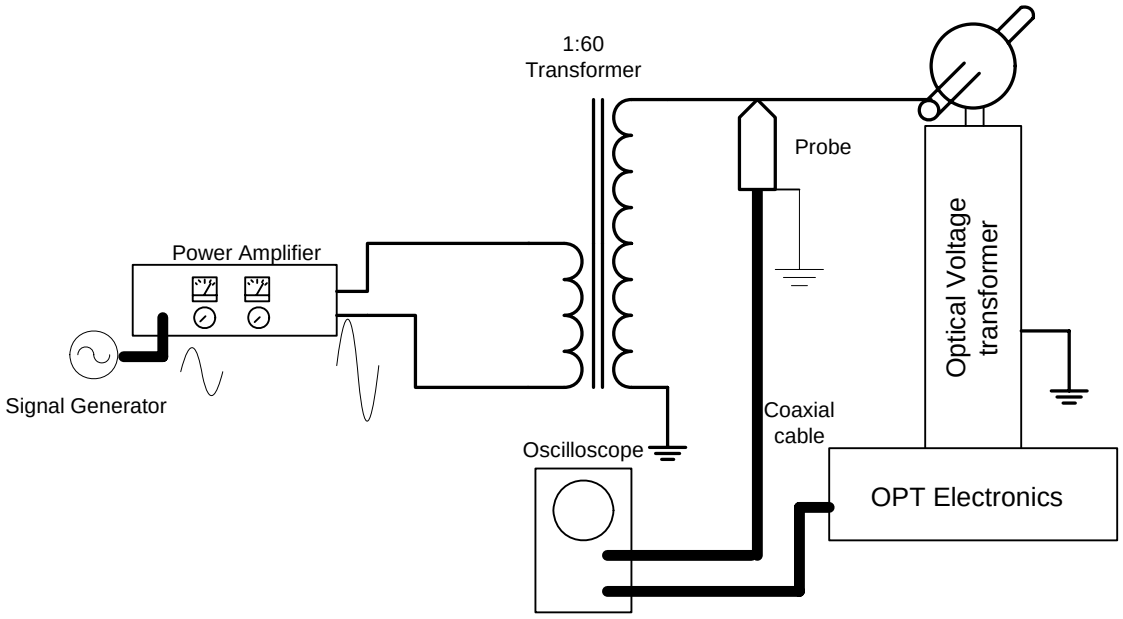

Figure 4.28 NXVT Frequency response test setup

A signal generator, with a 0 Hz to 1 MHz frequency range, has been used as a signal source. The variable-frequency output voltage of the signal generator was amplified by a 1000 W stereo amplifier. The stereo amplifier was set to mono-mode and it supplied 1:60 ratio of voltage transformer. The secondary side of the transformer was connected to the NXVT. The power amplifier drives around 35 V voltages through the transformer; this corresponds to 35x60 ≅ 2100 V. The frequency of the voltage was varied between 60 Hz ~ 20 kHz. The applied voltage was measured with a 1000:1 high voltage Tectonics probe at the secondary side of the 1:60 transformer. The probe was connected to the Tectonics digital oscilloscope as a channel 2. The other channel, input 1, has been used to measure the output voltage of the NXVT. Figure 4.29 shows the applied voltage and NXVT output voltage at 3 kHz frequency. The accuracy of the Tectonics probe and oscilloscope is > 2%

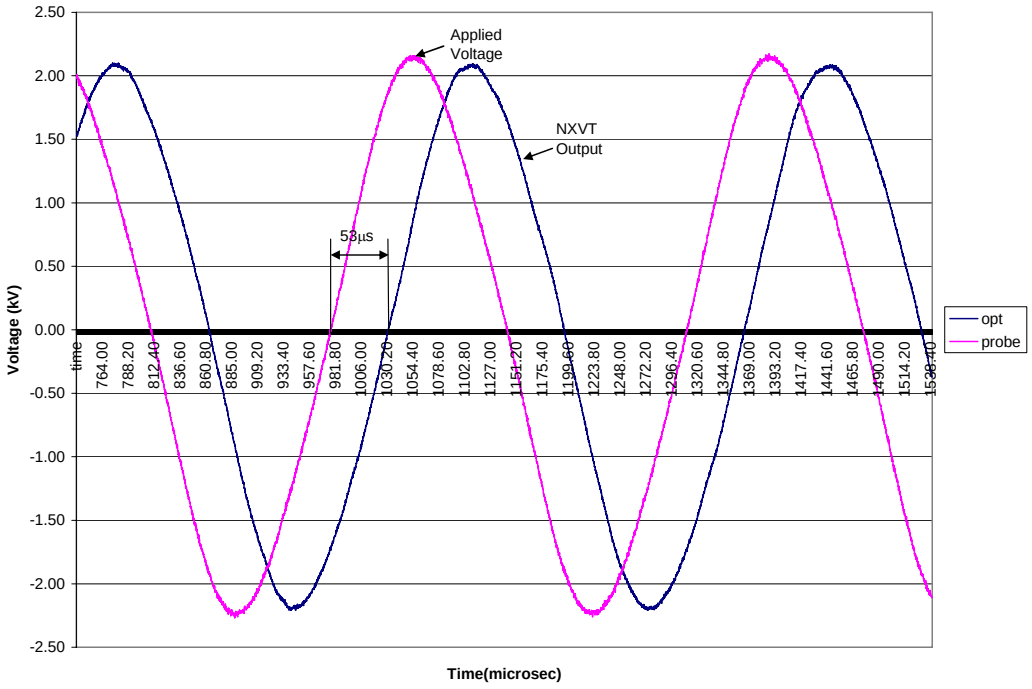

Figure 4.29 Applied voltage and NXVT output voltage at 3 kHz

Frequency tests have been performed in two different methods.

In the first method, the applied voltage was kept constant while the frequency was varied from 60 Hz to 15 kHz in steps of seventeen. The waveforms of both signals were recorded simultaneously. The RMS values were manually recorded using the digital oscilloscope. The phase differences corresponding to the time difference between the zero crossings of the signals were determined and converted to degrees using a feature of the digital oscilloscope. Figure 4.29 shows the signals at 3 kHz and demonstrates the method used for phase angle calculation. A digital oscilloscope noise filter had been used during this measurement in order to reduce the noise of the signals.

Figure 4.29 shows that the NXVT output is lagging and the phase difference is 53 µs. Phase angle calculations were verified by using the equation below:

$$\frac{54\times10^{-6}\times360}{\frac{1}{3000}}\cong57^{0}$$

Table 4.4 shows the results of the measurements and calculated phase differences.

Table 4.4 Frequency characteristics of the NXVT test results

Freq(Hz)	NXVT (V)	Voltage (kV)	Probe Voltage (V)	Applied Voltage (kV)	Normalized Amplitude	Lagging	Phase (deg)
60	2.156	1.509	1.501	1.501	1.000	NXVT	-0.804
500	2.156	1.509	1.496	1.496	1.003	NXVT	-10.24
1000	2.157	1.510	1.503	1.503	0.999	NXVT	-19.86
2000	2.163	1.514	1.5	1.5	1.004	NXVT	-38.13
3000	2.117	1.482	1.5	1.5	0.983	NXVT	-57.58
4000	2.052	1.436	1.499	1.499	0.953	NXVT	-78.57
5000	1.987	1.391	1.499	1.499	0.923	NXVT	-96.15
6000	1.921	1.345	1.503	1.503	0.890	NXVT	-113.6
7000	1.868	1.308	1.509	1.509	0.862	NXVT	-132.2
8000	1.794	1.256	1.492	1.492	0.837	NXVT	-147.9
9000	1.761	1.233	1.503	1.503	0.816	NXVT	-166
9743	1.727	1.209	1.499	1.499	0.802	NXVT	-179.5
11000	1.677	1.174	1.505	1.505	0.776	App Voltg	-199.6
12000	1.631	1.142	1.497	1.497	0.759	App Voltg	-217.1
13000	1.61	1.127	1.506	1.506	0.744	App Voltg	-234.6
14000	1.577	1.104	1.504	1.504	0.730	App Voltg	-252.4
15000	1.023	0.716	0.99	0.99	0.719	App Voltg	-268.99

Using the data in Table 4.4, the normalized amplitude-frequency and phase angle-frequency characteristics of the NXVT have been plotted in Figure 4.30 and Figure 4.31, respectively.

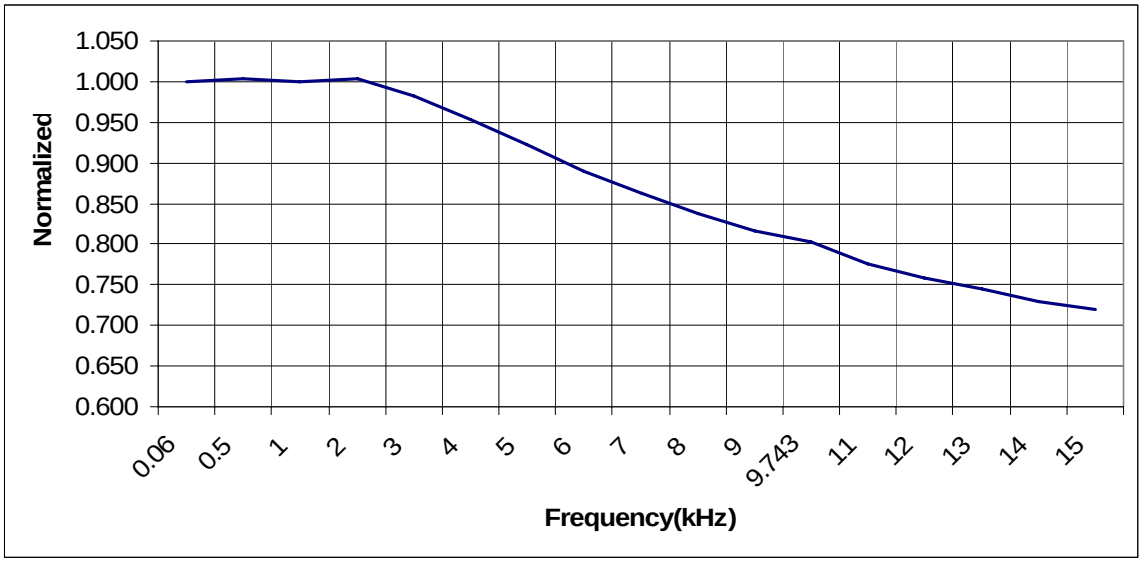

Figure 4.30 Normalized amplitude-frequency response

The phase shift at 60 Hz was 37 μs which corresponds to ~1 degree. According to the manufacturer, delay is due to the transit time required to transmit the light and digital signal processing.

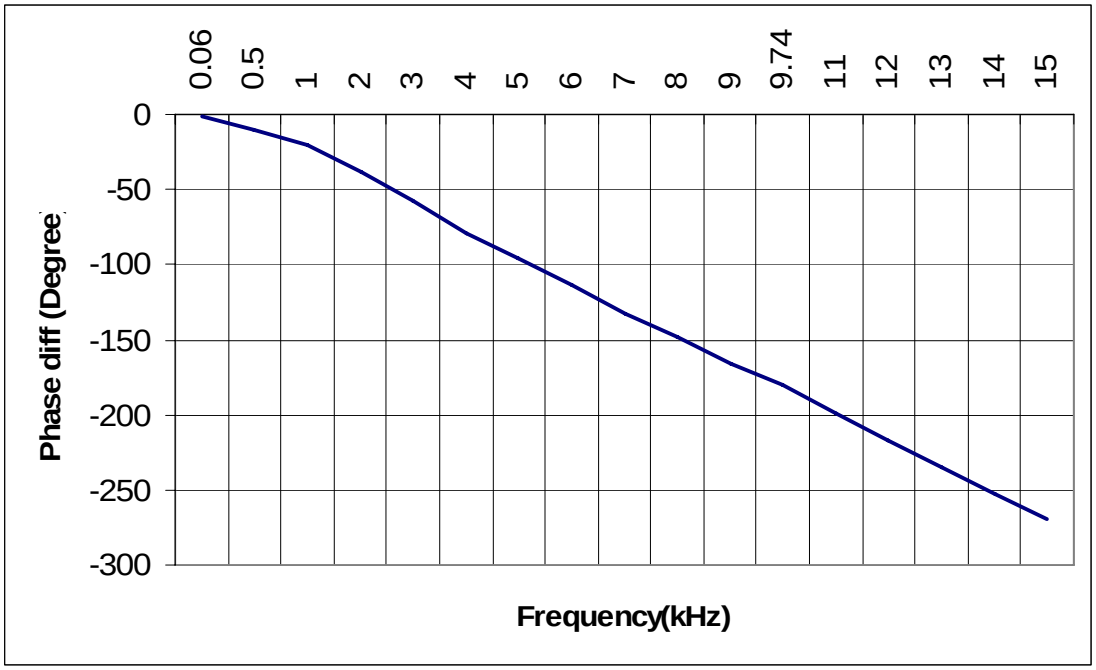

Figure 4.31 Phase angle-frequency characteristics

In the second method, the applied voltage was not kept constant while the frequency was varied from 60 Hz to 20 kHz in steps of twenty-two. The waveforms of both signals were recorded simultaneously. The RMS values were manually recorded using the digital oscilloscope. The phase difference corresponding to the time difference between the zero crossings of the signals was determined and converted to degrees using a feature of the digital oscilloscope. Same method used in method 1 was used to calculate the phase angle. Table 4.5 shows the results of the measurements and calculated phase differences.

Table 4.5 Frequency characteristics of the NXVT test results

Freq(Hz)	NXVT (V)	Voltage (kV)	Probe Voltage (V)	Applied Voltage (kV)	Normalized Amplitude	Lagging	Phase (deg)
60	2.912	2.038	2.011	2.011	1.000	NXVT	-0.495
500	2.996	2.097	2.076	2.076	0.997	NXVT	-10.62
1000	3.024	2.116	2.101	2.101	0.994	NXVT	-19.13
2000	3.11	2.177	2.157	2.157	0.996	NXVT	-38.49
3000	3.282	2.297	2.321	2.321	0.977	NXVT	-58.05
4000	3.551	2.485	2.592	2.592	0.946	NXVT	-76.96
5000	4.028	2.819	3.049	3.049	0.912	NXVT	-96.35
6000	4.969	3.478	3.893	3.893	0.881	NXVT	-114.7
7000	7.117	4.981	5.76	5.76	0.853	NXVT	-132.5
8000	11.16	7.812	9.31	9.31	0.828	NXVT	-149.1
9000	11.82	8.274	10.09	10.09	0.809	NXVT	-166.4
9764	9.279	6.495	8.08	8.08	0.793	NXVT	-179.9
11000	4.578	3.204	4.081	4.081	0.775	App Voltg	-200.1
12000	3.342	2.339	3.112	3.112	0.742	App Voltg	-217.3
13000	2.32	1.624	2.178	2.178	0.736	App Voltg	-233.9
14000	1.53	1.071	1.441	1.441	0.733	App Voltg	-252.1
15000	1.349	9.443	1.316	1.316	0.708	App Voltg	-270.36
16000	0.847	5.929	0.826	0.826	0.708	App Voltg	-285.11
17000	0.721	5.047	0.719	0.719	0.693	App Voltg	-302.2
18000	0.703	4.921	0.709	0.709	0.685	App Voltg	-320.4
19000	0.497	3.479	0.518	0.518	0.663	App Voltg	-335.3
20000	0.47	3.290	0.495	0.495	0.656	App Voltg	-352.01

Figure **4.32** shows the applied voltage and output voltage variations according to the frequency. It is seen that the max applied voltage was 10 kV at 9 kHz frequency.

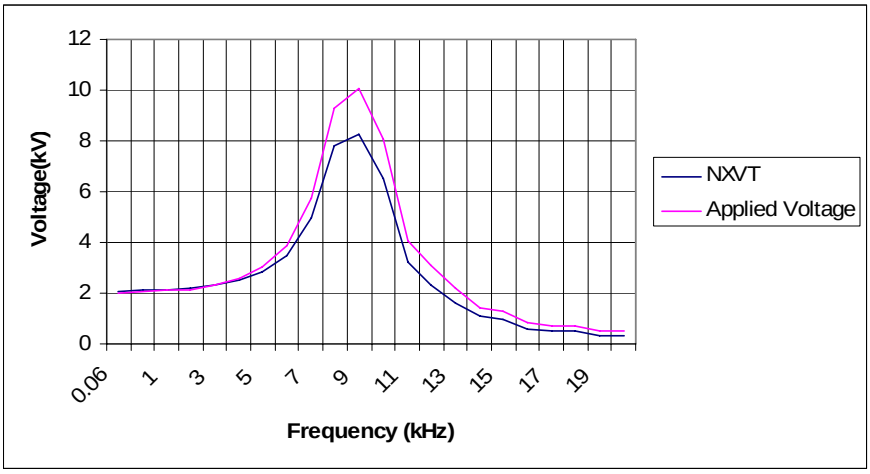

Figure 4.32 Applied voltage NXVT output voltage changing by frequency

Using the data in Table 4.5, the normalized amplitude-frequency and phase angle-frequency characteristics of the NXVT have been plotted in Figure 4.33 and Figure 4.34, respectively. These figures show the results obtained by the two methods. It can be seen that the difference between the two methods is small.

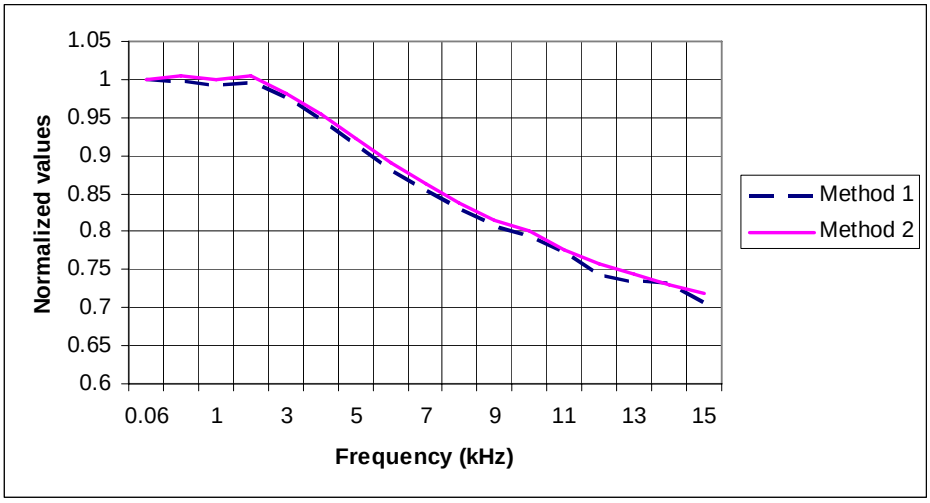

Figure 4.33 Normalized amplitude-frequency response

Figure 4.33 shows that the amplitude is gradually decreasing as frequency increases after 3 kHz. Between DC and 3 kHz, the amplitude is more or less independent from the frequency.

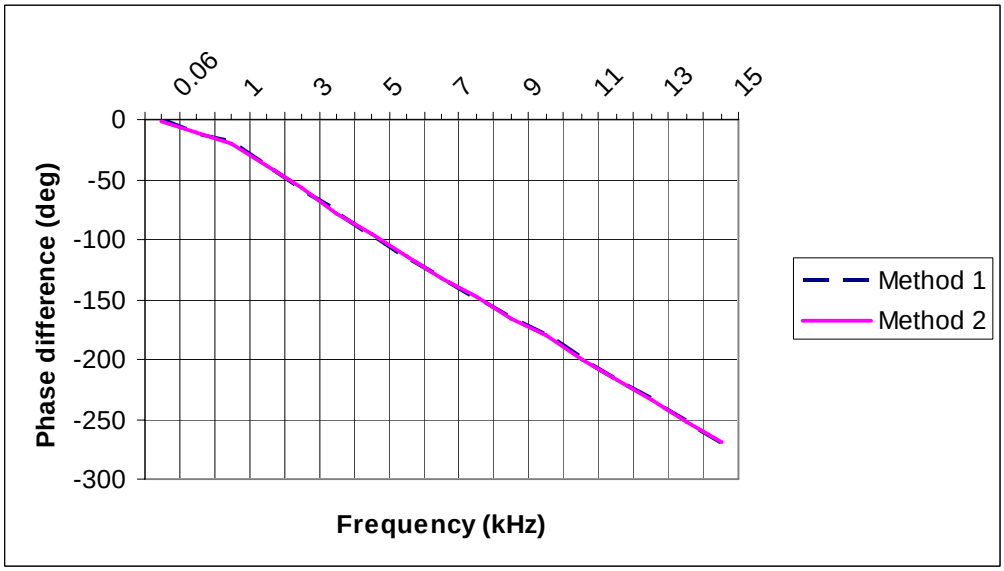

Figure 4.34 Phase angle-frequency characteristics

Figure 4.34 shows that the phase angle varies more or less linearly with the frequency. This corresponds to the manufacturer's claim that the delay caused by the optical system

is constant, independent from the frequency. The delay at 60 Hz was 22 μs. The 180 degree delay occurred at 9.764 kHz; this corresponds to a 51 μs delay.

Amplitude-frequency and phase- frequency relations obtained by the two methods are similar to each other. The second method generated higher voltage than the first method. The maximum generated voltage was 10 kV in method 2 and only 1.5 kV in the first method. The comparison of the results shows that the voltage does not have a significant effect on the frequency characteristics of OVT.

The manufacturer adjusted the phase delay to zero at 60 Hz; however, the test results showed 37 μs and 20 μs delay.

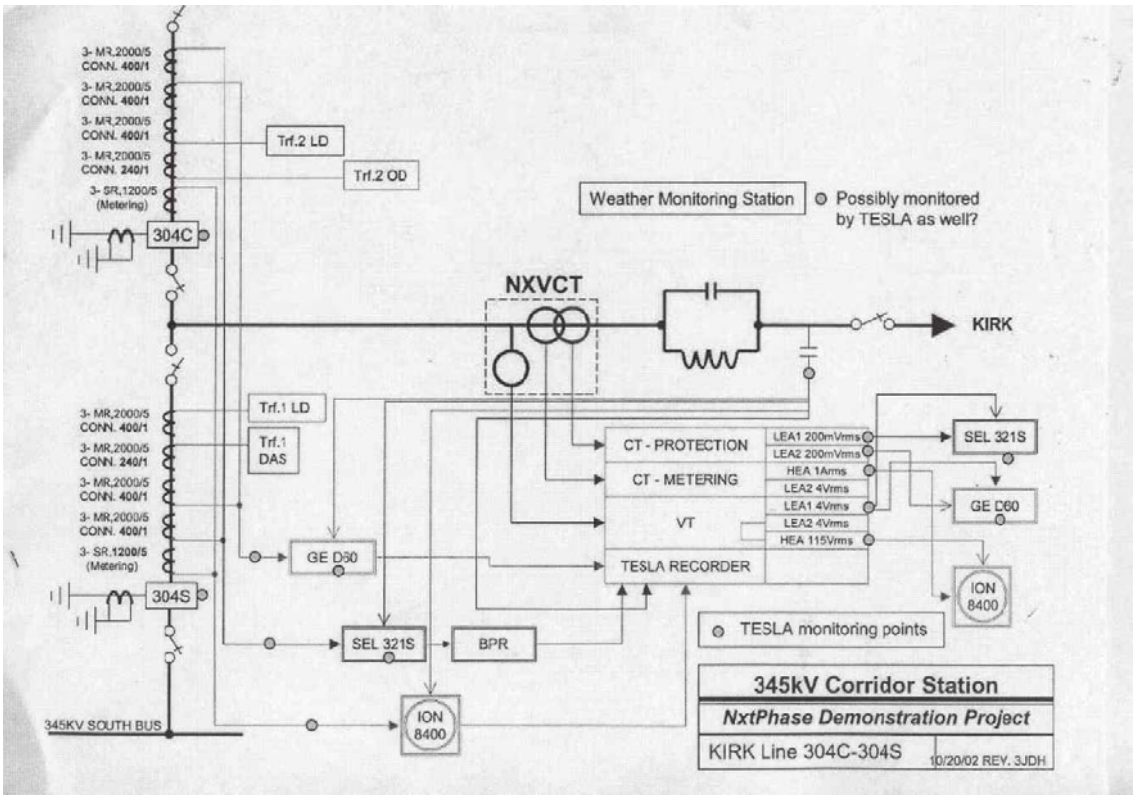

Figure 4.35 Corridor substation Instrument transformer connection

4.3 Comparison of Magnetic and Optical Instrument Transformers Operation Based On Field Data

American Electric Power has installed conventional and optical CTs for protection, and conventional and optical VTs and CTs for metering at the Corridor substation for each phase. The outputs of the instrument transformers were observed and recorded by a NxtPhase Tesla event recorder. The conventional CTs supplied two digital relays, (SEL321 and GE D60), which also recorded the current waveforms. The connection diagram of the instrument transformers can be seen in Figure 4.35 .

Eleven (11) events (faults) have been selected from the recorded events, and the instrument transformer's output signals were compared. The NxtPhase RecordBase View data viewer program was used to observe and analyze the recorded data. The data includes the time function of the sine waves (instantaneous values) during the event. The program permits the selection of an arbitrary point and measures the instantaneous value of all recoded data or an interval (window) can be selected and the program will calculate the RMS value and the maximum and minimum (peak) values of the sine waves in the window. The program will also analyze the data in the complete recorded interval and determines the maximum and minimum RMS values of the sine wave.

The program calculates the real (R) and reactive (X) components of the system impedance using the RMS values. The impedance trajectories of each phase are plotted. The trajectory is the X versus the R values plotted in each time interval. The procedure for the impedance trajectory calculation is:

- The computer selects a time value and a small interval (window) around this time value.
- The RMS value of the voltage and current is calculated in this window.
- The impedance is the RMS voltage is divided by the RMS current. This calculation gives an X and an R value belonging to the selected time point
- The calculation is repeated for each of the time points in the recorded interval.
- The obtained values are plotted in an X versus R diagram

Conventional CTs for protection are connected to the SEL321 and GE D60 impedance relays. The RMS maximums and minimums of the outputs of these relays were compared with the optical CT (LEA) protection output. The RMS maximums and minimums of selected cycles of the conventional CT for metering were compared with the optical CT for measurement of LEA and HEA outputs. Conventional VT outputs were compared with optical VT LEA and HEA outputs.

4.3.1 Case 1: Disturbance in C phase.

This event fault occurred in Phase C. The voltage and current of phase C (V_c, I_c) were recorded and analyzed in figures and tables.

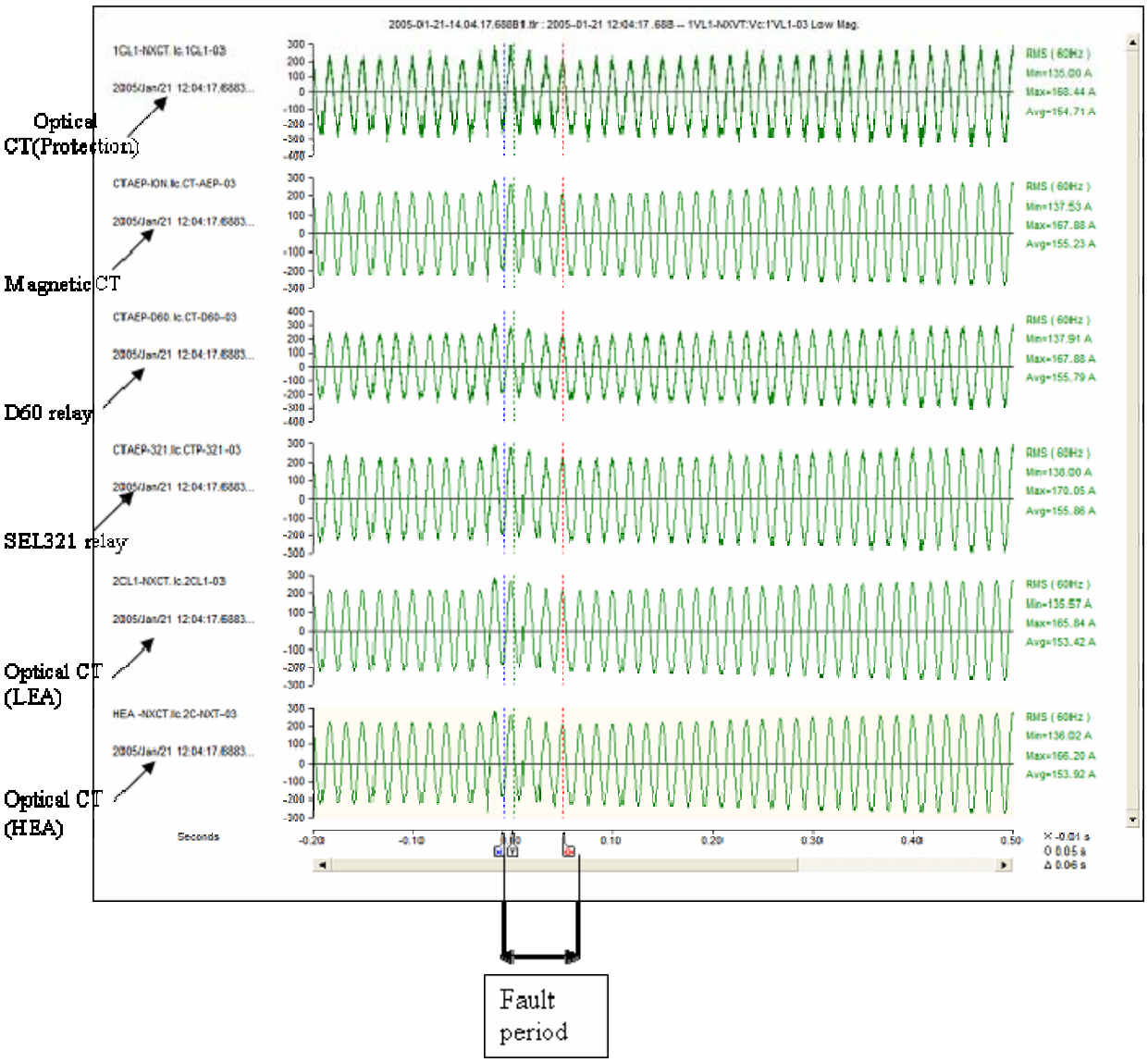

Figure 4.36 Current measurements Case 1

Figure 4.36 shows the current readings during the event:

- OCT for protection mode,
- magnetic CT metering mode,
- the currents recorded by SEL321 relay and D60 relay, which are supplied by magnetic CT with protection accuracy,
- Optical CT in metering mode with LEA output and HEA output.

4.3.1.1 Comparison of Metering CT Performance:

We selected a six cycle interval (window) before the fault and calculated the RMS value of the OCTs and magnetic CT currents, as well as the phase differences. The results are shows in Table 4.6.

Table 4.6 Metering current comparison Case 1

	I_{max} (A)	I_{min} (A)	I_{avg} (A)
I_c (Mag CT)	156.27	154.87	155.67
I_c (OCT-LEA)	153.95	154.47	154.19
I_c (OCT-HEA)	154.83	154.24	154.47
Errors			
OCT-LEA vs Mag.	1.48%	0.26%	0.95%
OCT-HEA vs. Mag	0.92%	0.41%	0.77%
OCT-HEA vs. LEA	0.57%	-0.15%	0.18%

The phase difference between the magnetic and optical CTs was measured. The results show no measurable phase difference.

Table 4.6 indicates that at low-current for 6 cycles, the deviation between magnetic CT and the optical LEA metering output maximum is 1.48%, the minimum is 0.26%, and the average is 0.95%. The difference between OCT LEA output and HEA output is a maximum 0.57%. This is much higher than 0.2% accuracy defined at the rated current.

Table 4.7 Comparison of fault currents Case 1

	Cycle 1	Cycle 2	Cycle 3
I_c (OCT-LEA)	167.60	165.86	168.92
I_c (Mag CT)	166.33	165.55	167.87
D60	166.57	166.76	167.88
SEL321	167.61	169.58	170.03
Errors			
Mag. CT vs. OCT LEA	-0.764%	-0.187%	-0.625%
OCT LEA vs. D60	0.615%	-0.543%	0.616%
OCT LEA vs. SEL321	-0.006%	-2.243%	-0.657%

4.3.1.2 Comparison of Protection CT Performance:

The protection must work during the fault. We calculated the RMS current of the first three cycles after the occurrence of the fault. We also measured the phase differences.

The fault current was not measured directly by the magnetic CT. We used the magnetic CT metering output for comparison. This gives conservative results because the relay loading reduces the accuracy of the magnetic CT. The results are presented in Table 4.7.

Table 4.7 shows that the difference between the magnetic and optical CT is less than 1%.

The phase differences between the sine waves were not measurable, mostly as a result of the noise. We estimate that the phase differences are negligible.

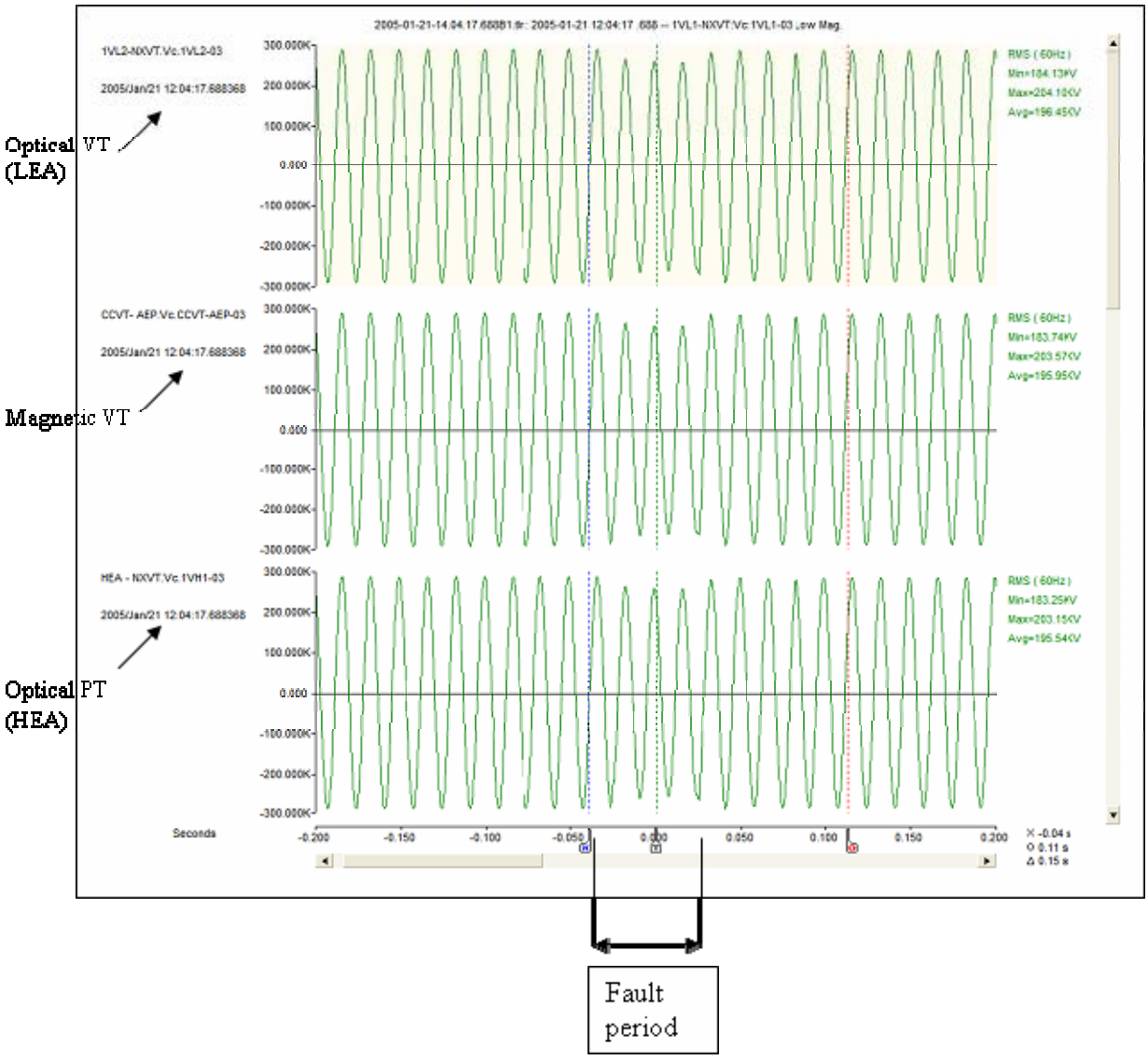

Figure 4.37 Voltage measurements

4.3.1.3 Comparison of Voltage Transformers Performance

Figure 4.37 shows the secondary voltage sine wave produced by the magnetic voltage transformer and the LEA and HEA output sine waves of optical PT. The fault produces voltage sag. The figure shows that the voltage sag does not produce any transient oscillation. The metering and protection mode is the same as in the case of voltage transformers. We selected six cycles before the fault for comparison. The results are shown in
Table 4.8.

Table 4.8 Comparison of voltages during the fault in Case 1

	V_{max} (kV)	V_{min} (kV)	V_{avg} (kV)
V_c (Mag VT)	205.50	205.26	205.38
Vc (NXVT-LEA)	206.00	205.74	205.87
Vc (NXVT-HEA)	205.92	204.79	204.92
Errors			
NXVT-LEA vs Mag.	-0.24%	-0.23%	-0.24%
NXVT-HEA vs. Mag	-0.20%	0.23%	0.22%
NXVT-HEA vs. LEA	-0.04%	-0.46%	-0.46%

Table 4.8 shows that the difference between the voltage transformers is significantly less than between the current transformers. The maximum error is less than 0.25%. It is interesting that there is around a 0.46% difference between the NXVT LEA and HEA output.

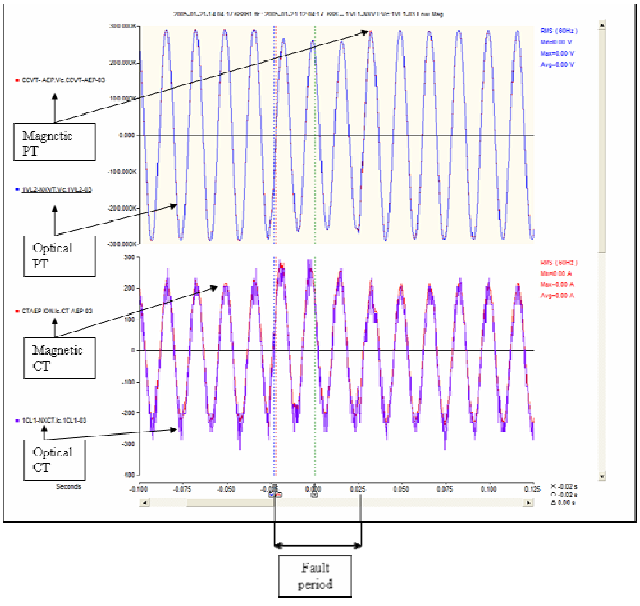

Figure 4.38 Voltage-current overlap sine waves

4.3.1.4 Direct Comparison of Wave Forms

Figure 4.38 shows the overlapped magnetic and optical CTs and the magnetic and optical VT's sine waves. The maximum difference between the peak values of voltage and sine waves is less than 0.5%. The difference between the CT's is larger, and the OCT output signal carries significant noise.

The instantaneous percentage difference between magnetic and optical VT sinusoidal output waves was calculated. The base was the peak value of the magnetic VT output voltage. Figure 4.39 shows the difference in percentage.

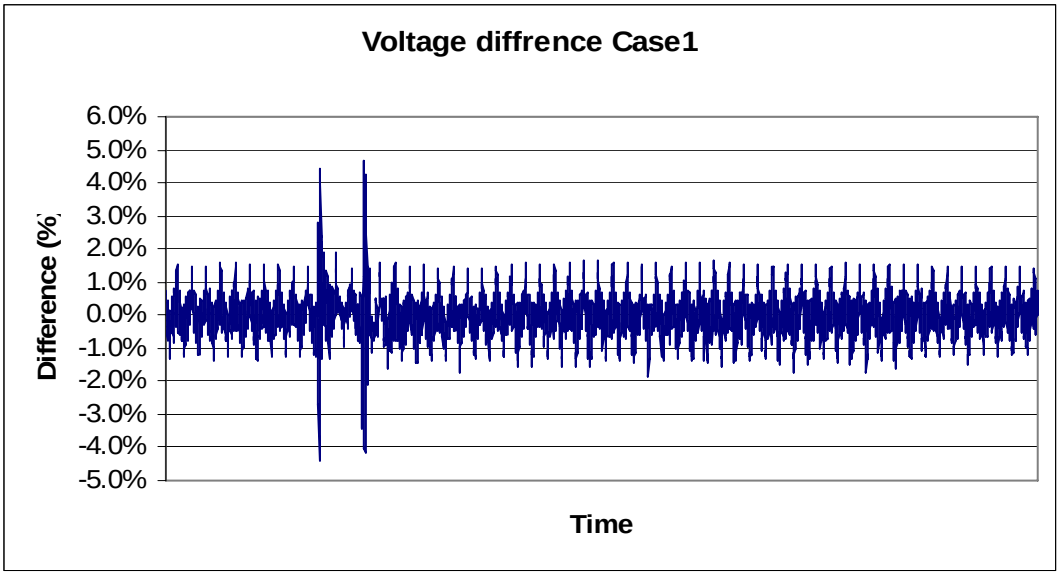

Figure 4.39 Comparison of voltage sine waves, Case 1

The voltage difference is a high-frequency (around 300 Hz) oscillation superimposed on a 60 Hz carrier wave. The small peaks occur at crossing where the output voltage is zero. The peak value of the oscillation is less than 1.8% disregarding the large disturbance (around 5%) that occurred at the time of the fault initiation and removal.

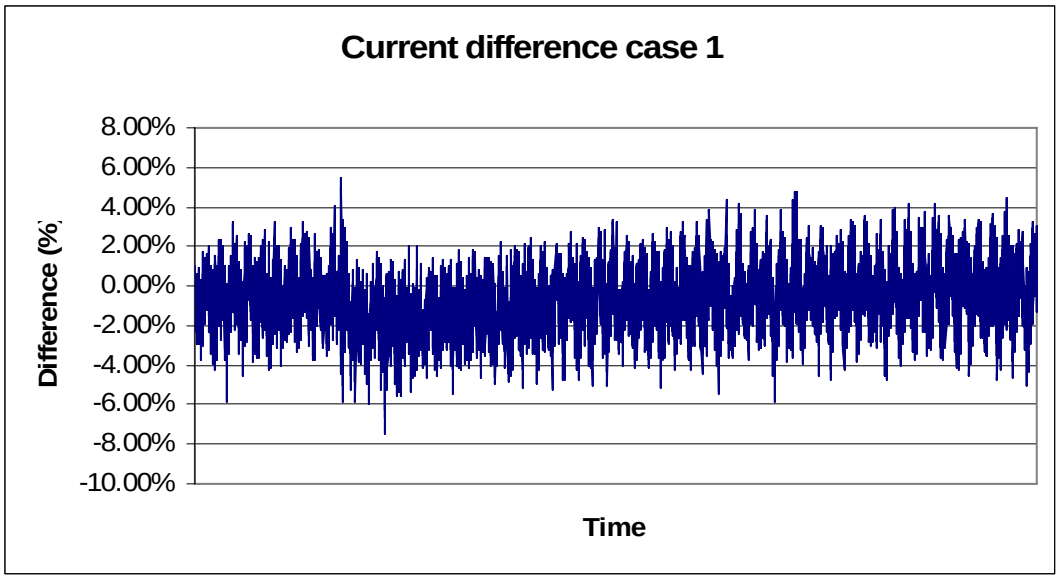

Figure 4.40 Comparison of current sine waves, Case 1

Figure 4.40 shows the percentage difference between the magnetic and optical CT output in measuring mode. The base is the peak value of the magnetic CT output current. The peak values are less than + 4% and -6%.

4.3.1.5 Impedance Trajectories

Figure 4.42 shows the impedance trajectories of Phase A, B, and C for magnetic and optical systems. The impedance trajectories are important for evaluations of the protection performance of the instrument transformers. The distance relays operate if the impedance is within a selected range.

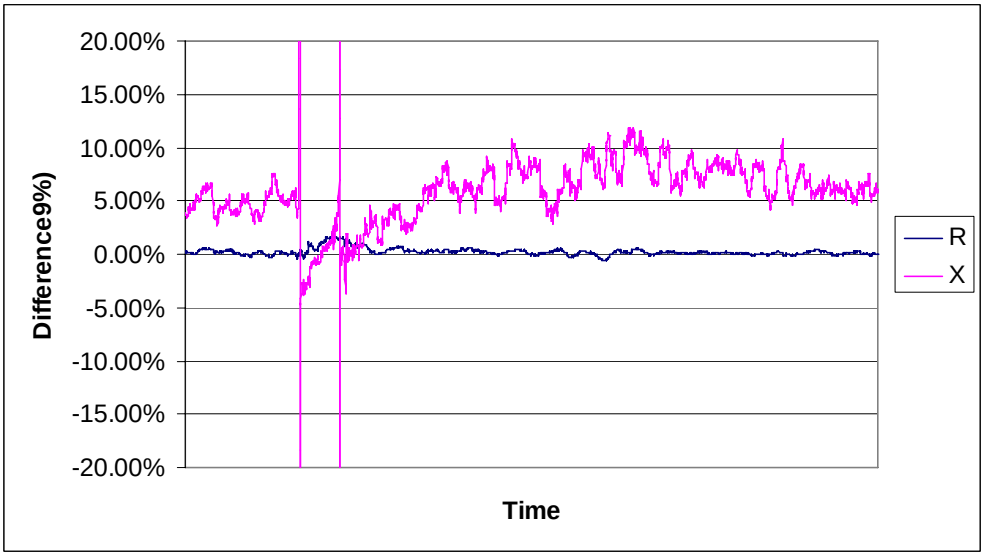

Figure 4.41 Percentage difference between the R and X values Case 1

The two impedance trajectories were compared by subtracting the R and X values the optical transformers produced from the magnetic transformer's generated R and X values. To obtain percentage differences, the calculated differences are divided by the magnetic instrument transformer provided R and X values. Figure 4.41 shows the percentage differences between the magnetic and optical instrument transformer's generated resistance and reactance of the impedance trajectories.

If the two peaks that occurred when the fault was initiated are disregard, Figure 4.41 shows that the error of reactance (X) is less than 11%. The difference in resistance is less than 2%.

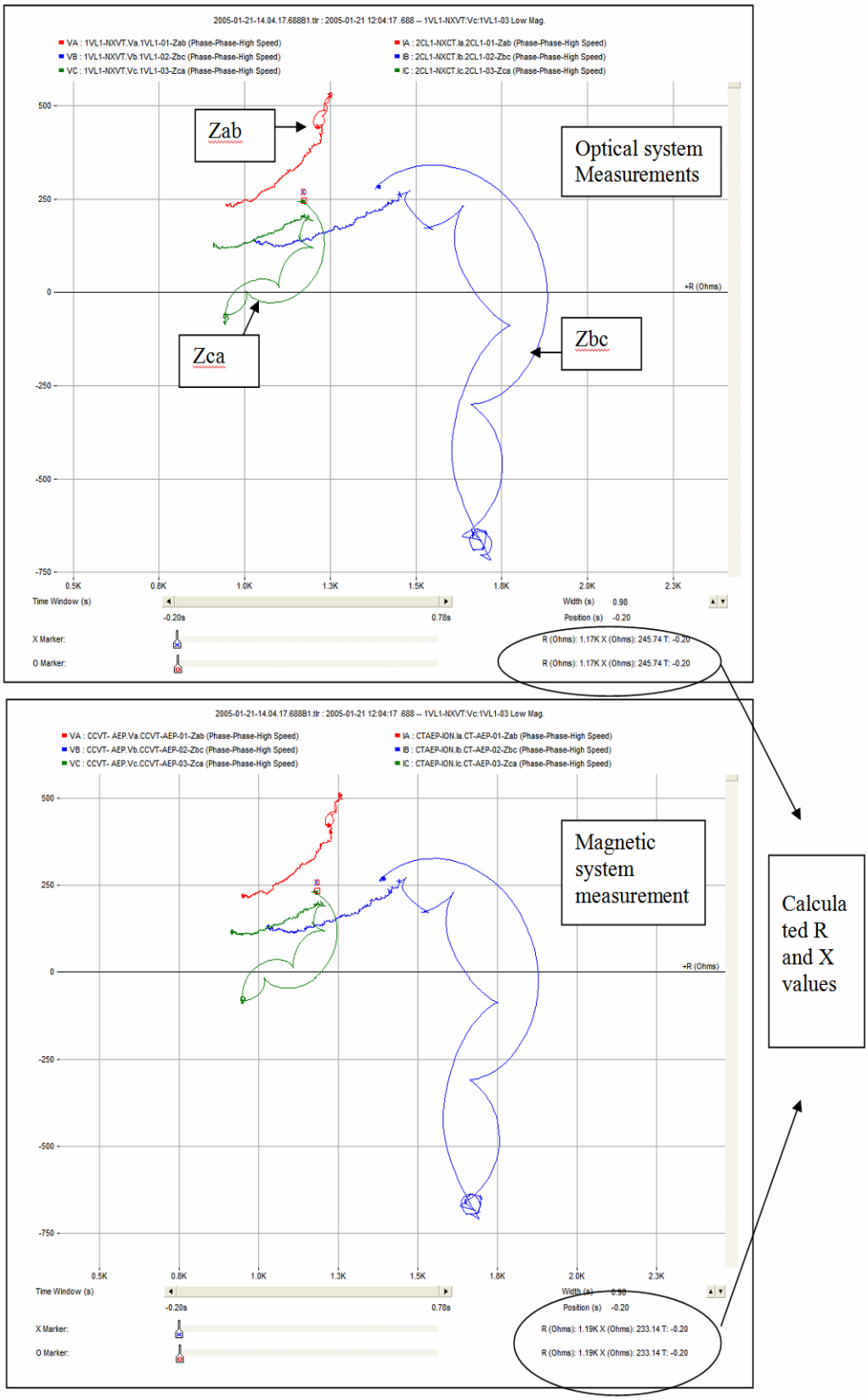

Figure 4.42 Impedance trajectories, Case 1

4.3.2 Case 2: Disturbance in Phase B

In this event, short circuit occurred in Phase B somewhere in the system. The protection interrupted the short circuit current after 3 cycles. The peak value of the short circuit current was close to 600 A. The peak value of the load current before and after short circuit interruption was around 140 A. The short circuit current was about 4 times the load current. The short circuit current has a significant DC component.

Figure 4.43 shows the current readings during the event:

- OCT for protection mode,
- magnetic CT metering mode,
- the currents recorded by SEL321 relay, and D60 relay, which are supplied by a magnetic CT with protection accuracy,
- Optical CT in metering mode with LEA output and HEA output

In Figure 4.43, Optical CT LEA measuring output is a distorted sine wave in the 2nd and 3rd cycles of fault current. It seems that the OCT chopped the current wave at the positive peak.

Table 4.9 indicates that at low-current for 6 cycles, the deviation between magnetic CT and optical LEA metering output the maximum is 0.68%, the minimum is 0.14%, and the average is 0.39%. The difference between OCT LEA output and HEA output is a maximum 0.20%.

Table 4.9 Metering current comparison Case 2

	I_{max} (A)	I_{min} (A)	I_{avg} (A)
I_b (Mag CT)	91.29	89.69	90.51
I_b (OCT-LEA)	90.85	89.86	90.38
I_b (OCT-HEA)	90.67	89.70	90.16
Errors			
OCT-LEA vs Mag.	0.48%	-0.19%	0.14%
OCT-HEA vs. Mag	0.68%	-0.01%	0.39%
OCT-HEA vs. LEA	-0.20%	-0.18%	-0.24%

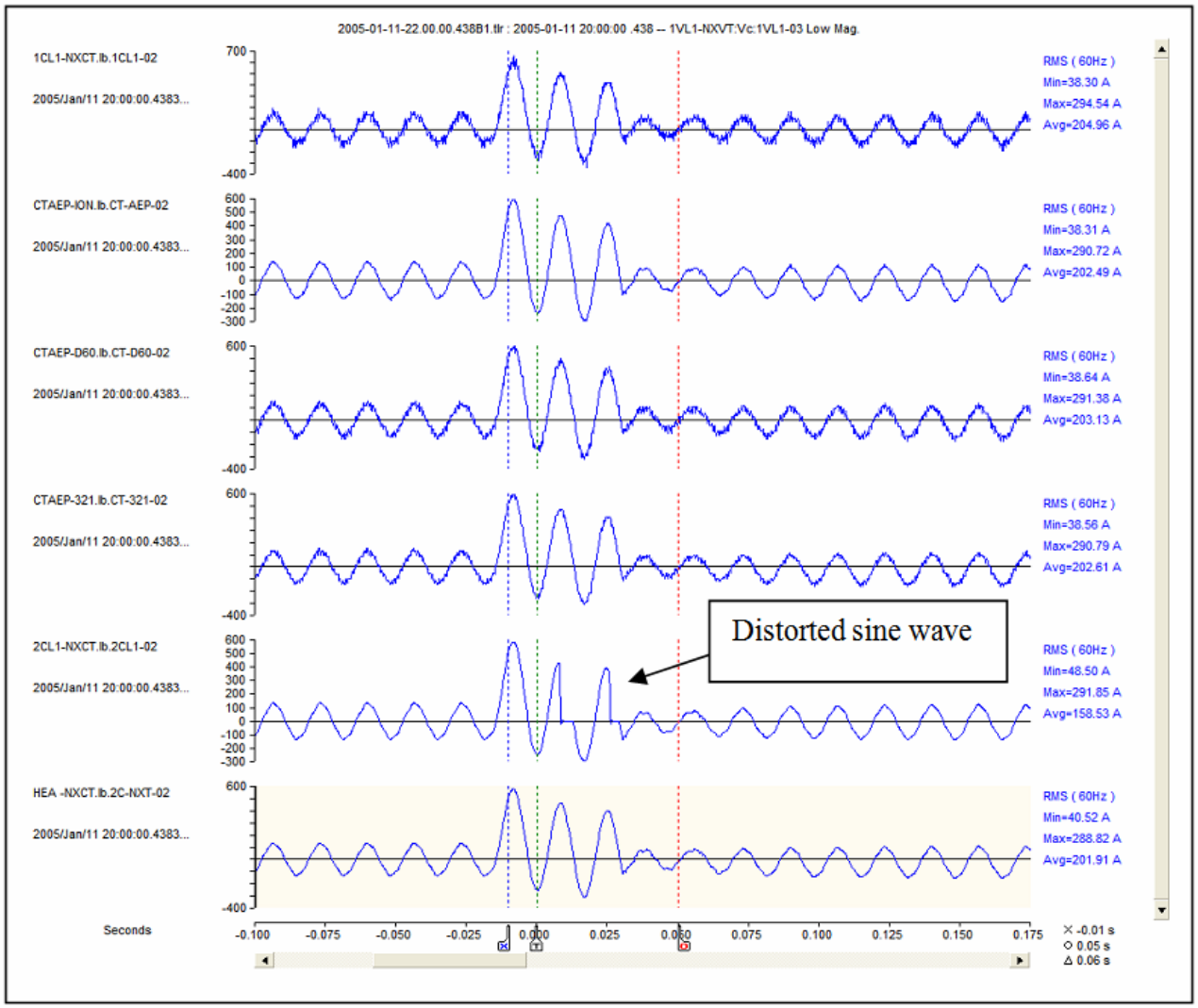

Figure 4.43 Current measurements Case 2

Table 4.10 shows reproduction of the short circuit current, when the optical CT was in protection mode.

Table 4.10 Comparison of fault currents Case 2

	Cycle 1	Cycle 2	Cycle 3
I_b (OCT-LEA)	297.86	275.83	266.73
I_b (Mag CT)	295.71	271.15	263.07
D60	296.48	272.37	264.21
SEL321	296.81	271.80	263.61
Errors			
Mag. CT vs. OCT LEA	-0.727%	-1.726%	-1.391%
OCT LEA vs. D60	-0.463%	-1.254%	-0.945%
OCT LEA vs. SEL321	-0.353%	-1.461%	-1.170%

The figure shows that the maximum difference in the RMS values of short circuit currents is less than 1.8%.

The voltage outputs of instrument transformers were recorded, but not reproduced here. Using the data, differences between the magnetic and optical VTs were calculated.

Table 4.11 Comparison of voltages during the fault in Case 2

	V_{max} (kV)	V_{min} (kV)	V_{avg} (kV)
V_b (Mag VT)	204.81	204.72	204.76
V_b (NXVT-LEA)	203.64	203.57	203.62
V_b (NXVT-HEA)	204.41	204.33	201.37
Errors			
NXVT-LEA vs Mag.	-0.57%	-0.56%	-0.56%
NXVT-HEA vs. Mag	-0.20%	-0.19%	-1.66%
NXVT-HEA vs. LEA	0.38%	0.37%	-1.12%

Table 4.11 shows that the difference between the voltage transformers is significantly less than between current transformers.

The impedance trajectories were calculated using the current and voltage outputs of the magnetic and optical instruments transformers.
Figure 4.44 shows the percentage difference between impedance trajectories, which are determined by magnetic and optical instrument transformers.

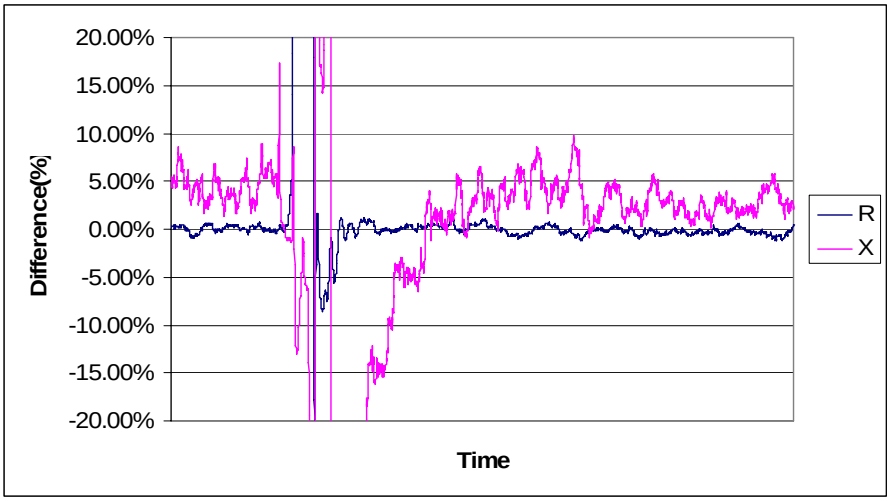

Figure 4.44 Percentage difference between the R and X values Case 2

The two impedance trajectories were compared by subtracting the optical transformer's produced R and X values from the magnetic transformers generated R and X values. The percentage difference was obtained by calculating differences divided by the magnetic instrument transformer's provided R and X values.

Figure 4.44 shows percentage differences between the magnetic and optical instruments transformers generated resistance and reactance in the impedance trajectories. The differences are significant, although the difference in instantaneous values is not affecting the protection operation.

4.3.3 Case 3: Disturbance in Phase B

The currents and voltages were recorded as in Case 1. Using these data we compared the current outputs of the magnetic and optical CT. The method is explained in case 1.

Table 4.12 compares the metering CT outputs. The results are very similar to Cases1 and 2. It is important that the maximum difference is larger than 0.4%.

Table 4.12 Metering current comparison Case 3

	I_{max} (A)	I_{min} (A)	I_{avg} (A)
I_b (Mag CT)	104.98	101.18	101.94
I_b (OCT-LEA)	105.01	101.64	102.01
I_b (OCT-HEA)	104.47	101.27	101.64
Errors			
OCT-LEA vs Mag.	-0.03%	-0.45%	-0.07%
OCT-HEA vs. Mag	0.49%	-0.09%	0.29%
OCT-HEA vs. LEA	-0.52%	-0.37%	-0.36%

Table 4.13 compares the reproduction of short circuit current by magnetic and optical CT in protection mode. The errors are similar to the previous cases.

Table 4.13 Comparison of fault currents Case 3

	Cycle 1	Cycle 2	Cycle 3
I_b (OCT-LEA)	397.97	382.68	380.46
I_b (Mag CT)	392.45	377.72	375.60
D60	393.10	377.95	375.56
SEL321	394.33	377.76	375.11
Errors			
Mag. CT vs. OCT LEA	-1.407%	-1.313%	-1.294%
OCT LEA vs. D60	-1.224%	-1.236%	-1.288%
OCT LEA vs. SEL321	-0.915%	-1.286%	-1.406%

The voltage outputs of instrument transformers were recorded, but not reproduced here. Using the data, differences between the magnetic and optical VTs were calculated. Table 4.14 shows that the performance of VTs is better than the performance of CTs. The calculated deviations are very similar to Cases 1 and 2.

Table 4.14 Comparison of voltages during the fault in Case 3

	V_{max} (kV)	V_{min} (kV)	V_{avg} (kV)
V_b (Mag VT)	203.97	203.69	203.85
V_b (NXVT-LEA)	202.74	202.46	202.63
V_b (NXVT-HEA)	203.50	203.23	203.39
Errors			
NXVT-LEA vs Mag.	-0.60%	-0.60%	-0.60%
NXVT-HEA vs. Mag	-0.23%	-0.23%	-0.23%
NXVT-HEA vs. LEA	0.37%	0.38%	0.37%

The impedance trajectories were calculated using the current and voltage outputs of the magnetic and optical instruments transformers. The percentage difference between impedance trajectories are determine by magnetic and optical instrument transformers.

Figure 4.45 and Figure 4.46 show the calculated impedance trajectories. These trajectories are different than those in Case 1 and 2.

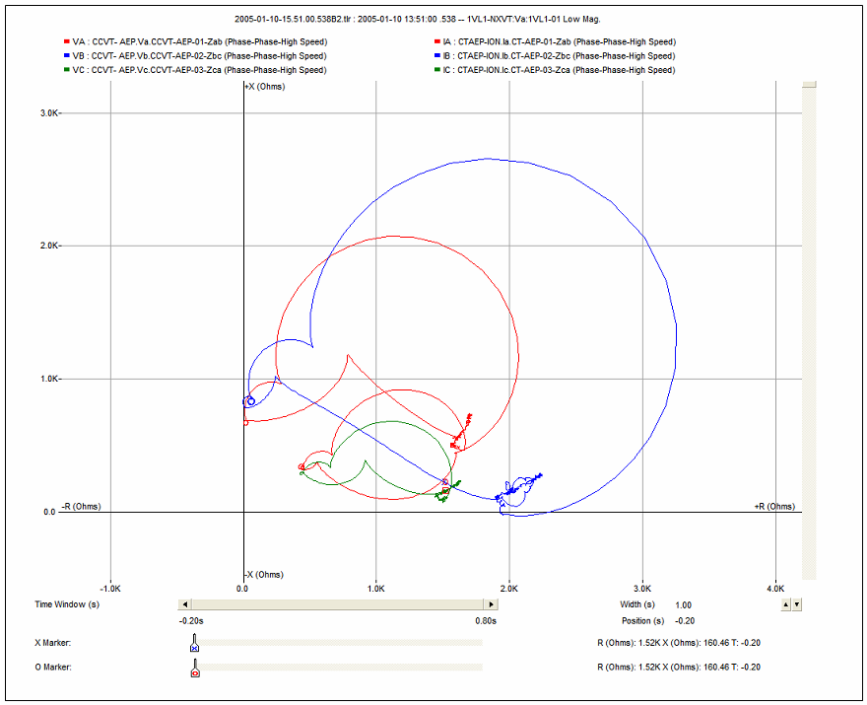

Figure 4.45 Impedance trajectories with magnetic transformers, Case 3

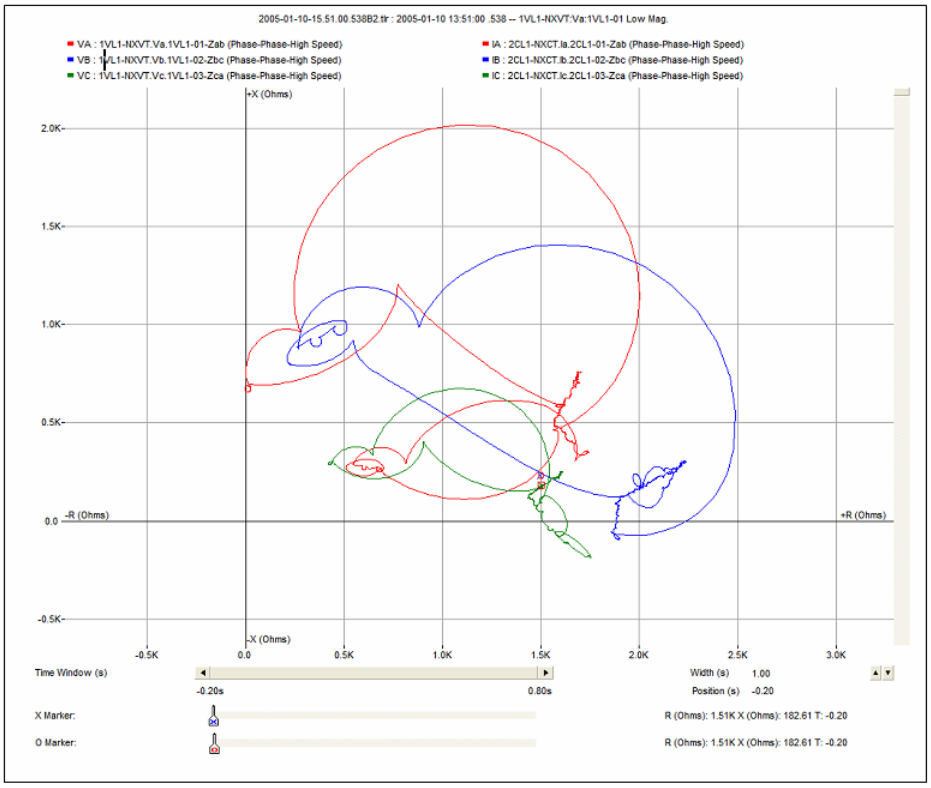

Figure 4.46 Impedance trajectories with optical transformers, Case 3

Figure 4.47 shows percentage differences between the magnetic and optical instrument transformer's generated resistance and reactance impedance trajectories.

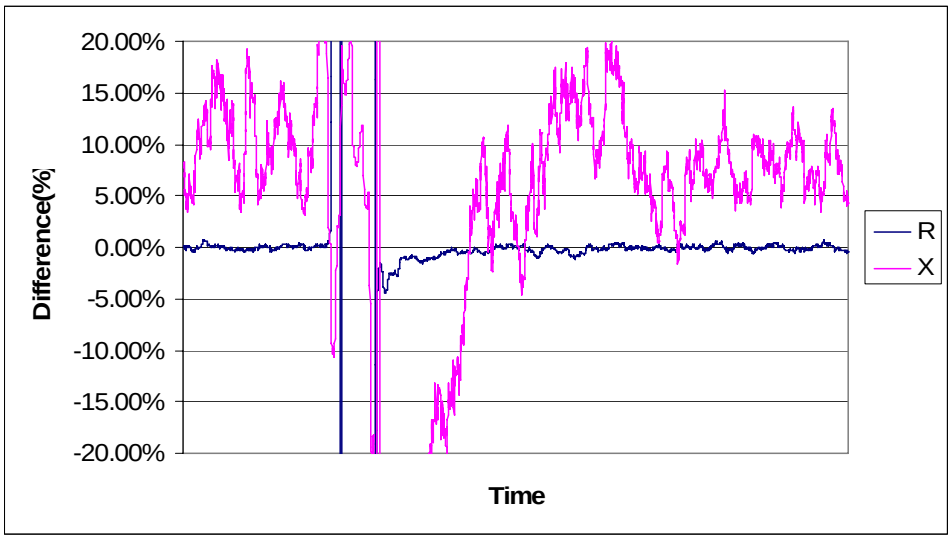

Figure 4.47 Percentage difference between the R and X values Case 3

The maximum reactance error is around 20% which is significantly larger than the close to 10% error in the previous cases.

4.3.4 Case 4: Disturbance in Phase A

In this case, short circuit occurred in Phase A. The current was interrupted after 2.5 cycles. The peak current was 3 times the load current. The currents and voltages were recorded as in the previous cases. Using these data, we compared the current outputs of the magnetic and optical CTs. The method is explained in Case 1.

Table 4.15 Compares the metering CT outputs. The results are very similar to the previous cases. The maximum difference between magnetic and optical CTs is 0.47%.

Table 4.16 Metering current comparison, Case 4

	I_{max} (A)	I_{min} (A)	I_{avg} (A)
I_a (Mag CT)	120.79	118.65	120.10
I_a (OCT-LEA)	120.76	119.21	120.07
I_a (OCT-HEA)	120.66	119.15	119.96
Errors			
OCT-LEA vs Mag.	0.02%	-0.47%	0.02%
OCT-HEA vs. Mag	0.11%	-0.42%	0.12%
OCT-HEA vs. LEA	-0.08%	-0.05%	-0.09%

Table 4.17 compares the RMS values of sine waves for first three cycles using the output of magnetic and optical CTs in protection mode. The maximum difference between CTs is less than 2%.

Table 4.17 Comparison of fault currents, Case 4

	Cycle 1	Cycle 2	Cycle 3
I_a (OCT-LEA)	460	450	450
I_a (Mag CT)	451.30	443.13	443.84
D60	452.11	443.29	444.07
SEL321	452.15	444.39	445.38
Errors			
Mag. CT vs. OCT LEA	-1.928%	-1.550%	-1.388%
OCT LEA vs. D60	-1.715%	-1.491%	-1.318%
OCT LEA vs. SEL321	-1.707%	-1.247%	-1.027%

The recorded voltage outputs of the VTs were analyzed, but the sine waves are not reproduced here. The differences between the VTs were calculated and presented in Table 4.18. The maximum difference is 0.43%.

Table 4.18 Comparison of voltages during the fault, Case 4

	V_{max} (kV)	V_{min} (kV)	V_{avg} (kV)
V_a (Mag VT)	203.62	203.45	203.46
V_a (NXVT-LEA)	202.75	202.59	202.69
V_a (NXVT-HEA)	202.80	202.62	202.73
Errors			
NXVT-LEA vs Mag.	-0.43%	-0.42%	-0.38%
NXVT-HEA vs. Mag	-0.40%	-0.41%	-0.36%
NXVT-HEA vs. LEA	0.02%	0.01%	0.02%

The impedance trajectories were calculated using magnetic and optical three phase current and voltage. The plotted trajectories are not presented here. The difference between plotted trajectories is in Figure 4.48.

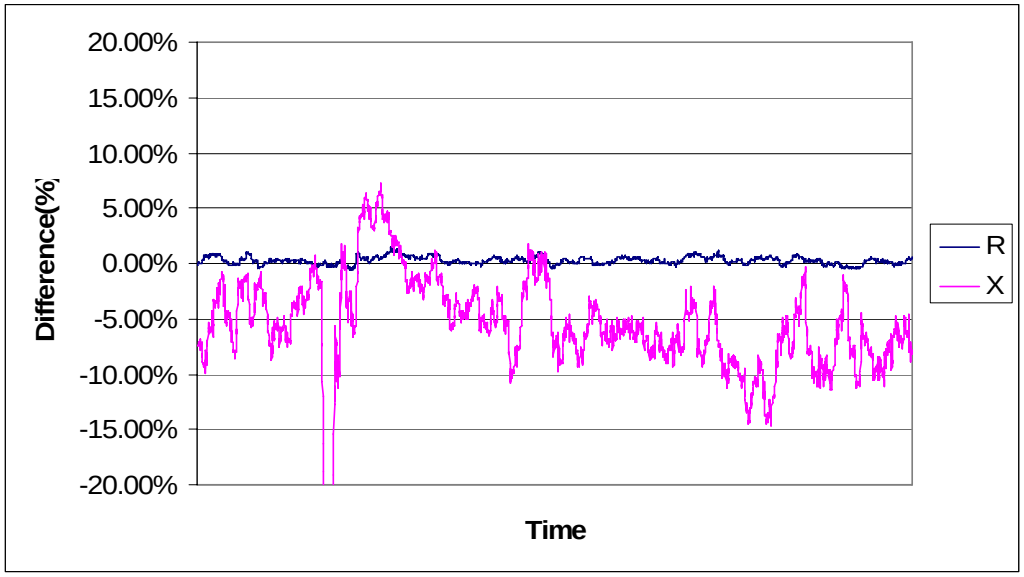

Figure 4.48 Percentage difference between the R and X values, Case 4

The calculated R and X values are changing by time. The difference between R and X values as calculated by magnetic and optical transformers are plotted in Figure 4.48. The maximum reactance error is around 15%, disregarding the peaks during the fault.

4.3.5 Case 5: Disturbance in Phase A

In this event case, Phase A voltages and current are recorded as a fault record and Phase A has been analyzed. A short circuit fault has been recorded. Figure 4.49 shows the recorded current sine waves.

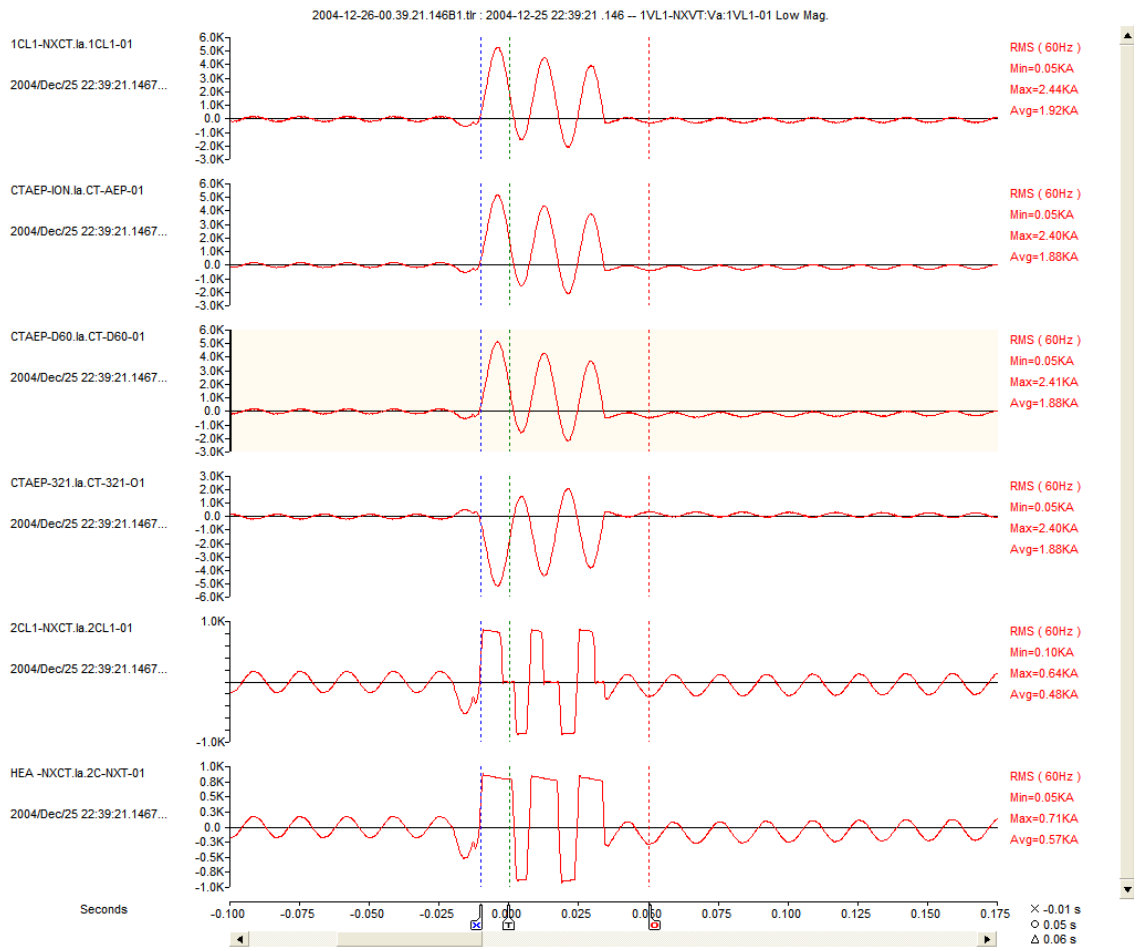

Figure 4.49 Current sine waves, Case 5

The load current before the event was around 200 A and the short circuit current is around 5200 A, which is 26 times the load current. When the sine waves are compared, it is seen that SEL321 sine wave instantaneous polarity is 180 with respect to the other traces. The wiring between the relay and Tesla recorder could cause the error. According to plotted current sine waves, comparisons between the metering CT results are presented in Table 4.19.

Table 4.19 Metering current comparison, Case 5

	I_{max} (A)	I_{min} (A)	I_{avg} (A)
I_a (Mag CT)	124.34	122.95	123.68
I_a (OCT-LEA)	124.26	123.84	124.05
I_a (OCT-HEA)	124.34	123.81	124.04
Errors			
OCT-LEA vs Mag.	0.06%	-0.72%	-0.30%
OCT-HEA vs. Mag	0.00%	-0.70%	-0.29%
OCT-HEA vs. LEA	0.06%	-0.02%	-0.01%

The maximum difference between the metering mode CTs is 0.70%.

Table 4.20 presents the comparison of RMS values of sine waves for first three cycles using the output of magnetic and optical CTs in protection mode. The maximum difference between CTs is less than 2.2%.

Table 4.20 Comparison of fault currents, Case 5

	Cycle 1	Cycle 2	Cycle 2.5
I_a (OCT-LEA)	239	227	226
I_a (Mag CT)	235	222	221
D60	235	222	221
SEL321	235	222	221
Errors			
Mag. CT vs. OCT LEA	-1.702%	-2.252%	-2.262%
OCT LEA vs. D60	-1.674%	-2.203%	-2.212%
OCT LEA vs. SEL321	-1.674%	-2.203%	-2.212%

Table 4.21 compares the reproduction of short circuit current by magnetic and optical CTs in protection mode. The errors are less than the previous cases.

The recorded voltage outputs of the instrument transformers were plotted, but not reproduced here. Using the data, differences between the magnetic and optical VTs were calculated.

Table 4.21 Comparison of voltages during the fault, Case 5

	V_{max} (kV)	V_{min} (kV)	V_{avg} (kV)
V_a (Mag VT)	204.56	204.46	204.52
V_a (NXVT-LEA)	203.76	203.67	203.71
V_a (NXVT-HEA)	203.79	203.71	203.75
Errors			
NXVT-LEA vs Mag.	-0.39%	-0.39%	-0.40%
NXVT-HEA vs. Mag	-0.38%	-0.37%	-0.38%
NXVT-HEA vs. LEA	0.01%	0.02%	0.02%

Table 4.21 shows the differences between recorded VT outputs during the fault. The maximum percentage difference is 0.40%.

The impedance trajectories were calculated using the current and voltage outputs of the magnetic and optical instruments transformers. Figure 4.50 shows the percentage difference between impedance trajectories, which are determined by magnetic and optical instrument transformers.

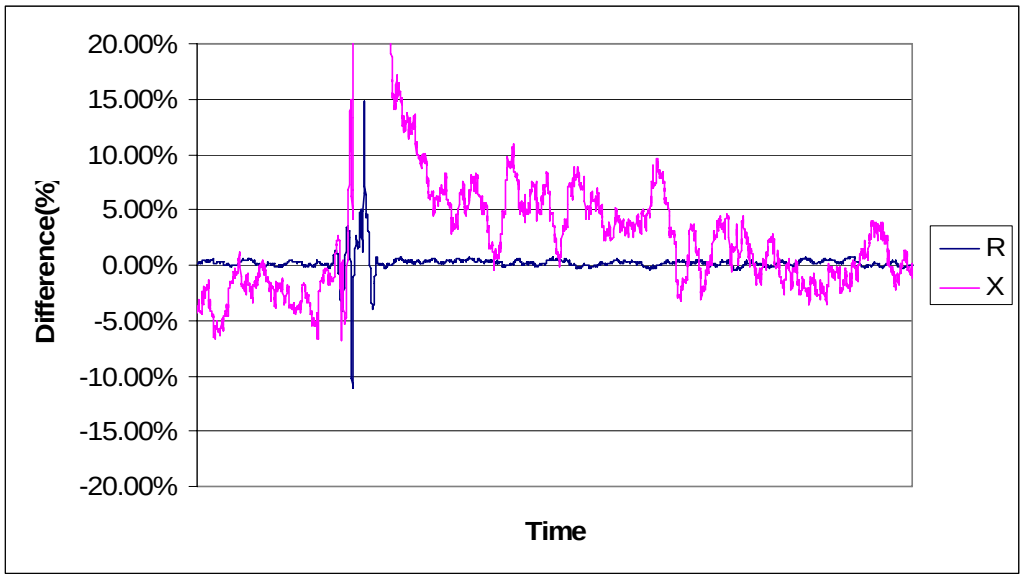

Figure 4.50 Percentage difference between the R and X values, Case 5

The reactance difference is very similar to the previous case results, and the maximum value is 10%, discarding the peaks during the fault.

4.3.6 Case 6: Disturbance in Phase A

In this event case, Phase A voltages and current are recorded as a fault record and Phase A has been analyzed. The phase ground type short circuit is recorded for two cycles. The plotted current and voltage sine waves are not reproduced here.

Table 4.22 shows differences between the metering mode CTs for cycles which are before the fault. The maximum difference between magnetic and optical CT is 0.49%.

Table 4.22 Metering current comparison, Case 6

	I_{max} (A)	I_{min} (A)	I_{avg} (A)
I_a (Mag CT)	82.14	80.85	81.50
I_a (OCT-LEA)	81.75	81.14	81.37
I_a (OCT-HEA)	81.74	81.11	81.37
Errors			
OCT-LEA vs Mag.	0.47%	-0.36%	0.16%
OCT-HEA vs. Mag	0.49%	-0.32%	0.16%
OCT-HEA vs. LEA	-0.01%	-0.04%	0.00%

The comparison of protection mode CTs were recorded for the first 2 cycles of fault current, due to the 2-cycle duration of the fault. Results are presented Table 4.23. The maximum difference between CTs is larger than the previous results.

Table 4.23 Comparison of fault currents, Case 6

	Cycle 1	Cycle 2
I_a (OCT-LEA)	306.02	305.55
I_a (Mag CT)	300.61	333.43
D60	300.93	333.99
SEL321	302.41	334.85
Mag. CT vs. OCT LEA	-1.800%	8.362%
OCT LEA vs. D60	-1.663%	9.308%
OCT LEA vs. SEL321	-1.180%	9.589%

Table 4.24 shows the comparison of VT outputs. The calculations were done according to the plotted sine waves. The maximum difference between magnetic VT and optical VT is 0.46%.

Table 4.24 Comparison of voltages during the fault, Case 6

	V_{max} (kV)	V_{min} (kV)	V_{avg} (kV)
V_a (Mag VT)	203.32	203.27	203.30
V_a (NXVT-LEA)	202.39	202.33	202.36
V_a (NXVT-HEA)	202.42	202.37	202.39
Errors			
NXVT-LEA vs Mag.	-0.46%	-0.46%	-0.46%
NXVT-HEA vs. Mag	-0.44%	-0.44%	-0.45%
NXVT-HEA vs. LEA	0.01%	0.02%	0.01%

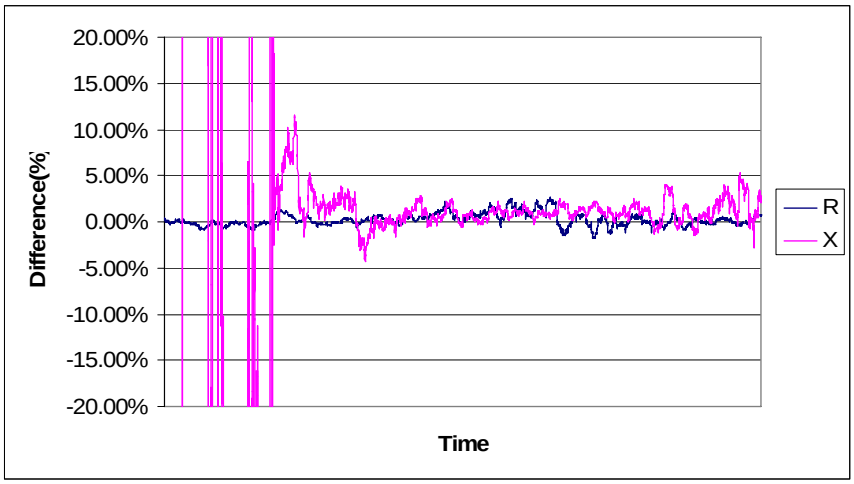

Figure 4.51 Percentage difference between the R and X values, Case 6

The impedance trajectories were calculated using the current and voltage outputs of the magnetic and optical instrument transformers. The method used in Case 1 was used to calculate the differences. Figure 4.51 shows the percentage difference between impedance trajectories. The maximum reactance difference is 10%, and is very similar to the previous cases.

4.3.7 Case 7: Disturbance in Phase C

In this event case, Phase C voltages and current are recorded as a fault record and Phase C has been analyzed. A short circuit fault has been recorded. The short circuit current is 10 times the load current. Figure 4.52 shows the overlapped current and voltage sine waves both for magnetic and optical systems. There is almost no difference between sine waves. The optical current sine wave has noise, compared to the magnetic CT output.

Table 4.25 compares the metering CT outputs. The results are very similar to the previous cases. The maximum difference between magnetic and optical CTs is 1.01%.

Table 4.25 Metering current comparison, Case 7

	I_{max} (A)	I_{min} (A)	I_{avg} (A)
I_c (Mag CT)	130.22	128.52	129.366
I_c (OCT-LEA)	128.90	128.37	128.61
I_c (OCT-HEA)	129.36	128.55	128.90
Errors			
OCT-LEA vs Mag.	1.01%	0.12%	0.58%
OCT-HEA vs. Mag	0.66%	-0.02%	0.36%
OCT-HEA vs. LEA	0.36%	0.14%	0.22%

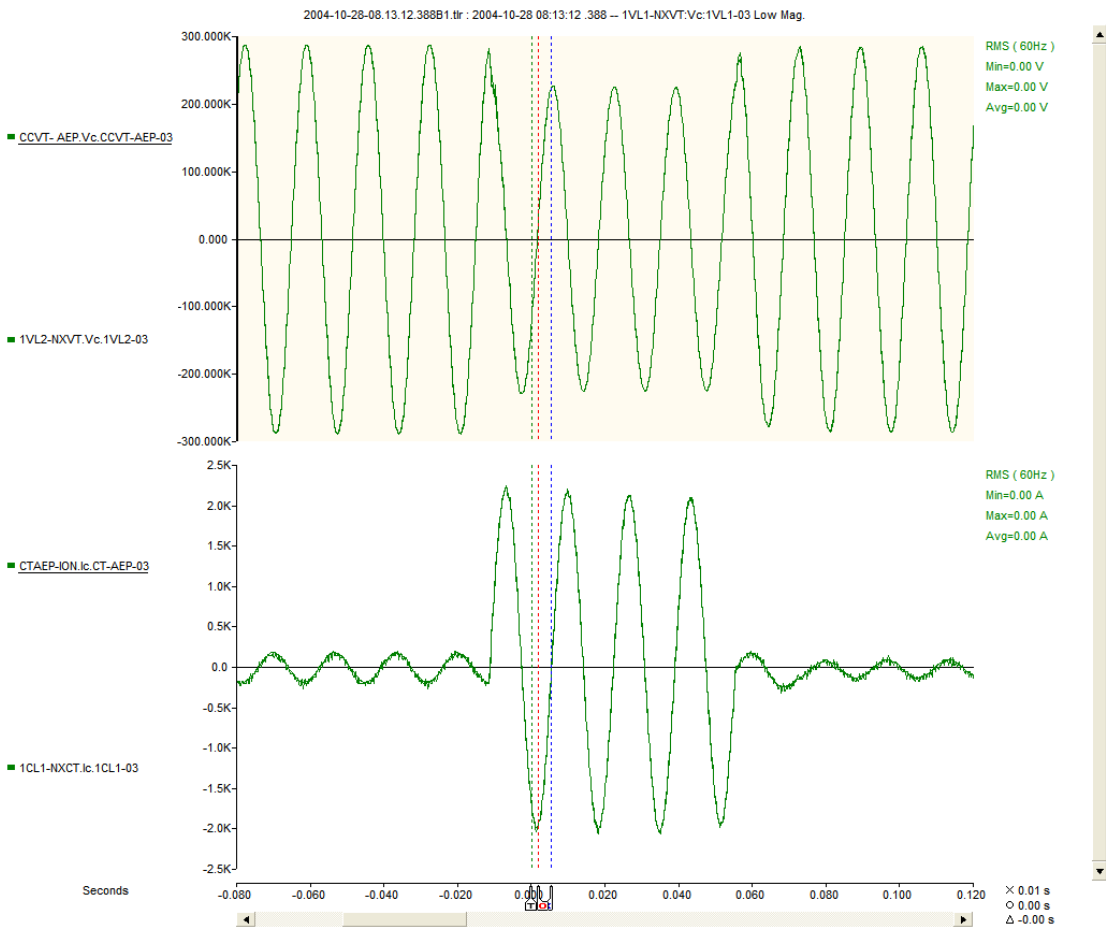

Figure 4.52 Voltage and current sine waves, Case 7

Table 4.26 compares the RMS values of sine waves for first three cycles using the output of magnetic and optical CTs in protection mode. The maximum difference between CTs is 0.6%.

Table 4.26 Comparison of fault currents Case 7

	Cycle 1	Cycle 2	Cycle 3
I_c (OCT-LEA)	1490	1480	1470
I_c (Mag CT)	1490	1470	1470
D60	148	1470	1460
SEL321	148	1470	1470
Errors			
Mag. CT vs. OCT LEA	0.000%	-0.680%	0.000%
OCT LEA vs. D60	-0.671%	-0.676%	-0.680%
OCT LEA vs. SEL321	-0.671%	-0.676%	0.000%

The recorded voltage outputs of the VTs are analyzed, but the sine waves are not reproduced here. The differences between the VTs were calculated and presented in Table 4.27. The maximum difference is 0.21%.

Table 4.27 Comparison of voltages during the fault, Case 7

	V_{max} (kV)	V_{min} (kV)	V_{avg} (kV)
V_c (Mag VT)	204.18	204.05	204.13
V_c (NXVT-LEA)	204.60	204.47	204.54
V_c (NXVT-HEA)	204.17	204.05	204.11
Errors			
NXVT-LEA vs Mag.	0.21%	0.21%	0.20%
NXVT-HEA vs. Mag	0.00%	0.00%	-0.01%
NXVT-HEA vs. LEA	-0.21%	-0.21%	-0.21%

The impedance trajectories were calculated using magnetic and optical three phase current and voltage. The plotted trajectories are not presented here. The difference between plotted trajectories is in Figure 4.53.

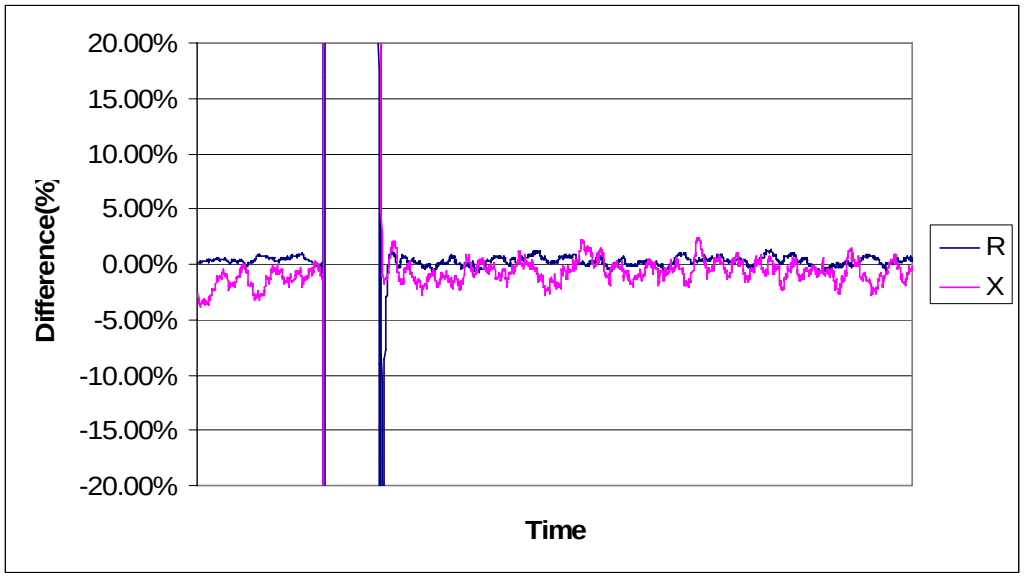

Figure 4.53 Percentage difference between the R and X values, Case 7

The calculated R and X values are changing by time. The difference between R and X values as calculated by magnetic and optical transformers are plotted in Figure 4.53 .The maximum reactance error is around 3%, disregarding the peaks during the fault. This difference is less than previous case results.

4.3.8 Case 8: Disturbance in Phase A

In this event case, Phase A voltages and current are recorded as a fault record and Phase A has been analyzed. Two short circuit faults have been recorded in a short time period. Figure 4.54 shows the recorded current sine waves.

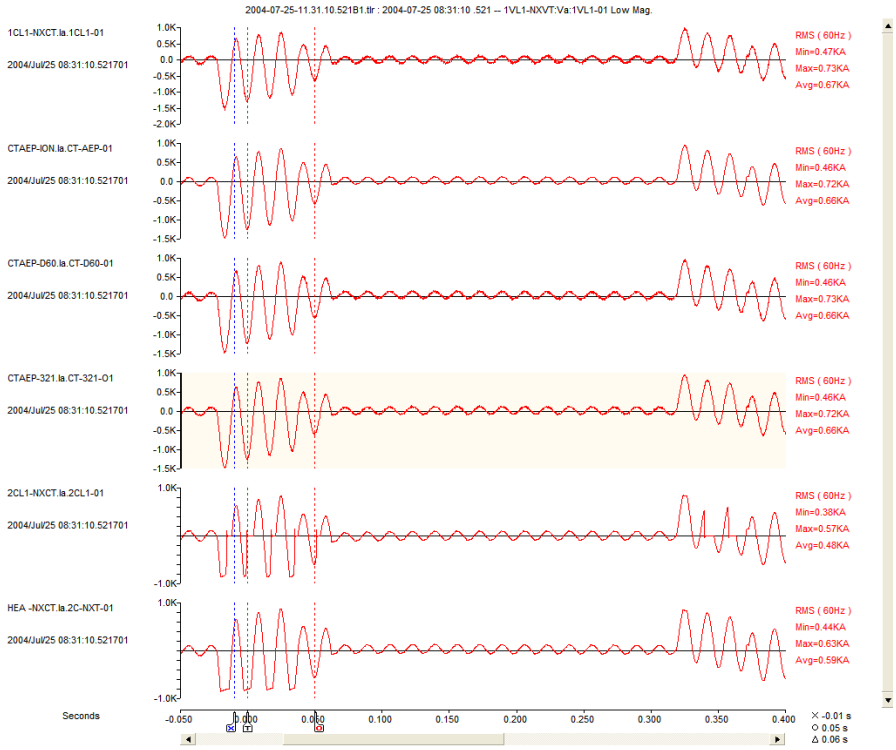

Figure 4.54 Recorded current sine waves, Case 8

In this record, the OCT-LEA output for measuring has a distorted sine wave. This distorted sine wave is very similar to the distorted sine wave in Case 2.

Table 4.28 Metering current comparison, Case 8

	I_{max} (A)	I_{min} (A)	I_{avg} (A)
I_a (Mag CT)	77.32	74.36	75.96
I_a (OCT-LEA)	77.43	74.57	76.26
I_a (OCT-HEA)	77.50	74.52	76.30
Errors			
OCT-LEA vs Mag.	-0.14%	-0.28%	-0.39%
OCT-HEA vs. Mag	-0.23%	-0.22%	-0.45%
OCT-HEA vs. LEA	0.09%	-0.07%	0.05%

Table 4.28 compares the metering CT outputs. The results are very similar to the previous cases. The maximum difference between magnetic and optical CTs is 0.45%.

Table 4.29 compares the RMS values of sine waves for the three cycles using the output of magnetic and optical CTs in protection mode. The maximum difference between CTs is much higher than the previous results. The program calculated the RMS values as rounded values and this increased the percentage difference.

Table 4.29 Comparison of fault currents, Case 8

	Cycle 1	Cycle 2	Cycle 3
I_a (OCT-LEA)	760	710	710
I_a (Mag CT)	750	700	700
D60	750	700	700
SEL321	750	700	700
Errors			
Mag. CT vs. OCT LEA	-1.333%	-1.429%	-1.429%
OCT LEA vs. D60	-1.316%	-1.408%	-1.408%
OCT LEA vs. SEL321	-1.316%	-1.408%	-1.408%

The recorded voltage outputs of the VTs are analyzed, but the sine waves are not reproduced here. The differences between the VTs were calculated and presented in Table 4.30. The maximum difference is 0.32%.

Table 4.30 Comparison of voltages during the fault, Case 8

	V_{max} (kV)	V_{min} (kV)	V_{avg} (kV)
V_a (Mag VT)	202.58	202.48	202.53
V_a (NXVT-LEA)	201.94	201.83	201.88
V_a (NXVT-HEA)	201.97	201.87	201.92
Errors			
NXVT-LEA vs Mag.	-0.32%	-0.32%	-0.32%
NXVT-HEA vs. Mag	-0.30%	-0.30%	-0.30%
NXVT-HEA vs. LEA	0.01%	0.02%	0.02%

The impedance trajectories were calculated using magnetic and optical three phase current and voltage. The plotted trajectories are not presented here. The difference between plotted trajectories is in Figure 4.55.

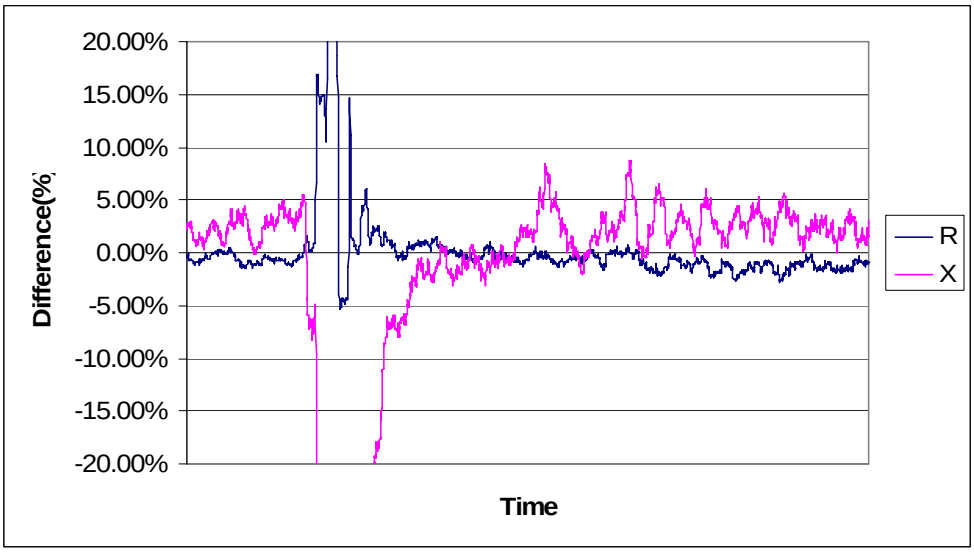

Figure 4.55 Percentage difference between the R and X values, Case 8

4.3.9 Case 9: Disturbance in Phase A

In this event case, Phase A voltages and current are recorded as a fault record and Phase A has been analyzed. Two cycle short circuit fault have been recorded. The fault current was 5 times greater than the load current.

Table 4.31 compares the metering CT outputs. The results are very similar to the previous cases. The maximum difference between magnetic and optical CTs is 0.62%.

Table 4.31 Metering current comparison, Case 9

	I_{max} (A)	I_{min} (A)	I_{avg} (A)
I_a (Mag CT)	170.15	169.02	169.58
I_a (OCT-LEA)	170.50	170.07	170.30
I_a (OCT-HEA)	170.61	169.82	170.17
Errors			
OCT-LEA vs Mag.	-0.21%	-0.62%	-0.42%
OCT-HEA vs. Mag	-0.27%	-0.47%	-0.35%
OCT-HEA vs. LEA	0.06%	-0.15%	-0.08%

Table 4.32 compares the RMS values of sine waves for first three cycles using the output of magnetic and optical CTs in protection mode. The maximum difference between CTs is much higher than the previous results. The program rounded the values while calculating the RMS values, and this increased the percentage difference.

Table 4.32 Comparison of fault currents, Case 9

	Cycle 1	Cycle 2	Cycle 3
I_a (OCT-LEA)	780	770	760
I_a (Mag CT)	760	750	740
D60	770	750	740
SEL321	760	750	740
Errors			
Mag. CT vs. OCT LEA	-2.632%	-2.667%	-2.703%
OCT LEA vs. D60	-1.282%	-2.597%	-2.632%
OCT LEA vs. SEL321	-2.564%	-2.597%	-2.632%

The recorded voltage outputs of the VTs are analyzed, but the sine waves are not reproduced here. The differences between the VTs were calculated and presented in Table 4.33. The maximum difference is 0.26% which is close to the accuracy of the manufacturer's specifications.

Table 4.33 Comparison of voltages during the fault, Case 9

	V_{max} (kV)	V_{min} (kV)	V_{avg} (kV)
V_a (Mag VT)	200.90	200.84	200.87
V_a (NXVT-LEA)	200.38	200.31	200.34
V_a (NXVT-HEA)	200.40	200.34	200.37
Errors			
NXVT-LEA vs Mag.	-0.26%	-0.26%	-0.26%
NXVT-HEA vs. Mag	-0.25%	-0.25%	-0.25%
NXVT-HEA vs. LEA	0.01%	0.01%	0.01%

The impedance trajectories were calculated using magnetic and optical three phase current and voltage. The plotted trajectories are not presented here. The difference between plotted trajectories is in Figure 4.56.

The calculated R and X values are changing by time. The difference between R and X values as calculated by magnetic and optical transformers are plotted in Figure 4.56. The maximum reactance error is around 15%, disregarding the peaks during the fault.

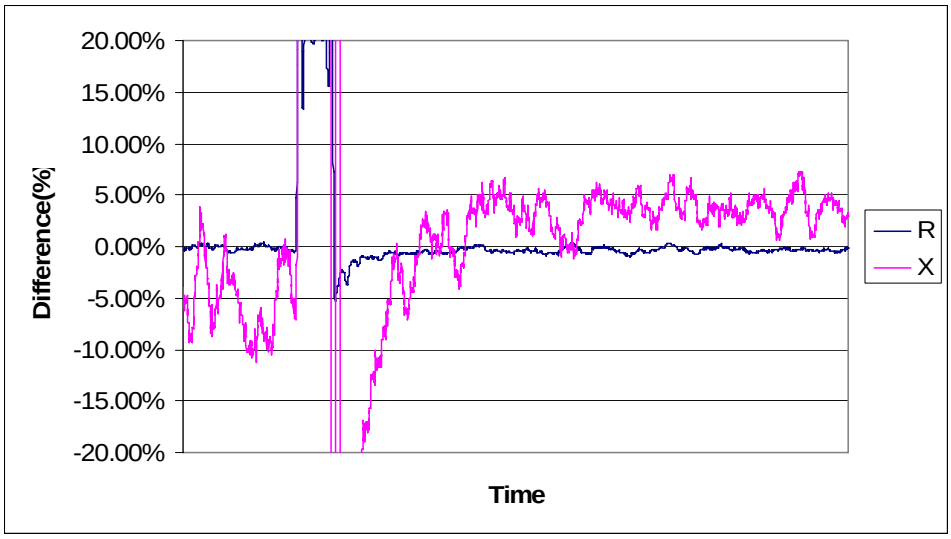

Figure 4.56 Percentage difference between the R and X values, Case 9

4.3.10 Case 10: Disturbance in Phase A

In this event case, Phase A voltages and current are recorded as a fault record and Phase A has been analyzed. A five cycle short circuit fault has been recorded. The fault current was 5 times greater than the load current. Two short circuits were recorded in a short period of time.

Table 4.34 compares the metering CT outputs. The results are very similar to the previous cases. The maximum difference between magnetic and optical CTs is 0.74%.

Table 4.34 Metering current comparison, Case 10

	I_{max} (A)	I_{min} (A)	I_{avg} (A)
I_a (Mag CT)	91.45	84.62	87.60
I_a (OCT-LEA)	90.77	85.02	87.81
I_a (OCT-HEA)	90.82	85.07	87.91
Errors			
OCT-LEA vs Mag.	0.74%	-0.47%	-0.24%
OCT-HEA vs. Mag	0.69%	-0.53%	-0.35%
OCT-HEA vs. LEA	0.06%	0.06%	0.11%

Table 4.32 compares the RMS values of sine waves for first three cycles using the output of magnetic and optical CTs in protection mode. The maximum difference between CTs is much higher than the previous results. The program rounded the values while calculating the RMS values and this increased the percentage difference as in Case 9 and 10.

Table 4.35 Comparison of fault currents, Case 10

	Cycle 1	Cycle 2	Cycle 3
I_a (OCT-LEA)	710	720	710
I_a (Mag CT)	700	700	700
D60	700	700	700
SEL321	700	700	700
Errors			
Mag. CT vs. OCT LEA	-1.429%	-2.857%	-1.429%
OCT LEA vs. D60	-1.408%	-2.778%	-1.408%
OCT LEA vs. SEL321	-1.408%	-2.778%	-1.408%

The recorded voltage outputs of the VTs are analyzed, but the sine waves are not reproduced here. The differences between the VTs were calculated and presented in Table 4.36. The maximum difference is 0.30% which is close to the accuracy of the manufacturer's specifications.

Table 4.36 Comparison of voltages during the fault, Case 10

	V_{max} (kV)	V_{min} (kV)	V_{avg} (kV)
V_a (Mag VT)	203.60	203.28	203.44
V_a (NXVT-LEA)	202.99	202.69	202.84
V_a (NXVT-HEA)	203.02	202.72	202.87
Errors			
NXVT-LEA vs Mag.	-0.30%	-0.29%	-0.29%
NXVT-HEA vs. Mag	-0.28%	-0.28%	-0.28%
NXVT-HEA vs. LEA	0.01%	0.01%	0.01%

The impedance trajectories were calculated using magnetic and optical three phase current and voltage. The plotted trajectories are not presented here. The difference between plotted trajectories is in Figure 4.57.

The calculated R and X values are changing by time. The difference between R and X values as calculated by magnetic and optical transformers are plotted in Figure 4.57. The maximum reactance error is around 11%, disregarding the peaks during the fault.

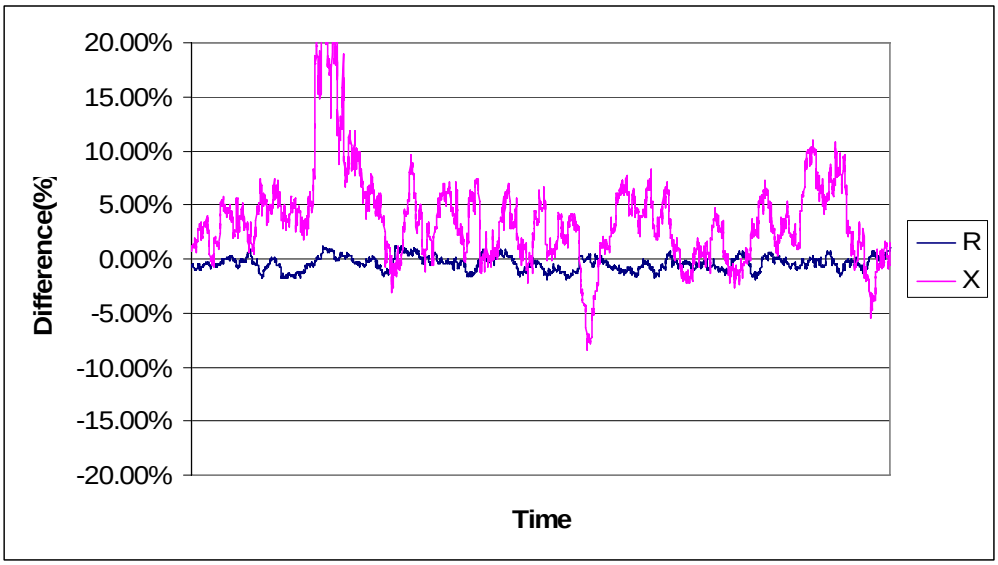

Figure 4.57 Percentage difference between the R and X values, Case 10

4.3.11 Case 11: Disturbance in Phase A

In this event case, Phase A voltages and current are recorded as a fault record and Phase A has been analyzed. A five cycle short circuit fault has been recorded. The fault current was 6 times greater than the load current.

Figure 4.58 shows the overlapped recorded sine wave for both magnetic and optical voltage and current transformers. There is no significant difference, and the optical current transformer output has noise.

Table 4.37 compares the metering CT outputs. The results are very similar to the previous cases. The maximum difference between magnetic and optical CTs is 0.67%.

Table 4.37 Metering current comparison, Case 11

	I_{max} (A)	I_{min} (A)	I_{avg} (A)
I_a (Mag CT)	193.41	191.84	192.76
I_a (OCT-LEA)	193.74	193.13	193.46
I_a (OCT-HEA)	193.52	193.11	193.31
Errors			
OCT-LEA vs Mag.	-0.17%	-0.67%	-0.36%
OCT-HEA vs. Mag	-0.06%	-0.66%	-0.29%
OCT-HEA vs. LEA	-0.11%	-0.01%	-0.08%

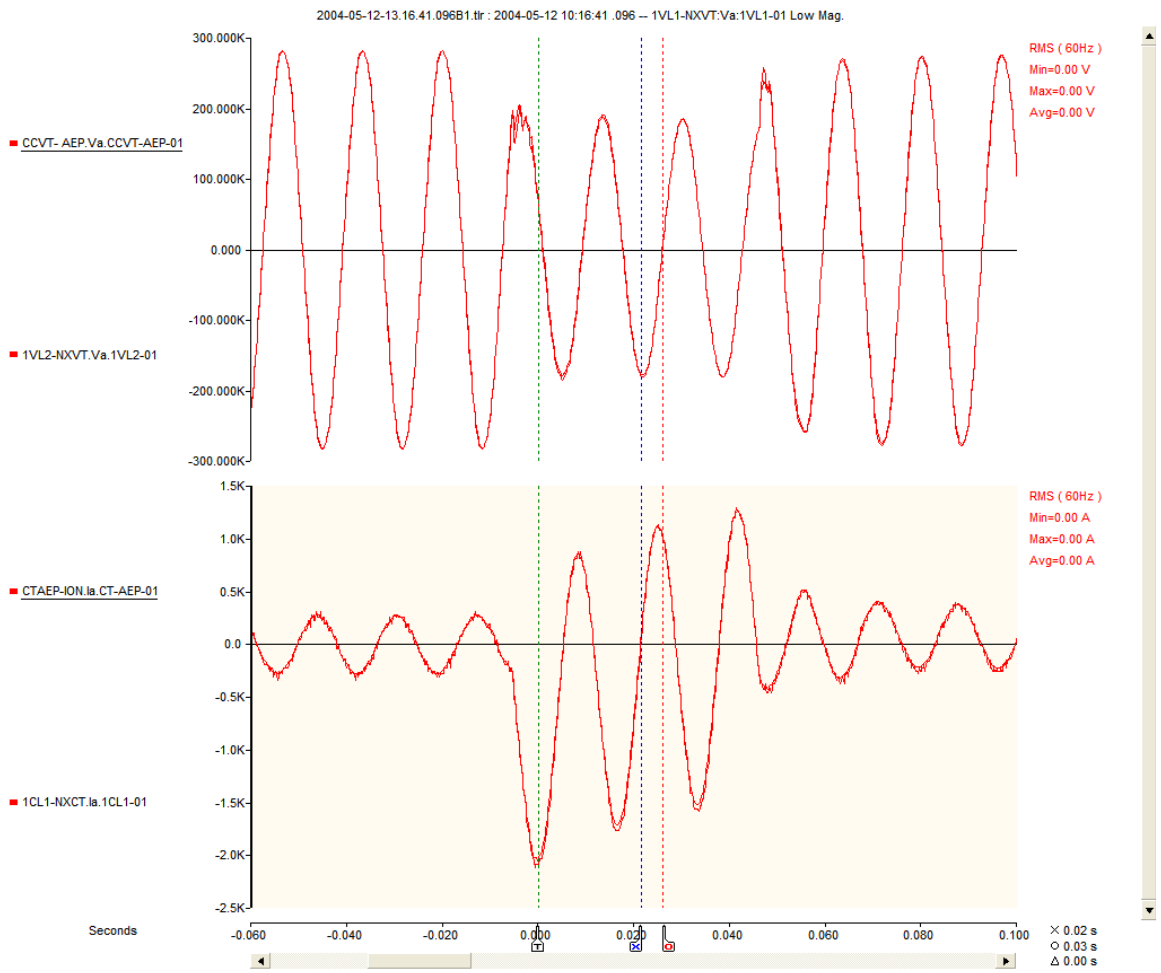

Figure 4.58 Voltage and current sine waves, Case 11

Table 4.37compares the RMS values of sine waves for first three cycles using the output of magnetic and optical CTs in protection mode. The maximum difference between CTs is much higher than the previous results. The program rounded the values while calculating the RMS values and this increased the percentage difference as in previous case.

Table 4.38 Comparison of fault currents, Case 11

	Cycle 1	Cycle 2	Cycle 3
I_a (OCT-LEA)	1050	980	980
I_a (Mag CT)	1040	970	960
D60	1040	970	960
SEL321	1030	960	960
Errors			
Mag. CT vs. OCT LEA	-0.962%	-1.031%	-2.083%
OCT LEA vs. D60	-0.952%	-1.020%	-2.041%
OCT LEA vs. SEL321	-1.905%	-2.041%	-2.041%

Table 4.39 shows the comparison of VT outputs. The calculations were done according to the plotted sine waves. The maximum difference between magnetic VT and optical VT is 0.46%.

Table 4.39 Comparison of voltages during the fault, Case 11

	V_{max} (kV)	V_{min} (kV)	V_{avg} (kV)
V_a (Mag VT)	200.03	200.17	200.10
V_a (NXVT-LEA)	199.45	199.58	199.52
V_a (NXVT-HEA)	199.45	199.58	199.52
Errors			
NXVT-LEA vs Mag.	-0.29%	-0.29%	-0.29%
NXVT-HEA vs. Mag	-0.29%	-0.29%	-0.29%
NXVT-HEA vs. LEA	0.00%	0.00%	0.00%

The impedance trajectories were calculated using magnetic and optical three phase current and voltage. The plotted trajectories are not presented here. The difference between plotted trajectories is in Figure 4.59. The reactance difference is around 5%.

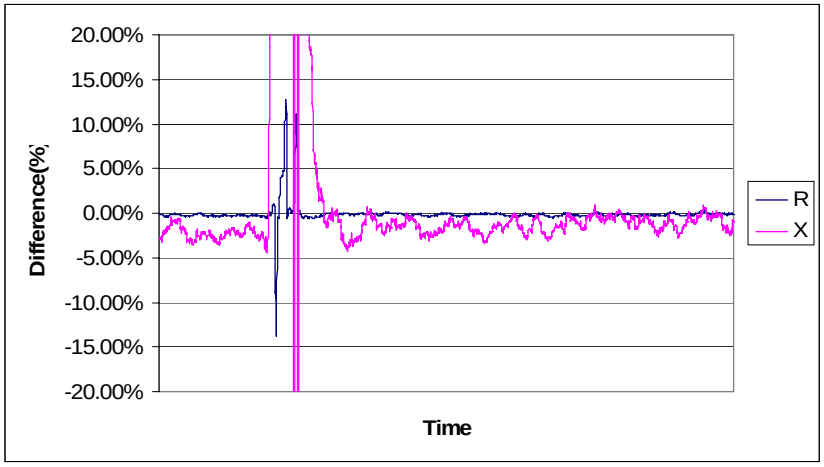

Figure 4.59 Percentage difference between the R and X values, Case 11

5 Conclusion

This report has presented the experimental comparison of the performance of magnetic and optical instrument transformers. The comparison has also been presented analyzing the actual field data. The study has been supported by theoretical concepts gained in the literature review. The study can be concluded as following:

1. The literature and market survey shows that several manufacturers produce optical instrument transformers. However, except for metering application, most of the products are experimental and used for pilot projects in a utility environment. Typically, few units of each product are installed in substations in parallel with conventional instrument transformers. The operation of the two systems is monitored and compared. We can conclude that the optical instrument transformer is viable product, but other than for revenue metering, it is not a well tested, mature product today.

2. The conventional instrument transformers have one output, 1 A or 5 A in the case of CT, and 69 V or 115 V in case of PT. The optical instrument transformers have three outputs:

    a. Digital
    b. Low Energy Analog (LEA). Optical CT = 4 V, Optical PT= 4 V
    c. High Energy Analog (HEA) Optical CT = 1 or 5 A Optical PT =69/120 V

3. The utilities buy high accuracy magnetic instrument transformers for metering. The load on these transformers must be less than the manufacturer specified value. The magnetic instrument transformer purchased for protection has less accuracy, higher load but in case of CT high short circuit current must not saturate the device.

    The optical CTs have metering and protection settings. The optical PT has only one setting, which can be used for metering or protection. The optical instrument transformer's accuracy is independent of the loading and burden, assuming that the load is less than the manufacturer's specified maximum value. The stated differences must be considered when OCT or OPT is used.

4. The metering accuracy of the NxtPhase provided OCT was measured using a high precision current transformer. We measured less than 0.2% error between 250 A and 760 A except one reading that was 0.22%. The results verified the manufacturer specified accuracy of less than 0.2%. The evaluation of the field measurements performed at the AEP Corridor substation gives around 2% differences between the OCT and the magnetic transformer measured RMS values, which is within the allowed limits of the test and recording equipment used.

5. ASU developed a current generator for testing current transformers. This generator can produce current up to 1200 A.

6. The steady state performance of NxtPhase-provided OCT and a standard magnetic CT was compared using the ASU's current generator. The OCT was in protection mode. The results show:
7. Observed white noise in LEA protection output of the OCT, with no impact on functionality,
    a. The RMS current difference between the two transformers was less than 2% in the 200 A-750 A range,
    b. Small phase shift (less than 1 degree) was observed between the two transformers. This is due to the fact that the OCT optical system has a 40 μs inherent delay (which wasn't compensated for in these tests).
    c. The field measurements showed around 2% deviation between the magnetic CT and optical CT output except one case, which is within the accuracy of test and recording equipment.
    d. The OCT output was not disturbed by neighboring magnetic field.

7. The steady state performances of NxtPhase provided OPT and a standard magnetic PT was compared in ASU's high voltage laboratory. The results show:
    a. The noise produced by the OPT HEA output is practically invisible.
    b. The magnetic PT saturated above the rated voltage. The difference between the two PTs is less than 1% under the rated voltage, but increases rapidly above the rated voltage due to saturation of magnetic PT.
    c. The OPT output is highly linear,
    d. The neighboring electric field did not disturb the OPT output.
    e. The comparison of wave shapes produced less than 3% differences and 42 μs phase delay.
    f. The field test shows less than 0.5% differences between the magnetic and optical PT, which is well within the accuracy of test and recording equipment.

8. The transient performance of NxtPhase-provided OCT was measured, comparing the reproduction of short circuit current and direct measurement of frequency characteristics. The results show:
    a. Laboratory testing shows around 2.3% differences in peak short circuit current reproduction,
    b. The field test shows maximum 2.8% differences in LEA output of OCT in the reproduction of RMS values of the first to third cycles after short circuit,
    c. Both the field and laboratory tests show around 2.5% differences between the instantaneous short circuit current values.
    d. The OCT response was tested using DC pulse. The OCT signal showed 68 μs delay and the rise time of the pulse appeared increased.

e. The frequency characteristics of the OCT were measured.
    i. The results showed that the amplitude decreases with the frequency. The slope is around 3 dB/octave. The amplitude is zero above around 20 kHz,
    ii. The phase angle changes more or less linearly by the frequency. At 7.6 kHz the phase angle is 180 degrees.

9. A circuit model was developed to represent the OCT in protection system performance analysis. The model consists of an ideal current transformer, a sixth order low-pass filter and an ideal amplifier, which converts the voltage signal to current.

10. The transient performance of NxtPhase provided OPT was evaluated, comparing the PT's response to short-circuit produced voltage drop in the field, a lightning impulse test, and direct measurement of frequency characteristics. The results show:
    a. The short circuit in the field generated voltage drop. The comparison of magnetic PT and OPT shows around less than 0.25% differences in RMS voltages. The comparison of instantaneous voltage values shows less than 1.8% differences.
    b. The lightning impulse test shows that the magnetic PT and the OPT's HEA output did not reproduce the lightning impulse. The LEA output reproduced the impulse fairly well. The amplitude was reduced about 60%, the signal was delayed by 40 μs, and the rise time increased from 1.2 μs to 13 μs. A higher bandwidth LEA is necessary for reproducing lightning impulses accurately.
    c. The frequency characteristic of the OPT was also measured.
        i. The results showed that the amplitude decreases with the frequency. The slope is around 3 dB/octave. The amplitude is zero above around 40 kHz,
        ii. The phase angle changes more or less linearly by the frequency. At 9.7 kHz the phase angle is 180 degree.

The field test permitted the calculation of impedance trajectories in the cases of different faults. The trajectories were calculated by using the optical instrument transformers as well as the magnetic instrument transformers provided data. The point-by-point comparison of the data shows around 10% deviation.

APPENDIX
Circuit Model for Optical Current Transformer

The frequency response of the Optical Current Transformer was measured and presented in Figure A. 1 and Figure A. 2. Preliminary investigation showed that this frequency response can be modeled by a six order filter. The selected filter circuit is shown in Figure A. 3. The parameters of the circuit were determined by trial and error method. First a set of parameter values were selected. After this, the circuit impedance is calculated vs. the frequency. This followed by the calculation of input current and output voltage vs. frequency. The R, L and C values were modified till the output voltage amplitude and phase angle frequency characteristics matched with the measured values.

The calculation below shows the step by step calculation of the amplitude and phase angle characteristics of the filter circuit modeling the Optical CT.

Measured amplitudes and phase angles

$$frq := \begin{pmatrix} 60 \\ 300 \\ 1000 \\ 2000 \\ 4000 \\ 6000 \\ 7670 \\ 8200 \\ 10000 \\ 12000 \\ 14000 \\ 16000 \\ 16800 \end{pmatrix} \quad ang := \begin{pmatrix} -0.86 \\ -7.78 \\ -25.2 \\ -52.42 \\ -104.54 \\ -149.47 \\ -181.13 \\ -197.05 \\ -223.2 \\ -259.78 \\ -301.54 \\ -339.26 \\ -353.95 \end{pmatrix} \quad ampl := \begin{pmatrix} 1 \\ 0.992 \\ 0.971 \\ 0.924 \\ 0.764 \\ 0.602 \\ 0.467 \\ 0.435 \\ 0.336 \\ 0.243 \\ 0.182 \\ 0.138 \\ 0.125 \end{pmatrix}$$

Vector representation

$length(frq) = 13$

Continues function

$angl(f) := linterp(frq, ang, f)$

$ampli(f) := linterp(frq, ampl, f)$

Equation describing the measured values

$$V_{out}(f) := \frac{ampli(f)}{ampli(0)} \cdot e^{j \cdot angl(f) \cdot deg} \qquad ampli(60) = 1 \qquad ampli(0) = 1.002$$

$$f := 0, 2000 .. 10000$$

$$V_{out}(f) = \begin{pmatrix} 1 + 0.015i \\ 0.562 - 0.731i \\ -0.191 - 0.738i \\ -0.518 - 0.305i \\ -0.438 + 0.085i \\ -0.244 + 0.23i \end{pmatrix}$$

$\arg(V_{out}(f)) =$ deg

0.87
-52.42
-104.54
-149.47
168.958
136.8

$angl(f) =$

0.87
-52.42
-104.54
-149.47
-191.042
-223.2

Resonance frequency

$f := 6000$ $\qquad f_{res} := root(angl(f) + 180, f) \qquad f_{res} = 7.61 \times 10^3$

$|V_{out}(f_{res})| = 0.471 \qquad f := 0, 1 .. 16800$

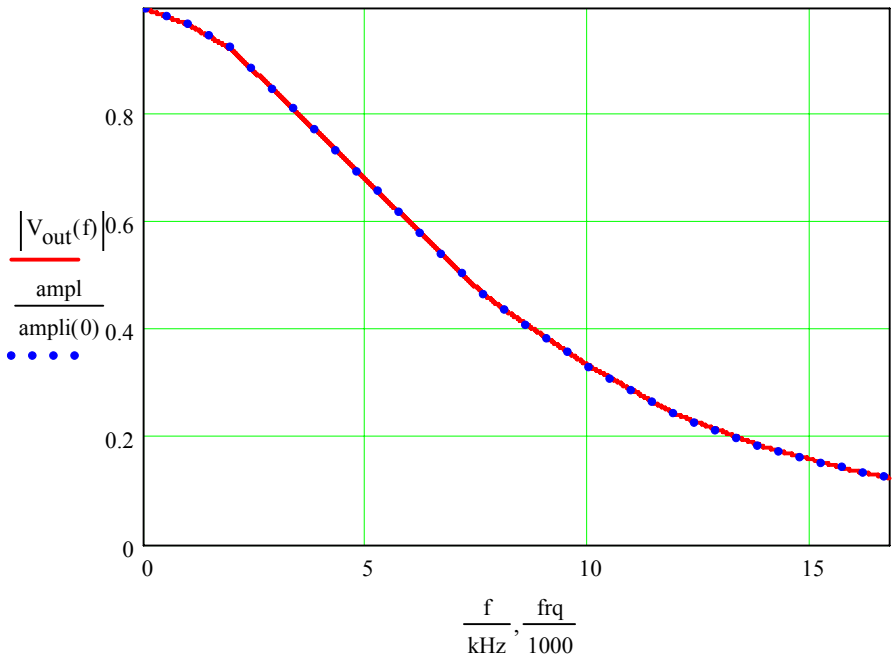

Figure A. 1 Experimental amplitude-frequency response

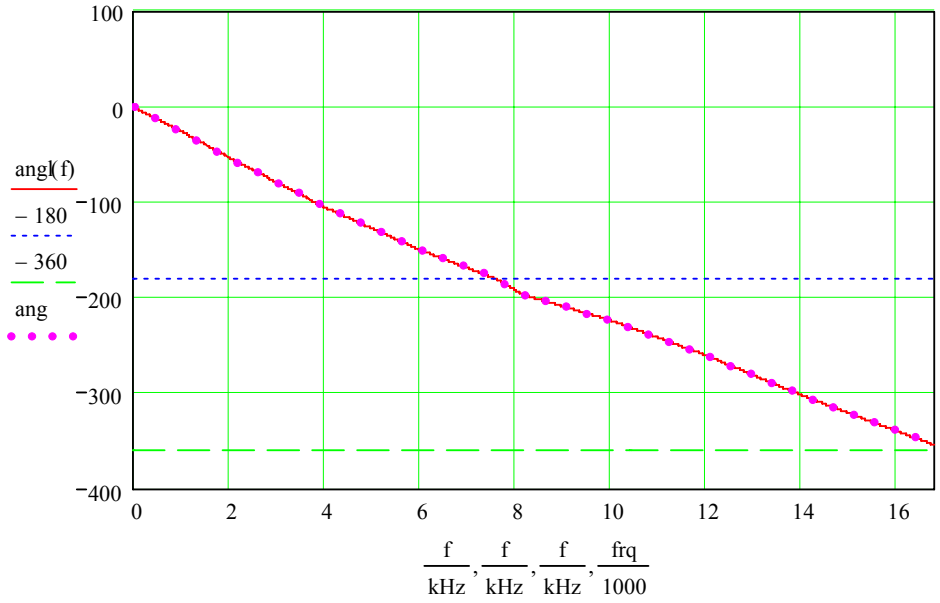

Figure A. 2 Experimental phase-frequency response

Ladder network

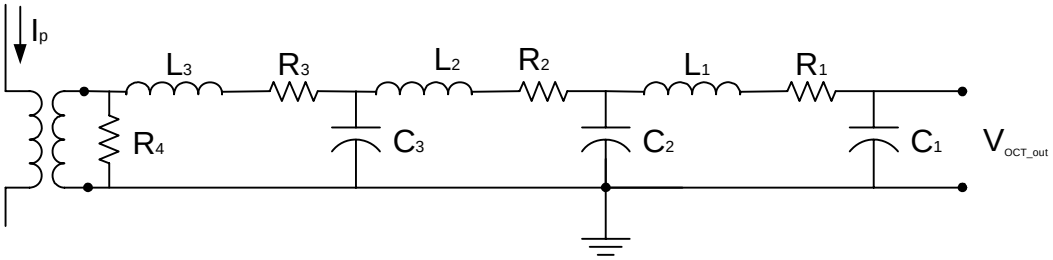

Figure A. 3 Ladder network

Filter data

$L_1 := 0.04\ H$ $C_1 := 15\ nF$ $R_1 := 1600\ \Omega$ $f_1 := \frac{1}{2\cdot\pi\cdot\sqrt{L_1\cdot C_1}}$ $f_1 = 6.497\ kHz$

$L_2 := 0.02\ H$ $C_2 := 13\ nF$ $R_2 := 1000\ \Omega$ $f_2 := \frac{1}{2\cdot\pi\cdot\sqrt{L_2\cdot C_2}}$ $f_2 = 9.87\ kHz$

$L_3 := 0.01\ H$ $C_3 := 12\ nF$ $R_3 := 600\Omega$ $f_3 := \frac{1}{2\cdot\pi\cdot\sqrt{L_3\cdot C_3}}$ $f_3 = 14.529\ kHz$

Ideal transformer data

$Turn := \frac{100}{1}$ $I_p := 1000\,A$ $R_4 := 0.1\Omega$

Impedance calculation

$w(f) := 2 \cdot \pi \cdot f$ $f := 1000Hz$

Loop one

$Z_{1c}(f) := \frac{1}{j \cdot w(f) \cdot C_1}$ $Z_{1s}(f) := j \cdot w(f) \cdot L_1 + R_1$

$Z_1(f) := Z_{1s}(f) + Z_{1c}(f)$ $Z_1(f) = 1.6 - 10.359i\,k\Omega$

Loop two

$Z_{2c}(f) := \frac{1}{j \cdot w(f) \cdot C_2}$ $Z_{2s}(f) := j \cdot w(f) \cdot L_2 + R_2$

$Z_{12c}(f) := \frac{Z_1(f) \cdot Z_{2c}(f)}{Z_1(f) + Z_{2c}(f)}$ $Z_{12c}(f) = 0.467 - 5.644i\,k\Omega$

$Z_2(f) := Z_{2s}(f) + Z_{12c}(f)$ $Z_2(f) := Z_{2s}(f) + Z_{12c}(f)$

Loop three

$Z_{3c}(f) := \frac{1}{j \cdot w(f) \cdot C_3}$ $Z_{3s}(f) := j \cdot w(f) \cdot L_3 + R_3$

$Z_{123c}(f) := \frac{Z_2(f) \cdot Z_{3c}(f)}{Z_{3c}(f) + Z_2(f)}$ $Z_{123c}(f) = 0.727 - 3.954i\,k\Omega$

$Z_3(f) := Z_{3s}(f) + Z_{123c}(f)$ $Z_3(f) = 1.327 - 3.891i\,k\Omega$

Input impedance

$$Z_{in}(f) := \frac{R_4 \cdot Z_3(f)}{Z_3(f) + R_4} \qquad Z_3(60Hz) = 1.315 - 66.309ik\Omega$$

$$Z_{in}(60Hz) = \left(0.1 - 1.507i \times 10^{-7}\right)\Omega \qquad Z_{in}(f) = 0.1 - 2.302i \times 10^{-6}\Omega$$

Input current transferred by ideal transformer

$$I_s(I_p) := \frac{I_p}{Turn} \qquad I_s(1000\ A) = 10\ A$$

The terminal voltage is

$$V_{R3}(I_P, f) := I_s(I_p) \cdot Z_{in}(f) \qquad V_{R3}(I_p, f) = \left(1 - 2.302i \times 10^{-5}\right) V$$

$$\arg\left(V_{R3}(I_p, f)\right) = -1.319 \times 10^{-3}\ deg \qquad \arg\left(V_{R3}(I_p, 60Hz)\right) = -8.637 \times 10^{-5}\ deg$$

Current entering into the filter is

$$I_3(f) := \frac{V_{R3}(I_p, f)}{Z_3(f)} \qquad I_3(f) = 0.079 + 0.23i\ mA$$

$$I_2(f) := I_3(f) \cdot \frac{Z_{3c}(f)}{Z_{3c}(f) + Z_2(f)} \qquad I_2(f) = 0.068 + 0.157i\ mA$$

$$I_1(f) := I_2(f) \cdot \frac{Z_{2c}(f)}{Z_{2c}(f) + Z_1(f)} \qquad I_1(f) = 0.043 + 0.082i\ mA$$

$$V_1(f) := I_1(f) \cdot Z_{1c}(f) \qquad V_1(f) = (0.872 - 0.451i)\ V$$

$$\arg\left(V_1(f)\right) = -27.351\ deg \qquad \left|V_1(f)\right| = 0.982\ V$$

The rated 1000A current produces at 60 Hz 1 volt output voltage but has -1.64 deg phase shift

$|V_1(60Hz)| = 1\ V$ $\qquad$ $\arg(V_1(60Hz)) = -1.642\ deg$

Time delay at 60 Hz is: $T_{delay} := \dfrac{\arg(V_1(60Hz))\cdot s}{360\cdot 60}$ $\qquad$ $T_{delay} = -1.327\mu s$

Deviation from the measured values: $\qquad |V_{out}(60)\cdot V| = 0.998\ V$

$error_{amp}(f) := \dfrac{|V_{out}(f)\cdot V| - |V_1(f\cdot Hz)|}{|V_{out}(60)\cdot V|}$ $\qquad$ $error_{amp}(60) = -0.194\ \%$

$error_{phase}(f) := \dfrac{\arg(V_{out}(f)) - \arg(V_1(f\cdot Hz))}{\arg(V_{out}(f))}$ $\qquad$ $error_{phase}(60) = -90.894\ \%$

Amplitude vs. frequency

$f := 0, 1 .. 16800$

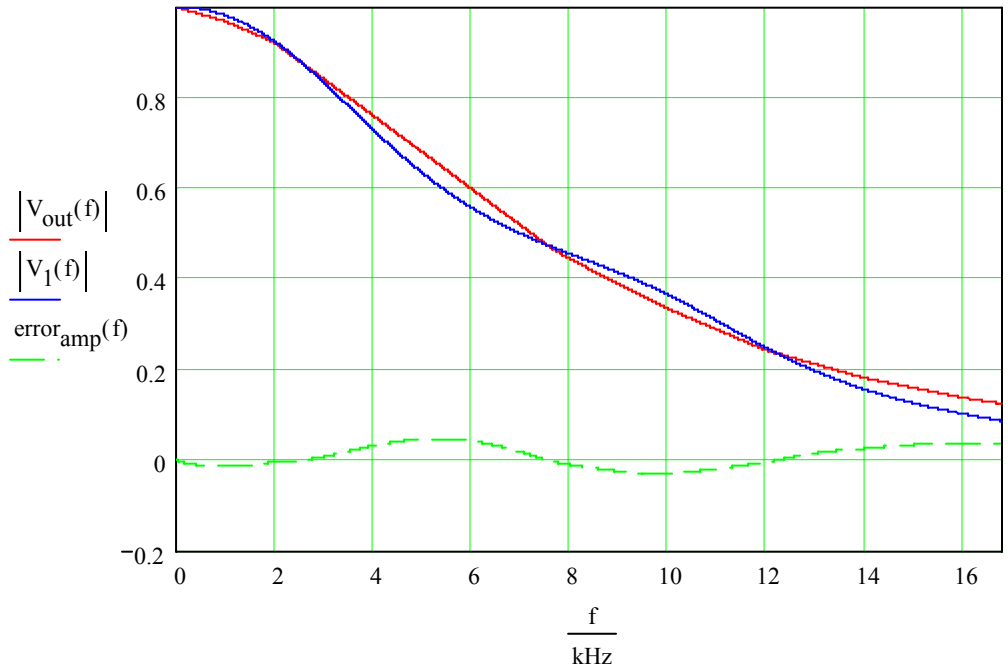

Figure A. 4 Experimental and calculated data, amplitude-frequency

Maximum and minimum errors

$f := 5000$

$$error_{amp}\left(Maximize\left(error_{amp}, f\right)\right) = 4.681\,\%$$

$$error_{amp}\left(Minimize\left(error_{amp}, f\right)\right) = -1.398\,\%$$

Phase angle vs. frequency

$f := 0, 1 .. 16800$

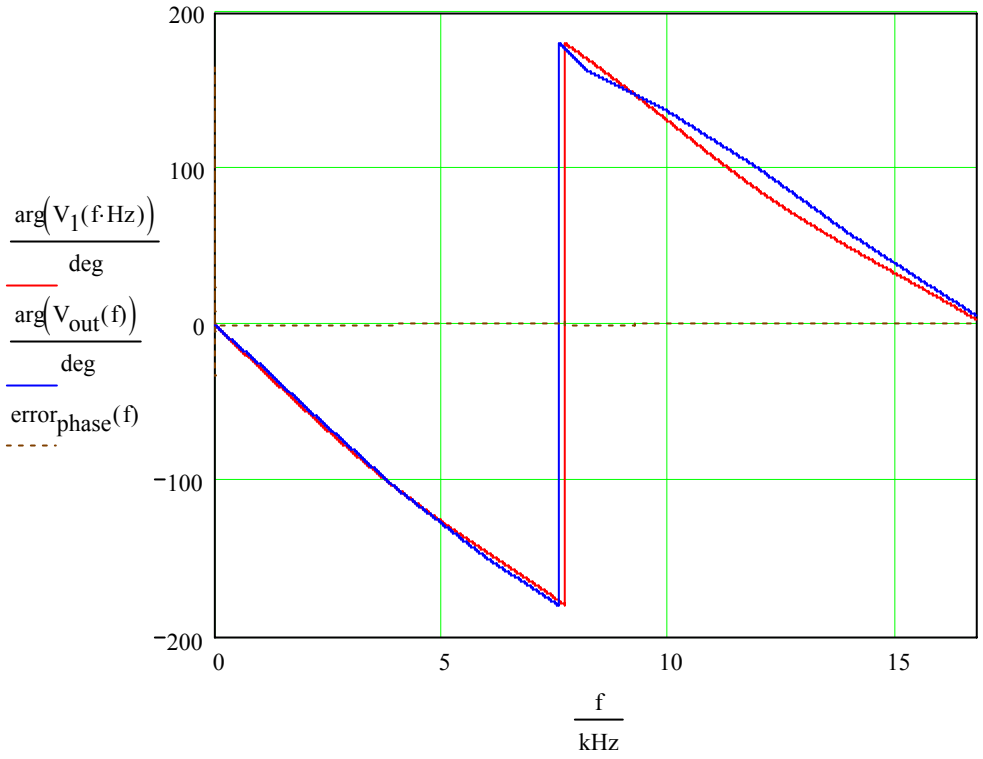

Figure A. 5 Experimental and calculated data, phase-frequency

Maximum and minimum errors

$f := 5000$

$$error_{phase}\left(Maximize\left(error_{phase}, f\right)\right) = 2.483\,\%$$

$$error_{phase}\left(Minimize\left(error_{phase}, f\right)\right) = -8.536\,\%$$

REFERENCES

[1] S. H. Horowitz, "Power System Relaying", Second Edition, 1995, page 39-51.

[2] T. Bosselmann, "Electric and Magnetic Field Sensing for High Voltage Applications," Technical Proceeding of SPIE Europe Series, v. 3099, 305, 1997.

[3] J.D.P, Hrabluik, "Optical current sensors eliminate CT saturation," Power Engineering Society Winter Meeting, v.2, January 27-31, 2002, pp. 1478-1481.

[4] J. Blake, W. Williams, C. Glasow, R. Bergh, K. Fetting, E. Hadley, G. Sanders, "Optical Current Transducers for High Voltage Applications," Intelligent Processing and Manufacturing of Materials 3rd International Conference, July 29, 2001, Vancouver.

[5] J. Blake, "Fiber optic current sensor calibration," Transmission and Distribution Conference and Exposition, 2001 IEEE/PES , v. 1 , Oct 28- Nov 2, 2001, pp.127 – 130.

[6] A. Tarely, A. Derossis (Alcatel Alstom), "A Current Sensor Remotely Powered and Monitored through an Optical Fiber Link," Optical Fiber Technology 1, 1999, pp.181-185.

[7] A.P Steer, S.J. Turner, P.R.B. Farrie, R.P Tatam, A.N. Tobin, J.D.C. Jones, D.A. Jackson, " Optical fiber current sensor for circuit protection", Developments in Power Protection, 1989., Fourth International Conference on , 11-13 Apr 1989
Pages:296 – 300

[8] T. Sawa, K. Kurosawa, T. Kaminishi, T. Yokota, "Development of optical instrument transformers," IEEE Transactions on Power Delivery, v.5, issue. 2, April 1990, pp.884 – 891.

[9] Y.C.L. Frankie, C.K.C. Wilson, M.S. Demokan, "Fiber-optic Current sensor developed for power system measurement," International Conference on Advances in Power System Control, Operation and Management (APSCOM), November 5-8, 1991, v.2, pp. 637 – 643.

[10] A. Cruden, J.R. McDonald, I. Andonovic, D. Uttamchandani, R. Porrelli, K. Allan, "Current measurement device based on the Faraday effect," Fifth International Conference on Developments in Power System Protection, 1993, pp. 69 – 72.

[11] A. Cruden, Z.J. Richardson, J.R. NcDonald, L. Andonovic, "Optical crystal based devices for current and voltage measurement," IEEE Transactions on Power Delivery, v.10, issue 3, July, 1995, pp. 1217 – 1223.

[12] P.G. Zhang, D. Irvine-Halliday, "Faraday effect optical current sensor," Canadian Conference on Electrical and Computer Engineering, 1996, v. 2 , May 26-29, 1996, pp.871 – 875.

[13] J.G. Werthen, A.G. Andersson, S.T. Weiss, H.O. Bjorklund, "Current measurements using optical power," IEEE Proceedings on Transmission and Distribution Conference, September 15-20, 1996, pp. 213 – 218.

[14] Y. Nie, X. Yin, Z. Zhang, "Optical current transducer used in high voltage power system," IEEE/PES Transmission and Distribution Conference and Exhibition 2002 Asia Pacific, v.3, October 6-10, 2002, pp.1849 – 1853.

[15] M. Willsch, T. Bosselmann, "Optical current sensor application in the harsh environment of a 120 MVA power generator," Optical Fiber Sensors Conference Technical Digest, v. 1, May 6-10, 2002, pp. 407 – 410.

[16] W.C. Michie, A. Cruden, P. Niewczas, W.I. Madden, J.R. McDonald, M. Gauduin, "Harmonic analysis of current waveforms using optical current sensor," IEEE Transactions on Instrumentation and Measurement, v. 51, No. 5, October, 2002, pp. 1023 – 1026.

[17] P. Mihailovic, S. Petricevic, Z. Stojkovic, J.B. Radunovic, "Development Of A Portable Fiber-Optic Current Sensor For Power Systems Monitoring," IEEE Transactions On Instrumentation and Measurement, v. 53, No. 1, February, 2004.

[18] J.D.P. Hrabliuk, "Interfacing optical current sensors in a substation," IEEE Power Engineering Society Summer Meeting, v. 1 , July 15-19, 2001, pp. 147 – 155.

[19] G. Nicholson, "Reliability considerations: optical sensors for the control and measurement of power," IEEE/PES Transmission and Distribution Conference and Exposition, v. 1, October 28- November 2, 2001, pp. 122 – 126.

[20] F. Rahmatian, P.P. Chavez, "SF6-Free 550 kV Combined optical voltage and current transducer system," IEEE Transmission and Distribution Conference, v. 1, September 7-12, 2003, pp. 379-382.

[21] J.N Blake, A.H. Rose, "Fiber-Optic Current Transducer Optimized For Power Metering Applications," IEEE Transmission and Distribution Conference, v. 1, September 7-12, 2003, pp. 405-408.

[22] T.W. Cease, J.G. Driggans, S.J. Weikel, "Optical Voltage and current sensors used in revenue metering system," IEEE Transactions on Power Delivery, v. 6, No.4 , October 1991.

[23] T.W. Cease, P.M. Johnston, "A magneto-optic current transducer," IEEE Transactions on Power Delivery, v. 5, No. 2, April, 1990, pp. 548-555.

[24] K. Bohnert, P. Gabus, and H. Brändle, "Fiber-Optic Current and Voltage Sensors for High-Voltage Substations," invited paper at 16th International Conference on Optical Fiber Sensors, October, 2003, Nara Lapan Technical Digest, pp 752-754.

[25] V. N. Filippov, A. N. Starodumov, Y. O. Barmenkov, and V. V. Makarov, "Fiber-Optic Voltage Sensor Based on a Bi 12 TiO 20 Crystal ," Applied Optics, v. 39, 2000, pp. 1389-1393.

[26] L.H. Christensen, "Design, construction, and test of a passive optical prototype high voltage instrument transformer," IEEE Transactions on Power Delivery, v. 10, No.3, July, 1995.

[27] P. Bauerschmidt, R. Lerch, "Optical voltage sensor based on a quartz resonator," IEEE Proceedings on Ultrasonics Symposium, v. 1, November 3-6, 1996, pp.383-387.

[28] J.C. Santos, M.C. Taplamacioglu, and K. Hidaka, " Pockels High-Voltage Measurement System," IEEE Transactions on Power Delivery, v. 15, No. 1, January, 2000.

[29] C. Li, X. Cui, “An optical voltage and current sensor with electrically switchable quarter waveplate,” Sensors and Actuators A: Physical, v. 126, No. 1, January 26, 2006, pp. 62-67.

[30] K. Kurosawa, S. Yoshida, E. Mori, G. Takahashi, S. Saito, “ Development of an optical instrument transformer for DC voltage measurement,” IEEE Transactions on Power Delivery, v. 8, No. 4, October, 1993, pp.1721 – 1726.

[31] P.G. Zhang, D. Irvine-Halliday, “ A practical hybrid optical fiber based high voltage sensor,” Canadian Conference on Electrical and Computer Engineering, 1996, v. 2 , May 26-29, 1996, pp.888– 890

[32] F. Rahmatian, P.P. Chavez, and N.A.F. Jaeger, “138 kV and 345 kV Wide-Band SF6-Free Optical Voltage Transducers,” IEEE PES Winter Power Meeting, v. 2, January 27-31, 2002, pp. 1472 – 1477.

[33] F. Rahmatian, P.P. Chavez, and N.A.F. Jaeger, “A 230 kV Optical Voltage Transducer Using Multiple Electric Field Sensors,” IEEE Transaction on Power Delivery, v. 17, No. 2, April, 2002, pp.417-422.

[34] F.Rahmatian, P. Chavez, and N.A.F. Jaeger, “Wide-Band 138 kV Distributed-Sensor Optical Voltage Transducer: Study of Accuracy under Pollution and other Field Disturbances,” IEEE PES Summer Meeting, v. 1, July 15-19, 2001, pp.156-161.

[35] F.Rahmatian, D. Romalo, S. Lee, A. Fekete, S. Liu, N.A.F. Jaeger, and P.P. Chavez, “Optical Voltage Transducers for high-voltage applications,” Proceedings of 2nd EPRI Optical Sensor Systems Workshop, January 26-28, 2000.

[36] F. Rahmatian, P.P. Chavez, and N.A.F. Jaeger, “Resistively Shielded Optical Voltage Transducer,” IEEE Transmission & Distribution Conference, v. 1, October 28-November 2, 2001, pp. 117-121.

[37] General Electric, “Instrument Transformer Burden Data”, Data sheet GET-1725D.

[38] P.P. Chavez, F. Rahmatian, , and N.A.F. Jaeger, “Accurate voltage measurement with electric field sampling using permittivity-shielding,” IEEE Transactions on Power Delivery, v. 17, No. 2, April, 2002, pp. 362 – 368.

[39] P.P. Chavez, N.A.F. Jaeger, F. Rahmatian, “Accurate Voltage Measurement by the Quadrature Method,” IEEE Transactions on Power Delivery, v. 18, No. 1, January, 2003, pp. 14-19.

[40] F. Rahmatian, P. P. Chavez, and N. A. F. Jaeger, “A Wide-Band SF6-Free Optical Voltage Transformer,” 3rd EPRI Sensor Systems Workshop, Pittsburgh, October 17-19, 2001.

[41] Wikipedia The Free Encyclopedia

http://en.wikipedia.org/wiki/Pockels_effect

[42] NxtPhase T&D Corporation, http://www.nxtphase.com/